STATUS OF THESIS

Title of thesis | **A Study on the Effect of Nozzle Type on the Hydrodynamics of Ejector-Induced Cocurrent Upflow Bubble Column**

I **FAUZAN RAHMAN** hereby allow my thesis to be placed at the Information Resource Center (IRC) of Universiti Teknologi PETRONAS (UTP) with the following conditions:

1. The thesis becomes the property of UTP
2. The IRC of UTP may make copies of the thesis for academic purposes only
3. This thesis classified as

☐ Confidential

☑ Non-confidential

If the thesis is confidential, please state the reason:

_____

_____

The contents of the thesis will remain confidential for _____ years.
Remarks on disclosure:

_____

Endorsed by

Signature of Author

Jl. Karya Wisata,
Perumahan Taman Johor Baru
Blok B2/14 – Medan – 20144
Indonesia

Date: June, 9th, 2008

Signature of Supervisor

Department of Chemical Engineering
Universiti Teknologi PETRONAS
Bandar Seri Iskandar, Perak
Malaysia

Date: 09.06.08

APPROVAL

UNIVERSITI TEKNOLOGI PETRONAS

Approval by Supervisors

The Undersigned certify that they have read, and recommend to The Postgraduate Studies Programme for acceptance, a thesis entitled "**A Study on the Effect of Nozzle Type on the Hydrodynamics of Ejector-Induced Cocurrent Upflow Bubble Column** " Submitted by **Fauzan Rahman** for the fulfillment of the requirements for the degree of Master of Science in Chemical Engineering.

09.06.2008
Date

Signature : 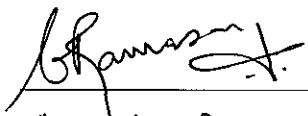
Supervisor : Dr. M. RAMASAMY
Date : 09-06-2008

UNIVERSITI TEKNOLOGI PETRONAS

A Study on the Effect of Nozzle Type on the Hydrodynamics of Ejector-Induced Cocurrent Upflow Bubble Column

By

Fauzan Rahman

A THESIS

SUBMITTED TO THE POSTGRADUATE STUDIES PROGRAMME

AS A REQUIREMENT FOR THE DEGREE OF MASTER OF SCIENCE

IN CHEMICAL ENGINEERING PROGRAMME

BANDAR SERI ISKANDAR

PERAK

JUNE 2008

DECLARATION

I hereby declare that the thesis is based on my original work except for quotations and citations which have been duly acknowledged. I also declare that it has not been previously or concurrently submitted for any other degree at UTP or other institutions.

Signature :

Name : FAUZAN RAHMAN

Date : June, 9th, 2008

This thesis is dedicated to my loving parents, Fathur Rahman and Cut Mena Muria, who always instill the importance of hard work and higher education, and whose words of encouragement and push for tenacity always ring in my ears.

A special gratitude goes to my loving, caring, understanding and supportive wife, Widyastuti. I would not have done it without your support and encouragement.

ACKNOWLEDGMENTS

First and foremost I am very grateful towards the Almighty, the Bountiful and the Merciful Allah SWT, with His bestow, I have the strength to finish this thesis. Praise be upon Him, with His grace extends my existence to show my gratitude to whom I am going to mention in these following paragraphs.

My most sincere gratitude also goes to my former supervisor, Late Prof. V.R. Radhakrishnan for his expert guidance and brilliant idea in designing such masterpiece research equipment, the ejector-induced cocurrent upflow bubble column. For a long time, we will deeply feel this bereavement and remembrance. I would also like to extend my deepest gratitude and appreciation to my supervisor, Assoc. Prof. Dr. Marappagounder Ramasamy, for his continuous guidance, cooperation, support and valuable advices throughout the period of this research. I also want to express my gratitude to Prof. Dr. Duvvuri Subbarao for brightening my mind with his expert guidance during the completion of this research. I also wish to thank Prof. Binay Dutta and Assoc. Prof. Dr. Thanapalan Murugesan for insightful discussions.

I thank Chemical Engineering Department and Postgraduate Studies Program, Universiti Teknologi PETRONAS, which have provided all necessary supports. I would also like to express my gratitude all postgraduate office staffs, especially Pn. Kamaliah, En. Fadil, Kak Norma and Kak Aida. I wish to thank Mr. Cheng (S/V Technics), Najad (SOLTEQ), Fazli, Azzudin, Amie, Firman, Wawan, Aqsha (University of Calgary), Dhany Saputra, Sue and all technicians in Unit Operation Lab.; Shahafizan, Khairul and Asnizam, for their kind efforts in helping me doing the research.

Tremendous thanks to all members of PPI UTP, especially Erman, Zulfan, Ayu, Anisa, Amank, Munir, Surya, Bu Anti, Amelia, Faisal, Barkah, Iqbal, Kiki, Tri Chandra, Roil, Teguh and Ariyanti. I really enjoyed every single moment I have spent with you guys; you are all unquestionably great friends to me. Last but not least, I would like to thank my family for their patience, open-mindedness and endless support. They are, always have been and always will be, in my heart.

ABSTRACT

Bubble columns as gas-liquid cocurrent contactors have gained a considerable attention due to various advantages they offer. The effectiveness of gas distributors in the bubble columns determines the mass transfer efficiency of the column. Ejector is one of the most widely used devices as the gas distributors in the bubble columns. Although empirical correlations for the ejectors have been reported in literature, no study based on the principle of fluid mechanics has been carried out on the effect of ejector geometry on its important hydrodynamic characteristics. A better understanding of the ejectors is essential for an improved design of the ejector itself and the bubble column.

In the present work, the experimental setup consists of an ejector integrated with upflow bubble column and a gas-liquid separator at the top of the column. Experimental investigations have been carried out on the effect of ejector nozzle geometry on the hydrodynamics of cocurrent upflow bubble column. Gas entrainment rate, gas hold-up, pressure drop and energy dissipation for water-air system are studied and reported. Experiments have been conducted using convergent and orifice nozzles with different types and sizes.

It is found experimentally that nozzle with smaller nozzle diameter develops higher vacuum and entrains more air as the suction fluid, for a given flow rate of water as the motive fluid. This also means that nozzle with smaller nozzle diameter gives higher gas hold-up and dissipates more energy to create intense mixing between the two phases. In terms of nozzle type, orifice nozzles present higher vacuum level than convergent nozzles for the same nozzle diameter. The pressure drop across the nozzle and the air entrainment rate have been modeled and analyzed by applying Bernoulli's principle. Predicted values of air entrainment rate as a function of water flow rate through the nozzle by the theoretical model developed show good agreement with experimental values. Gas hold-up data has also been analyzed using drift flux model. The analysis agrees well with the previous works.

ABSTRAK

Kolum Gelembung (bubble columns) sentuhan sama arah arus gas-cecair telah mendapat banyak perhatian disebabkan oleh keistimewaan yang ia tawarkan. Keberkesanan alat pengagihan gas menentukan keupayaan perpindahan jisim setiap kolum. Ejektor (ejectors) telah digunakan secara meluas sebagai pengagihan gas didalam kolum gelembung. Walaupun hubung kait empirikal untuk ejektor telah dilaporkan didalam kajian reviuw literatur, tetapi masih tiada kajian teori dijalankan untuk kesan tindak-balas saiz dan bentuk ejektor kepada sifat penting hidrodinamik kolum gelembung. Kefahaman ejektor yang mendalam adalah penting untuk membaiki reka bentuk ejektor itu sendiri dan juga kolum gelembung.

Bagi kerja-kerja yang dikendalikan, eksperimen dilakukan menggunakan penyepaduan ejektor bersama kolum gelembung sentuhan sama arah arus ke atas dan pemisah gas-cecair yang terletak diatas kolum. Di antara kerja-kerja yang dikendalikan, kajian eksperimen telah dijalankan untuk mengkaji tindak balas nozel ejektor yang berlainan bentuk dan saiz kepada tindak-balas hidrodinamik kolum gelembung sentuhan sama arah arus ke atas. Kadar kuantiti gas yang terperangkap, kejatuhan tekanan dan kehilangan tenaga dari system air-udara itu dikaji dan dilaporkan.. Eksperimen telah dijalankan menggunakan nozel jenis convergen (convergent) dan orifis (orifice) dengan pelbagai jenis saiz nozel.

Dalam kerja hari ini, didapati nozel bersaiz diameter yang kecil menghasilkan lebih vakum dan sedutan angin yang lebih banyak bagi eksperimen yang mengunakan aliran air sebagai bendalir penggerak utama. Ini juga bermakna nozel bersaiz diameter yang kecil dapat memerangkap lebih gas dan menggunakan lebih tenaga untuk menghasilkan percampuran yang kuat diantara dua jenis bendalir. Dari segi jenis nozel pula, nozel berjenis orifis menghasilkan lebih vakum berbanding nozel berjenis convergen untuk perbandingan menggunakan nozel bersaiz diameter yang sama. Susutan tekanan dalam nozel dan kadar pengaliran udara telah dimodelkan dan dianalisis menggunakan prinsip Bernoulli. Nilai-nilai yang diperoleh bagi kadar udara sebagai fungsi dari kadar pengaliran air yang terperangkap dari model yang dihasilkan adalah munasabah dan sama

seperti nilai-nilai eksperimen. Data kuantiti gas yang terperangkap telah dianalisa menggunakan model "drift flux". Keputusan analisa adalah munasabah dan betul mengikut kerja-kerja yang telah dijalankan.

TABLE OF CONTENTS

	Page
STATUS OF THESIS	i
APPROVAL	ii
TITLE PAGE	iii
DECLARATION	iv
DEDICATION	v
ACKNOWLEDGMENTS	vi
ABSTRACT	vii
ABSTRAK	viii
TABLE OF CONTENTS	x
LIST OF TABLES	xiii
LIST OF FIGURES	xiv
NOMENCLATURES	xvii
CHAPTER I: INTRODUCTION	1
1.1 Objective of Research	6
1.2 Scope of Research	6
1.3 Thesis Outline	6
CHAPTER II: LITERATURE REVIEW	8
2.1 Early Investigations on Liquid-Gas Ejector	8
2.2 Effect of Nozzle Geometry on the Ejector Performance	9
2.3 Gas Entrainment Rate in Liquid-Gas Ejector	10
2.4 Pressure Drop in Ejector-Induced Bubble Column	11
2.4.1 Frictional pressure drop and friction factor in Ejector-Induced Bubble Column	13
2.5 Energy Dissipation in Ejector-Induced Bubble Column	15
2.6 Gas Hold-Up in Ejector-Induced Bubble Column	17
2.6.1 Gas hold-up measurement techniques	17
2.6.2 Gas hold-up modeling techniques	19
2.6.2.1 Homogeneous flow model	19

2.6.2.2 Variable density model 20
2.6.2.3 Momentum exchange model 20
2.6.2.4 Slip velocity model 21
2.6.2.5 Lockhart-Martinelli model 22
2.7 Summary 22

CHAPTER III: RESEARCH METHODOLOGY 24
3.1 Introduction 24
3.2 Experimental Setup 25
3.3 Experimental Procedure 31
3.3.1 Equipment start-up procedure 31
3.3.2 Preliminary experiments 31
3.3.3 Pressure drop measurement 33
3.3.4 Gas hold-up measurement 33
3.3.5 Shut down procedure 34
3.3.6 Changing and aligning the nozzles 34
3.4 Data Processing 35
3.4.1 Pressure drop 35
3.4.2 Friction factor 35
3.4.3 Energy dissipation 36
3.4.4 Derivation of Bernoulli Equation for water flow through nozzle 36
3.4.5 Determination of coefficient of discharge, C_v 37
3.4.6 Derivation of Bernoulli Equation for air flow through air inlet line 38
3.4.7 Gas hold-up 39
3.5 Equipment Identification 41
3.6 Summary 45

CHAPTER IV: RESULTS AND DISCUSSIONS 46
4.1 Pressure Profile Observations 46
4.2 Pressure Drop across nozzle 52
4.3 Pressure Drop for Air Flow across the Air Inlet Line 55

4.4 Observations on Water Flow Rate and Air Entrainment Rate 56
4.5 Pressure Recovery in the Ejector 57
4.6 Pressure Drop in the Ejector and the Total System 58
4.6.1 Friction factor in the total system 61
4.7 Application of Bernoulli Principle for Water Flow through the Nozzle 63
4.8 Application of Bernoulli Principle for Air Flow through Air Inlet Line 65
4.9 Correlation between Water Flow Rate and Entrained Air Flow Rate 66
4.9.1 Correlation between predicted values of water flow rate and air entrainment rate 67
4.10 Energy Dissipation in Ejector-Induced Bubble Column 68
4.11 Gas Hold-Up Analysis 70
4.12 Summary 74

CHAPTER V: CONCLUSIONS AND RECOMMENDATIONS 76
5.1 Conclusions 76
5.2 Recommendations 77

PUBLICATIONS 79
REFERENCES 80
APPENDIX A: PHYSICAL PROPERTIES AND CONSTANTS 91
APPENDIX B: EXPERIMENTAL DATA 92

LIST OF TABLES

	Page
Table 1.1 Classification of ejector based on the motive and suction fluids	4
Table 2.1 Empirical correlations given by various authors	11
Table 3.1. Sizes of nozzles	29
Table 3.2. Distance of pressure transducers	29
Table 3.3. Dimensions of the ejector-bubble column assembly	30
Table 3.4. Optimum position of nozzle in the suction chamber	32
Table 3.5. Data table for pressure drop measurement	35
Table 3.6 Data table for friction factor calculation	35
Table 3.7. Data table for energy dissipation calculation	36
Table 3.8. Data table for gas hold-up measurement	39
Table 3.9. Data table for gas hold-up analysis with drift-flux model	40
Table 4.1. C_v values for various nozzles	64
Table 4.2. Comparison of gas and liquid superficial velocities, and gas hold-up	72
Table 4.3. Values of drift-flux parameters	73
Table 4.4. Comparison of distribution parameter and drift velocity for different works	74
Table A.1. Physical properties and constants used in calculations	91
Table B.1. Pressure measurement for convergent nozzles	93
Table B.2. Pressure measurement for orifice nozzles	94
Table B.3. Nozzle pressure drop calculation for various nozzles	95
Table B.4. Air pressure drop calculation for various nozzles	96
Table B.5. Calculation of pressure recovery in the ejector for various nozzles	97
Table B.6. Calculation of friction factor for convergent nozzles	99
Table B.7. Calculation of friction factor for orifice nozzles	99
Table B.8. Calculation of air entrainment prediction for various nozzles	100
Table B.9. Calculation of energy dissipation in the ejector for various nozzles	101
Table B.10. Calculation of gas hold-up in the ejector for various nozzles	102

LIST OF FIGURES

	Page
Figure 1.1. Schematic drawing of an ejector	4
Figure 3.1. Research flow diagram	25
Figure 3.2. Schematic diagram of ejector-induced bubble column experimental setup	26
Figure 3.3. Sectional drawing of ejector-bubble column assembly	27
Figure 3.4. Detail drawing of nozzle construction (a) Orifice (b) Convergent	28
Figure 3.5. Schematic drawing of important sections in preliminary experiments	32
Figure 3.6. Drift-flux correlation chart	40
Figure 3.7. Ejector-Induced Cocurrent Upflow Bubble Column	41
Figure 3.8. Ejector Assembly (E) and pressure transducers (PI)	42
Figure 3.9. Nozzles used in the experiments from left to right: NC6, NC8, NC10, NO6 and NO8	42
Figure 3.10. Water storage tank (T)	43
Figure 3.11. Flow meter (FI-14a) and pump (P)	43
Figure 3.12. Gas-liquid separator (SE)	44
Figure 3.13. Suction pump (P-3)	44
Figure 4.1. Observed pressure profiles for different water flow rates in the system using 6 mm convergent nozzle (NC6), with distance, z, measured from the tip of the nozzle	47
Figure 4.2. Observed pressure profiles for different water flow rates in the system using 8 mm convergent nozzle (NC8), with distance, z, measured from the tip of the nozzle	48
Figure 4.3. Observed pressure profiles for different water flow rates in the system using 10 mm convergent nozzle (NC10), with distance, z, measured from the tip of the nozzle	49
Figure 4.4. Observed pressure profiles for different water flow rates in the system using 6 mm orifice nozzle (NO6), with distance, z, measured from the tip of the nozzle	50
Figure 4.5. Observed pressure profiles for different water flow rates in the	51

system using 8 mm orifice nozzle (NO8), with distance, z, measured from the tip of the nozzle

Figure 4.6. Schematic diagram of important locations at the nozzle 52

Figure 4.7. Upstream pressure (P_l) developed as a function of water flow rates for different nozzles 52

Figure 4.8. Effect of water flow rates on the suction pressure (P_s) developed for different nozzles 53

Figure 4.9. Effect of water flow rate on the pressure drop across the convergent nozzles 54

Figure 4.10. Effect of water flow rate on the pressure drop across the orifice nozzles 54

Figure 4.11. Schematic diagram of important locations at the suction chamber 55

Figure 4.12. Effect of suction pressure on the air flow rate with different nozzles 56

Figure 4.13. The relationship between the observed water flow rate and the air entrainment rate fort different nozzles 57

Figure 4.14. Comparison between the observed values of ($P_d - P_s$) 58

Figure 4.15. Effect of water flow rate on ejector pressure drop 59

Figure 4.16. Effect of air entrainment rate on ejector pressure drop, $R^2 = 0.816$ 59

Figure 4.17. Effect of mixture flow rate at the suction chamber on ejector pressure drop 60

Figure 4.18. Effect of water flow rate on total system pressure drop 61

Figure 4.19. Effect of superficial water Reynold's number on the two-phase friction factor 62

Figure 4.20. Correlation of water pressure drop across the nozzle 63

Figure 4.21. Correlation of water pressure drop across the nozzle with C_v^2 64

Figure 4.22. Correlation between the pressure drop across the air inlet line, $R^2 = 0.894$ 65

Figure 4.23. Comparison of the experimental values of entrained air flow rate 67

Figure 4.24. Correlation between the predicted values of water flow rate and air entrainment rate 68

Figure 4.25. Effect of mixture flow rate at the suction chamber on the dissipated energy for different nozzles 69

Figure 4.26. Relationship between energy dissipation in the ejector and the 70

third power of mixture flow rate at the suction chamber
Figure 4.27. The effect of entrained air flow rate on gas hold-up for various nozzles 71
Figure 4.28. Drift-flux correlation for ejector bubble column 73
Figure B.1. Optimization of nozzle position for convergent nozzles 93
Figure B.2. Optimization of nozzle position for orifice nozzles 94

NOMENCLATURES

A_a	crossectional area of air inlet line, m^2
A_c	crossectional area of column, m^2
A_n	crossectional area of nozzle, m^2
A_i	crossectional area of nozzle upstream line, m^2
A_t	area of throat, m^2
C_o	distribution parameter, dimensionless
C_v	coefficient of discharge, dimensionless
D_a	diameter of air inlet line, m
D_c	diameter of bubble column, m
D_i	diameter of water inlet line (nozzle upstream), m
D_n	diameter of nozzle, m
D_s	diameter of suction chamber, m
D_t	diameter of throat, m
E_c	energy consumed for compressing gas phase, W
E_D	energy dissipation, W
E_{De}	energy dissipation at the ejector, W
E_j	energy supplied by high velocity jet, W
F	frictional loss, W
f	Fanning friction factor, dimensionless
f_m	two-phase friction factor, dimensionless
g	gravitational acceleration, m/s^2
H	jet velocity head, m
h_b	height of bubble column, m

H_s	height of suction chamber, m
h_l	height of clear liquid, m
h_n	height of nozzle tip from the chamber base, cm
h_t	height of total mixture, m
K	Bankoff factor, dimensionless
K_{di}	diffuser loss coefficients, dimensionless
K_n	nozzle loss coefficients, dimensionless
K_{th}	throat loss coefficients, dimensionless
L_d	length of diffuser, m
L_n	length of nozzle head, m
L_t	length of throat, m
M	molecular weight of air, kg/kmol
m_G	mass of gas, kg
m_L	mass of liquid, kg
P	pressure, Pa
P_A	atmospheric pressure, Pa
P_d	pressure in diffuser outlet, Pa
P_h	hydrostatic pressure in the bubble column, Pa
P_l	pressure in nozzle upstream, Pa-a
P_s	pressure in the suction chamber, Pa-a
Q	volumetric flow rate, m^3/s
Q_G	volumetric flow rate of gas phase, m^3/s
Q_L	volumetric flow rate of liquid phase, m^3/s
Q_M	volumetric flow rate of two-phase mixture, m^3/s
$Q_{M,d}$	volumetric flow rate of two-phase mixture in the diffuser outlet, m^3/s

$Q_{M,s}$	volumetric flow rate of two-phase mixture in the suction chamber, m^3/s
R	Ideal gas constant, 8.314 $m^3 \cdot Pa/mol \cdot K$
$Re_{L,c}$	Superficial liquid Reynold's number across the column, dimensionless
$Re_{L,n}$	Superficial liquid Reynold's number across the nozzle, dimensionless
R_m	gas to liquid volumetric flow rate ratio, dimensionless
T	temperature, K
u_G	true velocity of gas, m/s
u_L	true velocity of liquid, m/s
v_D	drift velocity, m/s
V_G	volume of gas phase or unoccupied space, m^3
v_G	velocity of gas phase, m/s
$v_{G,A}$	velocity of gas phase in the atmosphere, m/s
$v_{G,s}$	velocity of gas phase at the air inlet line, m/s
v_L	velocity of liquid phase, m/s
$v_{L,l}$	velocity of liquid phase at the nozzle upstream, m/s
$v_{L,s}$	velocity of liquid phase at the nozzle tip, m/s
v_M	velocity of two-phase mixture, m/s
v_{SG}	superficial gas velocity, m/s
v_{SL}	superficial liquid velocity, m/s
V_T	volume of total system, m^3
W	external work, W
z	distance, mm
z_{nt}	distance between the nozzle tip and the throat entry, cm

Greek symbol

ΔF	irreversible pressure loss, Pa
ΔP_e	pressure drop across the ejector, Pa
ΔP_F	frictional pressure drop, Pa
ΔP_n	pressure drop across the nozzle, Pa
ΔP_T	pressure drop across the total system, Pa
ε_G	gas hold-up, dimensionless
ε_L	liquid hold-up, dimensionless
μ	viscosity, Pa.s
ρ_G	density of gas phase, kg/m^3
ρ_L	density of liquid phase, kg/m^3
ρ_M	density of two-phase mixture, kg/m^3
σ	surface tension, N/m
ϕ_m	gas to liquid mass flow rate ratio, dimensionless

CHAPTER 1

INTRODUCTION

Separation processes are common in chemical, petroleum, petrochemical, pulp and many other industries. Most of the capital and operating expenses in these industries come from one or more separation processes. However, the existence of efficient separation processes in an industry has significant contribution on the economics.

Many processing equipment are devoted to separate one phase or one material from another. Separation processes in chemical engineering commonly involve gas, liquid and/or solid phases. Separation processes can be classified into two broad categories, namely mechanical separations and diffusional separations.

Mechanical separations of heterogeneous mixtures usually include methods of separating solid particles from gases or liquids, liquid drops from gases or other liquids, and separating one type or size of solids from a mixture of particles. Diffusional transfer operations are more extensively found in industries that involve gas and liquid phases like in petrochemical plants, oil refineries and gas processing plants. This type of separation processes is based on the transfer of material from one homogeneous phase to another. The driving force in mass transfer-based separation processes is the difference in concentration, vapor pressure, solubility and diffusivity. Several well-known separation techniques are carried out based on mass transfer operations such as distillation, gas absorption, adsorption, liquid extraction, dehumidification, leaching and membrane separations.

The efficiency of separation processes depends on the mass transfer coefficient between the two phases and the interfacial area. In order to achieve a good mass transfer between phases, various types of contacting devices have been used. Wetted wall columns, packed towers, distillation columns, spray towers and bubble columns are some of the established devices in performing effective mass transfer operations.

In terms of the flow direction of the fluids, gas-liquid contacting devices can be broadly classified as cocurrent, counter current and cross current systems. Counter current

operations are ubiquitous in industries because they present good mass transfer between the phases due to many equilibrium stages that can be achieved, while cocurrent and cross current operations are rare practices in industries. Cocurrent operations are not often used in industries because they can only perform one equilibrium stage. Hence, compared to countercurrent operations, cocurrent operations give lesser mass transfer coefficient.

Despite not having very wide applications in industries, cocurrent operations have some beneficial features that make them still competitive with other flow modes. Due to their simplicity, ability to handle high superficial velocities without flooding, low pressure drop, high interfacial area and reasonable mass transfer coefficients, and low capital cost, cocurrent operations may be an attractive alternative to counter current operations in situations requiring only one equilibrium stage. Improvements have been made on many aspects of such equipment to increase the mass transfer and separation efficiency such as the usage of various types of gas distributors on cocurrent bubble columns to enhance the dispersion efficiency.

An attractive cocurrent device for mass transfer operation is a bubble column. Bubble columns allow good contact between gas phase and liquid phase, and have been extensively used in wide industrial applications such as in biotechnological areas (Schugerl et al., 1977), antibiotic fermentation (Fregapane et al., 1999), hydrotreating process (Dautzenberg and de Deken, 1984) and Fischer-Tropsch process (Jager and Espinoza, 1995). Bubble columns have also gained a considerable attention over the past few decades due to various advantages they offer such as lower capital and operating cost, higher interfacial area which leads to excellent mass transfer, simpler in construction, operation and maintenance (Cui, 2005). From recent work carried out by many researchers (Pal et al., 1979; Deckwer, 1992; Chaumat et al., 2005; Dhaouadi et al., 2007), it is known that cocurrent systems are also capable of performing very efficiently in several separation processes.

In bubble column operations, gas distributor is required to disperse the gas phase into the liquid phase. The design of the distributor has a strong effect on gas dispersion. Spargers are the commonly used gas distributors in bubble columns. In sparger type systems, the gas sparger is fixed at the top or bottom side of bubble column. Liquid is forced through the column at high velocity and as it moves it shears the gas from the sparger in the form

of bubbles. Yet, nowadays, it is known that jet type distributors such as ejectors, venturis, nozzles and other similar devices are also good alternatives for gas-liquid contacting. Generally, these devices utilize kinetic energy of high velocity fluids to achieve fine dispersion and intense mixing between the two phases.

Venturis have been used for a century to measure fluid flow rates. In recent times, venturis have been found with wider applications such as removing particles from gas streams and also acting as gas dispersion device. Several studies have been reported on the performance characteristics of venturis (Bauer et al., 1962; Jackson et al., 1964; Elenkov and Boyadzhiev, 1967; Huynh et al., 1991). However, venturis still need external energy source to make effective dispersions between the phases since they do not have the ability to develop suction and entrain fluids into the system. In the last few decades, ejectors, which have analogous physical shape as venturis, are becoming popular as efficient gas distributors. According to several earlier researchers, ejectors have been used as gas distributing devices in bubble columns (Rylek and Zahradnik, 1984; Zahradnik et al., 1985; Havelka et al., 1997) and in aerobic fermenters (Moresi et al., 1983).

Ejectors have become popular due to their simplicity and high reliability. They give greatest preference for industries in creating vacuum in many processes. Ejectors are essentially designed to convert the pressure energy of a motivating fluid to kinetic energy to entrain a suction fluid. Numerous advantageous features are provided by ejectors, which can be summarized as:

1. Ejectors provide good mixing between the motive fluid and the suction fluid
2. Ejectors have no mechanically moving parts, hence, maintenance is low and operation is fairly constant when corrosion is not a factor
3. Dispersion efficiencies of ejectors are reasonably good
4. Ejectors can be designed compactly, and easily fabricated in all sizes and installed
5. Capital cost is low due to their simplicity in design

Due to the wide variety of liquids, gases or vapors, which may be used as either the motive or as the suction fluid, a wide variety of ejector configurations are possible. Ejectors from the point of view of the motive and suction fluids may broadly be classified into four types as shown in Table 1.1.

Table 1.1 Classification of ejector based on the motive and suction fluids

System	Motive Fluid	Suction Fluid
Gas-Gas	Gas	Gas
Gas-Liquid	Gas	Liquid
Liquid-Liquid	Liquid	Liquid
Liquid-Gas	Liquid	Gas

Ejectors basically consist of four major sections as shown in Figure 1.1, namely nozzle, suction chamber, throat and diffuser.

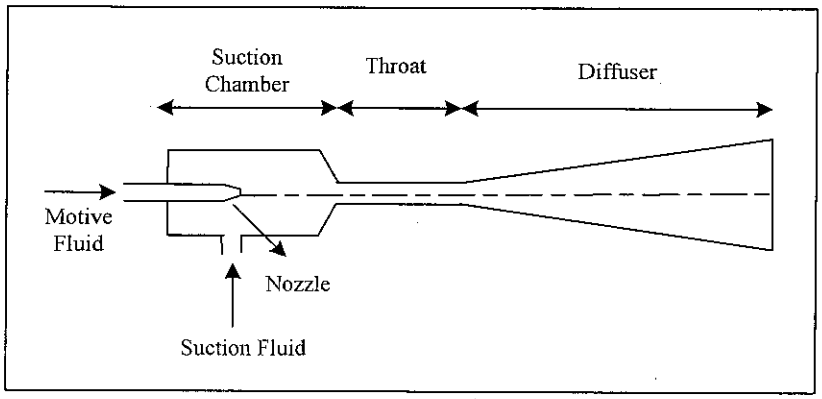

Figure 1.1. Schematic drawing of an ejector

When a motive fluid is pumped through the nozzle of an ejector at a high velocity, vacuum condition is created in the suction chamber. The suction fluid is entrained because of this condition. The dispersion of the entrained fluid in the throat of the ejector with the motive fluid jet emerging from the nozzle leads to intimate mixing between the two phases. A diffuser section after the throat helps in the pressure recovery.

Nozzle is a vital part in an ejector since it determines the vacuum level and the amount of suction fluid that can be entrained into the suction chamber. Nozzles in an ejector can be of two different types; single-jet nozzle or multi-jet nozzle. Nevertheless, ejectors with single-jet nozzle are the simplest and most commonly used design. They are normally recommended for pressures from atmospheric to 3 mmHg. Ejectors with multi-jet nozzle are used where lower suction pressure is specified. Moreover, these designs are frequently used when the low fixed cost is more important than operating economy, where the supply of motive fluid is limited, and for intermittent use.

Integration of bubble column and ejector is expected to give more advantageous features in gas-liquid contacting process (Radhakrishnan and Mitra, 1984; Mandal et al., 2005; Majumder et al., 2006). Bubble columns with ejector are gaining importance because of its self-sucking characteristics of gas phase and efficient dispersion of gas phase into the liquid phase. As a gas dispersing device, the good aspect of the ejector is that it is very simple in design and no extra energy is required for gas dispersion as the gas phase is spontaneously sucked and dispersed by the high velocity liquid jet. Therefore, from energy point of view, it is very attractive as energy is required only for pumping liquid. These advantages of ejectors integrated with bubble columns make their integration as a potential alternative to replace conventional devices and be used in many chemical engineering applications such as for carbon dioxide absorption from natural gas, desorption and scrubbing, gas-liquid reactions, aerobic fermentation, waste water treatment etc.

Depending upon the direction of flow of fluids, ejector-induced cocurrent bubble columns may be classified into upflow and downflow columns. Although ejector-induced cocurrent downflow bubble column gives higher residence time and gas hold-up, it has been found from previous works (Mandal et al., 2005) that downflow systems have significant disadvantage due to the limitation of handling large flow rates in the system. Therefore, ejector induced cocurrent downflow bubble columns are not suitable for high capacity processes. On the contrary, this limitation can be avoided when using upflow columns.

However, researches that provide useful knowledge in improving the design, scaling-up and optimization of ejector-induced cocurrent upflow bubble column are still relatively scanty. Hydrodynamics is one important aspect that has to be considered for the design and characterization of this equipment. Important parameters in the hydrodynamics of ejector-induced cocurrent upflow bubble column that need further investigations are fluid flow rates, pressure drop, gas hold-up and energy dissipation. Since nozzle is an indispensable part in the ejector, investigation of the effect of nozzle geometry on those hydrodynamic parameters is essential to provide a better design of ejector-induced cocurrent upflow bubble columns.

1.1 Objective of Research

Based on the discussions made in the earlier section, the hydrodynamic phenomena that occur in ejector-induced bubble column needs further investigations. Furthermore, since the nozzle is a vital part in the ejector in creating excellent gas dispersion into the liquid phase (Lapple, 1951; Das and Biswas, 2006), a study on the effect of ejector's nozzle geometry on several important hydrodynamic parameters such as gas entrainment rate, pressure drop, gas hold-up and energy dissipation is required. Therefore, the objectives of the present research work are stated as follows:

- To study the effect of nozzle geometry on hydrodynamic parameters of ejector-induced cocurrent upflow bubble column such as gas entrainment rate, pressure drop, energy dissipation and gas hold-up,
- To analyze the experimental data based on fundamental principle of fluid mechanics.

1.2 Scope of Research

This research involves the use of water, as the motive fluid, and atmospheric air, as the suction fluid, in an ejector-induced cocurrent upflow bubble column. The research activities will include the observation of pressure profiles along the column, observation of gas entrainment rate, measurement of the pressure drop, calculation of friction factor, calculation of energy dissipation, and measurement of gas hold-up, for various flow rates of motive fluid for two nozzle types with different sizes (in diameter) of nozzles. The two nozzle types that will be used in the experiments are convergent and orifice,. Moreover, mathematical models to interpret the hydrodynamics in the system will also be developed by using fundamental principles of fluid mechanics.

1.3 Thesis Overview

This thesis includes five chapters. Chapter 2 presents a critical review on the literature related to the present research. Results from previous studies on several important aspects such as pressure drop, energy dissipation and gas hold-up are presented.

Chapter 3 outlines the experimental approach used in this study on the effect of nozzle type on the hydrodynamics of ejector-induced bubble column. Details on the equipment, experimental conditions, and experimental procedures are included.

Chapter 4 presents the experimental results of this study in detail, and provides the analysis of experimental results. Comparison between the results obtained in this study and those reported in literature are also provided. Mathematical models based on the fundamental principles are developed to predict the hydrodynamics in the column.

CHAPTER 2

LITERATURE REVIEW

Ejectors have been widely used in several industrial applications such as in chemical and biochemical industries. Currently, ejectors are used as pumps, mixers, heaters, coolers, to generate vacuum, and also as bubble generators. Ejectors show important advantages over other devices because of its simplicity in operation, low capital and operating costs and the ability to mix two streams intimately (Balamurugan et al., 2008). Numerous works have been conducted to examine the performance of ejectors (Miller, 1969; Evans et al., 2001; Gamisans et al., 2003; Das and Biswas, 2006). Liquid-gas ejector is one of ejector types that have great contribution in generating efficient dispersion between liquid phase and gas phase which are the motive fluid and the suction fluid in the ejector, respectively. Design and performance characterization of a liquid-gas ejector depend highly on several aspects such as pressure drop, gas hold-up, energy dissipation, interfacial area and mass transfer coefficient.

2.1 Early Investigations on Liquid-Gas Ejector

Some of the earliest reported investigations on liquid-gas ejector used water as the motive fluid and air as the suction fluid (Hoefer, 1922; Von Pawel-Rammingen, 1936; Flugel, 1938 and Witte, 1966). Von Pawel-Rammingen (1936) found that when the suction fluid gets sucked into the suction chamber of the ejector, the gas and liquid flows are initially coaxial consisting of an annular suction fluid flow around a core of the motive fluid jet. This jet flow persists for a certain distance in the mixing throat. At a particular location, the jet flow changes into a froth flow. Beyond this location, the suction fluid is dispersed in a continuous motive fluid stream. The change from coaxial jet flow to froth flow is called "mixing shock". This phenomenon is also indicated with sudden throat pressure rise in the liquid jet ejector.

A remarkable and contributive work on flow processes in the throat and the mixing shock was done by Witte (1969). The work experimentally demonstrated high volumetric entrainment ratios by means of multiple nozzles and a relatively greater mixing shock. By

applying the momentum balance equations, Witte (1969) derived theoretical curves relating the compression ratio with the flow ratio under isothermal and adiabatic conditions. Despite providing useful knowledge on the liquid-gas ejector, these researchers have stressed solely on the throat section of the ejector.

Studies on liquid-gas ejector at the early period of its development were mostly done using horizontal type of ejectors (Bhat et al., 1972; Cunningham, 1974; and Biswas et al., 1975). They successfully examined the effect of area ratio and liquid property group on the performance of a single-jet horizontal liquid-gas ejector, and developed a mathematical model from the experimental data involving both variables and a modified Euler number. Furthermore, effort on developing a model derived from momentum and continuity equations together with an overall frictional loss coefficient was also carried out.

2.2 Effect of Nozzle Geometry on the Ejector Performance

According to Cunningham and Dopkin (1974), the location of mixing shock zone is of key importance for the ejector performance. The optimum ejector dispersion efficiency is reported to be achieved when the liquid jet breaks up just at the end of the mixing throat. If the jet disintegration occurs earlier, the flow of the homogeneous gas-liquid mixture through the remaining part of the mixing throat results in excessive frictional losses. If, on the other hand, the mixing throat is too short, the jet does not break up and accordingly the momentum transport between the phases does not occur. As a result, the ejector efficiency in such a case strongly decreases. Obviously, the occurrence of the jet break-up and the position of the mixing shock zone in the mixing throat depend generally on the liquid and entrained gas flow rates, on the pressure drop and on its geometrical parameters i.e. nozzle geometry, diameter and length of mixing throat, and opening angle of diffuser.

Among previously mentioned factors, flow rate of the motive fluid, and nozzle geometry have greater contribution in determining vacuum level developed in the suction chamber. Higher vacuum in the suction chamber means that more amount of gas phase can be sucked into the system. Consequently, the gas phase gets dispersed into the liquid phase

along its path through the mixing throat and diffuser. Numerous works have been reported in the literature in modifying the nozzle design to entrain more gas phase and create better dispersion between gas phase and liquid phase such as application of slot nozzles (Zlokarnik, 1979; Rylek and Zahradnik, 1984), nozzles with a divergent outlet (Cunningham and Dopkin, 1974) and multi-orifice nozzles (Witte, 1969; Das and Biswas, 2006). Das and Biswas (2006) carried out investigations on the nozzle loss coefficients and the entrainment rates at various suction conditions for single-orifice and multi-orifice nozzle arrangements in a downflow ejector. However, their discussions on the effect of nozzle geometry on the suction developed and gas entrainment rate is rather limited. Havelka et al. (1997) found that, in an upflow ejector, the highest values of gas entrainment rate and ejector efficiency were achieved for ejector configurations with single-orifice nozzle and with swirl body for zero length of mixing throat.

2.3 Gas Entrainment Rate in Liquid-Gas Ejector

Many researchers have developed mathematical correlations to predict the gas entrainment rate. The most common way to characterize the rate of gas entrainment is using momentum balance and mass balance equations across the ejector (Davies et al., 1967; Bhat et al. 1972; Acharjee et al., 1975; Biswas et al., 1975). The gas entrainment rate is usually correlated by dimensional analysis using dimensionless groups such as $\Delta P/\rho_G v_G^2$ (ratio of the energy supplied by the motive fluid, i.e. the pressure drop, to the momentum gained by entrained fluid), A_t/A_n (ratio of the throat area to the nozzle area), and $g\mu_L^4/\rho_L\sigma_L^3$ (related to physical properties of the motive fluid). Table 2.1 summarizes various empirical correlations for estimation of gas entrainment rate. Most of these correlations have similar form, where only the indices of various terms differ with the difference of the sizes of the nozzle and the diffuser.

Table 2.1 Empirical correlations given by various authors

Geometry and Range Investigated	**Correlation**	**Authors**
Flow – upward D_n = 0.808 – 2.676 mm, D_t/D_n = 4.75 – 15.72	$\frac{m_G}{m_L} = k\left(\frac{\mu_L}{D_n \rho_L v_L}\right)^{0.76} (A_r)^{0.4} \left(\frac{g\mu_L^4}{\rho_L \sigma_L^3}\right)^{-0.04} \left(\frac{\rho_L - \rho_M}{\rho_M}\right)^{0.63}$	Davies et al. (1967)
Flow – horizontal D_n = 1.9 – 4.49 mm, D_t/D_n = 2.06 – 4.87	$\frac{m_G}{m_L} = 8.5\times10^{-2} \left(\frac{\Delta P}{\rho_G v_G}\right)^{-0.3} (A_r)^{0.46} \left(\frac{g\mu_L^4}{\rho_L \sigma_L^3}\right)^{-0.02}$	Bhat et al. (1972)
Flow – upward D_n = 1.7 – 5.5 mm, D_t/D_n = 2.31 – 7.13	$\frac{m_G}{m_L} = 5.2\times10^{-4} \left(\frac{\Delta P}{\rho_G v_G}\right)^{-0.305} (A_r)^{0.68} \left(\frac{g\mu_L^4}{\rho_L \sigma_L^3}\right)^{-0.305}$	Acharjee et al. (1975)

Another method which is being intensely recently developed to predict entrainment rate of suction fluid in an ejector is using Computational Fluid Dynamics (CFD) simulation. Work on CFD to predict entrainment of suction fluid in an upflow gas-liquid ejector has been reported by Balamurugan et al. (2008). They have shown good agreement between liquid entrainment rate values obtained experimentally by Davies et al. (1967) with the liquid entrainment rate values predicted using their CFD simulation. In the present work, prediction of gas entrainment rate has been done using mathematical model developed from fundamental principle of fluid mechanics since it offers simplicity in calculations and also gives reliable results.

2.4 Pressure Drop in Ejector-Induced Bubble Column

Pressure drop in the ejector is an important design parameter to indicate the performance of an ejector-induced bubble column. The knowledge of pressure drop helps in modeling the system as it forms the basis of assessment of equipment performance. In liquid-gas ejector-induced bubble column, pressure drop is a key indicator to know the amount of energy being consumed to create intense contact between the gas phase and the liquid phase. There are three factors that are responsible for pressure changes in the system i.e.: pressure change due to the hydrostatic head, acceleration and irreversible losses which include pressure loss due to friction and dispersion between two phases.

Considerable research efforts have been carried out by previous researchers on the study of pressure drop in ejector-induced bubble columns. Radhakrishnan and Mitra (1984) studied frictional pressure drop in an ejector-induced cocurrent upflow bubble column with multi-orifice nozzles. Water-air system was used in the pressure drop experiment. Total pressure drop in the system was measured experimentally from the reading in manometers placed along the column. It was observed that total pressure drop decreases with the increase of air flow rate due to the increase in air hold-up and consequent reduction in hydrostatic head. An attempt to predict two-phase friction factor by correlating it with several variables like liquid flow rate, area ratio and number of nozzles was also carried out by dimensional analysis.

Cramers and Beenackers (2000) studied the pressure drop in a downflow liquid-gas ejector with the presence of a swirl device in the upstream section of the nozzle. They discovered that ejector with swirl devices gives higher gas phase pressure drop for the same gas to liquid volumetric ratio than other devices. In other words, more energy is used for gas compression instead of for gas dispersion when using swirl device in the ejector.

Quite similar to findings of Radhakrishnan and Mitra (1984) who conducted experiments in an ejector-induced cocurrent upflow bubble column, Mandal et al. (2005) performed experimental study on pressure drop in an ejector-induced cocurrent downflow bubble column with a single nozzle. They found out that frictional pressure drop increased with increasing gas flow rate at constant liquid flow rate. The increase in pressure drop occurs due to the fact that an increase of gas flow rate causes greater air entrainment into the system or higher population of gas bubbles, which consequently increases the true liquid velocity. Work on downflow column have also been conducted by several other researchers such as Kandakure et al. (2005), and Das and Biswas (2006). Both workshowed that pressure drop in the downflow ejector system decreased with the increase in area of throat to nozzle. Kandakure et al. (2005) also showed that the air entrainment rate can be correlated with the pressure drop between the air entry line and the throat exit. They found out that the pressure drop between the air entry and the throat exit is proportional to the power of 1.5 of the air entrainment rate.

Efforts on modeling the pressure drop in ejector-induced bubble column have also been reported. Recently, Majumder et al. (2006) formulated a theoretical model to predict pressure drop for gas-liquid dispersion in an ejector-induced cocurrent downflow bubble column. The model uses the knowledge of single phase pressure drop to predict the two phase pressure drop. The effect of bubble formation and two-phase interfacial friction was taken into account in this model.

2.4.1 Frictional pressure drop and friction factor in Ejector-Induced Bubble Column

Unlike in horizontal two-phase flow, the frictional pressure drop in vertical flow systems cannot be directly obtained because the measured pressure drop is the sum of the frictional pressure drop and the column hydrostatic head. The column hydrostatic head or potential energy component depends on the insitu mixture density which in turn is a function of gas hold-up. For determining the frictional component from the total pressure drop, two methods of analysis have been used.

In the first method, the two-phase mixture is assumed to be homogeneous so that the frictional pressure drop may be obtained from the following equation,

$$\frac{\Delta P_T}{g\,z} = \frac{m_L + m_G}{Q_L + Q_G} + \frac{\Delta P_F}{g\,z} \tag{2.1}$$

which relates the total pressure, hydrostatic head, and the frictional pressure drop. Many workers, notably, Govier et al., (1957), Baxendell and Thomas (1961), Hughmark and Pressburg (1961) and Hagedorn and Brown (1964) have used this method for calculating the frictional pressure drop.

In the second method of analysis, the frictional pressure drop is calculated from the total pressure drop using estimated insitu two-phase density as expressed by the following equation:

$$\frac{\Delta P_T}{\rho_L g\,z} = \left[\rho_G \varepsilon_G + \rho_L (1-\varepsilon_G)\right] + \frac{\Delta P_F}{\rho_L g\,z} \tag{2.2}$$

This method has been used by Griffith and Wallis (1961), Ros (1961), and Hagedorn and Brown (1965).

In the present work, an ejector-induced upflow bubble column has been used and the studies have been made in the bubble flow regime, and therefore, the assumption that the mixture is homogeneous will be justified. Hence, the first approach for calculating the frictional pressure drop component from the total pressure drop has been adopted.

A mechanical energy balance over the column neglecting the kinetic energy term leads to,

$$\frac{\Delta P_T}{\rho_L g\, z} = \frac{m_L + m_G}{Q_L + Q_G}\frac{1}{\rho_L} + \frac{\Delta P_F}{\rho_L g\, z} \tag{2.3}$$

where the first term on the right hand side is the potential energy term and the second term is due to the irreversibilities which include, beside frictional loss, the contribution due to the gas-liquid slip. Equation (2.3) can be rewritten as,

$$\frac{\Delta P_T}{\rho_L g\, z} = \frac{1 + R_m}{1 + \varphi_m} + \frac{\Delta P_F}{\rho_L g\, z} \tag{2.4}$$

Based on thermodynamic analysis Govier et al. (1957) obtained an expression for the total pressure drop for the two-phase flow in a vertical column as,

$$\frac{\Delta P_T}{\rho_L g\, z} = \frac{1 + R_m}{1 + \varphi_m} + \frac{1}{1 + \varphi_m}\left[\frac{\Delta F}{\rho_L g\, z}\right]_L \tag{2.5}$$

where the second term on the right hand side is the irreversibility component for two-phase vertical flow. On comparing Equations (2.4) and (2.5) we get,

$$\left[\frac{\Delta F}{\rho_L g\, z}\right] = (1 + \varphi_m)\frac{\Delta P_F}{\rho_L g\, z}_L \tag{2.6}$$

In the limiting case with no gas flow $R_m = \phi_m = 0$, Equation (2.5) reduces into,

$$\frac{\Delta P_T}{\rho_L g z} = 1 + \frac{\Delta F}{\rho_L g z} = 1 + \frac{\Delta P_F}{\rho_L g z} \tag{2.7}$$

Equation (2.7) represents the mechanical energy balance for the vertical flow of liquid. In Equation (2.7), the term $\frac{\Delta F}{\rho_L g z}$ is the same as frictional pressure drop per unit height of the column due to single-phase liquid flow, and therefore may be expressed as,

$$\frac{\Delta F}{\rho_L g z} = \frac{2 f u_L^{\,2}}{D_c g} \tag{2.8}$$

where f is the Fanning friction factor. Similarly, for two-phase flow a friction factor f_m may be defined based on liquid superficial velocity by the following equation:

$$\frac{\Delta F}{\rho_L g z} = \frac{2 f_m v_L^{\,2}}{D_c g} \tag{2.9}$$

Combining Equations (2.6) and (2.9) we get,

$$f_m = (1 + \varphi_m) \frac{\Delta P_F}{\rho_L g z_L} \frac{D_c g}{2 v_L^{\,2}} \tag{2.10}$$

Equation (2.10) defines the two-phase friction factor f_m based on superficial velocity. The two-phase friction factor f_m will be a function of primary variables of the system.

2.5 Energy Dissipation in Ejector-Induced Bubble Column

The kinetic energy in an ejector is caused by the motive fluid of high pressure that flows through the nozzle. This energy is partly converted into useful work by increase in the pressure energy associated with the motive and suction streams. The difference between the input energy and the useful work is the energy lost as irreversible losses. The irreversible losses are made up of the frictional losses and the energy loss associated with jet expansion and mixing. It is the energy utilized for jet expansion and mixing which is

of importance in gas-liquid contacting. The higher this energy is the better the dispersion and the higher the interfacial area. It is therefore necessary to know the amount of energy dissipated in the system to determine the interfacial area and mass transfer coefficient.

Basically, energy dissipation can be calculated using the pressure drop information as expressed in Equation (2.11) (Havelka et al., 1997)

$$E_D = \Delta P\, Q_L \tag{2.11}$$

Cunningham (1974), and Cunningham and Dopkin (1974) have developed equations to model the momentum transfer and pressure recovery in ejectors. They have presented momentum balance equations for the throat and diffuser section. The losses in the nozzle, throat and diffuser were accounted for by the three loss coefficients for each section. These coefficients represent the fraction of the jet momentum which is lost as irreversible losses. The mathematical expression to calculate the energy dissipated in the ejector developed is given in Equation (2.12) as follows,

$$E_D = Q_L H(K_n + K_{th} + K_{di}) \tag{2.12}$$

where H is the jet velocity head given by $\rho_L v_L^2/2$. Values for the loss coefficients have been presented by Cunningham (1974). For well-designed square edged nozzles, the nozzle coefficient can be taken as zero (Cunningham, 1974). Cunningham (1974) recommends throat loss coefficients K_{th} values in the range of 0.32 to 0.46 and diffuser loss coefficient K_{di} values of 0.26 to 0.35. The model presented by Cunningham (1974) was for ejectors used as liquid jet pumps for gas compression. As such their gas/liquid flow ratio did not exceed a value of 1.6. In this range of flow ratio the throat loss coefficient was essentially constant with value of about 0.4. This method has also successfully been applied by Evans et al. (2001) in a confined plunging liquid jet bubble column.

In gas-liquid dispersion, a part of energy is lost as friction and only the remaining energy is used for jet expansion and interfacial area generation. The frictional losses are one

order of magnitude smaller and hence the energy used for mixing can be approximately taken to be equal to the total energy dissipated in the system.

A different approach in calculating energy dissipation in the ejector has been performed by Cramers and Beenackers (2000). According to them, the energy dissipation rate effectively used for gas dispersion can be calculated as

$$E_D = E_j - E_c \tag{2.13}$$

where E_j is the energy supplied by a high velocity jet which is a function of liquid flow rate and jet velocity at nozzle exit, and E_c is the energy consumed for compressing gas phase which is a function of gas phase pressure drop and gas flow rate.

2.6 Gas Hold-Up in Ejector-Induced Bubble Column

Gas hold-up or voidage, which is the fraction of two-phase mixture occupied by the gas phase, is one of most frequent properties measured in a two-phase flow. It is an important property for design purposes, both because of its direct influence on column size and because it is indirectly related to the gas-liquid surface area and hence to mass transfer. Gas hold-up information also facilitates the determination of the flow regime inside the system (such as homogeneous, heterogeneous or transition regime) for a given set of operating conditions.

2.6.1 Gas hold-up measurement techniques

The measurement of two-phase system parameters like gas hold-up is of inevitable importance for interpreting, understanding and predicting the overall performance of the equipment. Several techniques exist to measure gas hold-up either globally or as a function of position in a two-phase flow system. The simplest method is using flow isolation technique which is done by noting change in dispersion height due to the presence of gas bubbles. According to flow isolation technique, when a steady state condition was reached, the total height of the gas-liquid mixture was noted. Then all the

inlet valves were shut simultaneously. This causes an immediate termination of the flow of both fluids. When the gas-liquid mixture inside the column got arrested, the liquid phase was allowed to settle down whereby all the gases got separated. The clear liquid height inside the column was then noted. Using the information of total mixture height (h_t) and clear liquid height (h_l) in the column and assuming that the fluids behave as a homogeneous mixture, overall gas hold-up (ε_G) in the column can be calculated from the following equation

$$\varepsilon_G = \frac{h_t - h_l}{h_t} \tag{2.14}$$

Due to its simplicity and reliability, this method has been applied by many authors in their works such as Radhakrishnan and Mitra (1984), Kundu et al. (1995), Havelka et al. (1997), Zahradnik et al. (1997), Evans et al. (2001), Mandal et al. (2002 and 2005) etc. However, this method is only applied well in a transparent system where liquid height is clearly visible and the presence of foam in the system might lead to significant errors in the measurement.

Measuring the pressure difference between two levels in a column is another method to calculate gas hold-up. This method was firstly applied by Hills (1976) with an air lift reactor and more detail works was conducted by Tang et al. (2006) in a cocurrent bubble column. Nevertheless, gas hold-up measurement via pressure difference can lead into problematic issue in condition where the pressure tappings experience fouling. Another way in measuring gas hold-up is using probe techniques, using conductivity measurement (Kocamustafaogullari et al., 1994; Sun et al., 2005) or optical measurement (Schweitzer et al., 2001). But then again, these methods can be subject to fouling which consequently would provide inaccurate measurement. More sophisticated methods using Gamma Ray tomography and laser-based equipments have become recent trends in measuring gas hold-up in a two-phase flow system (Deshpande et al., 2000; Kulkarni et al., 2001; Patel et al., 2008). However, these measurement techniques involve expensive devices with complex operating procedures and safety precautions.

In this present work, gas hold-up measurement using flow isolation technique has been chosen due to its simplicity and ability to give accurate measurement. Possible drawbacks like foaming presence can be eliminated since experimental setup in this research only involves mixture of air and water. Moreover, compared to radiation attenuation and laser-based techniques, this technique is much safer.

2.6.2 Gas hold-up modeling techniques

Gas hold-up modeling in two-phase cocurrent flow has been investigated by a number of researchers. In most of these studies, the experimental data has been correlated on the basis of one of the following models.

2.6.2.1 Homogeneous flow model

In the homogeneous flow model it is assumed that the fluids behave as homogeneous mixture. Therefore, the velocity of the two phases is the same and the mixture density can be calculated from the input mass and volumetric flow rates. These assumptions permit the application of the mechanical and total energy relations to the two-phase mixture for calculating the gas hold-up from the inlet volumetric flow rates by the following relationship:

$$\varepsilon_G = \frac{Q_G}{Q_G + Q_L} \tag{2.15}$$

Isbin et al. (1957) showed that the homogeneous model can be successfully used for the prediction of gas hold-up in situations where the pressure losses are relatively small and the two-phase system can be considered as a pseudo-homogeneous mixture.

2.6.2.2 Variable density model

The effect of the non-uniformity in bubble concentration with radial position on the hold-up has been considered by several workers. Armand (1946) and Bankoff (1960) suggested that the bubble concentration is not flat but the concentration of bubbles is higher at the axis and decreases radially. Also, it is assumed that there is no velocity slip between the liquid phase and the gas phase but there is more gas in the centre region where the velocity is high. Therefore, the cross-sectional average gas velocity would be higher than the cross-sectional average liquid velocity. By assuming a power law distribution for both the velocity and bubble concentration profiles in the radial direction, Bankoff (1960) arrived at the following relationship between the fractional gas hold-up and the input flow rates,

$$\varepsilon_G = K \frac{Q_G}{Q_G + Q_L} \tag{2.16}$$

where the Bankoff factor, K, is related to the input and insitu volume fractions. Zuber and Findlay (1965) has considered the effect of both local and relative velocities and the concentration gradient on the insitu hold-up and derived a general relationship for the hold-up. The variable density model has been found to be valid for two-phase flow when both the phases enter the system at almost equal velocities.

2.6.2.3 Momentum exchange model

Prediction of gas hold-up in two-phase horizontal flow by a momentum exchange model has been proposed by Levy (1966). The model was based on the hypothesis that when the frictional and hydrostatic head losses in the two-phases are equal, there would be a rapid exchange of momentum between the two-phases for maintaining an equilibrium condition. On the basis of this assumption the following relationship for gas hold-up was reported:

$$\frac{1}{\varepsilon_G (1+R_m)^2} + \frac{1}{\varepsilon_G (1+R_m)} \frac{\rho_L}{\rho_G} = \frac{1}{2(1-\varepsilon_G)^2 (1+R_m)^2} \tag{2.17}$$

This model has been found to give reasonably good agreement with experimental data only in horizontal flow with high voidage.

2.6.2.4 Slip velocity model

The slip velocity model was developed on the consideration that the buoyancy in two-phase vertical flow will tend to accelerate the lighter phase, and therefore, there will be local slip between the phases. Behringer (1936) proposed a model taking this local slip into consideration but neglecting the effect of radial concentration and velocity profiles. The Zuber and Findlay (1965) drift flux model is widely recommended for modeling of gas hold-up in two-phase flow columns. This model takes into account the effect of non-uniform flow and gas hold-up as well as the effect of local relative velocity between the two phases. The model suggested by Zuber and Findlay (1965) has been applied by several researchers in their works to analyze the gas hold-up data in two-phase flow in simple pipeline contactors. Chandrakar et al. (1985) has successfully applied this model for the analysis of gas hold-up in an ejector-induced upflow with air-carboxy methyl cellulose (CMC) mixture. Ohkawa et al. (1986) have also used the model in a downflow bubble column with plunging jet water system. Gas hold-up analysis using drift-flux model is done by plotting the average gas velocity, $\bar{v}_G$, against the gas-liquid mixture velocity, v_M ($v_{SG} + v_{SL}$), as shown in the following equation

$$\bar{v}_G = \frac{v_{SG}}{\varepsilon_G} = C_o v_M + v_D \qquad (2.18)$$

where C_o is called the distribution parameter, which accounts for effect of non-uniform flow (for a uniform radial gas hold-up profile, $C_o = 1$; for a centre peaked radial gas hold-up profile, $C_o > 1$) and concentration profiles and v_D is called the weighted average drift velocity which indicates the effect of the local relative velocity. The value of the distribution parameter has been obtained from the slope of the plot, whereas the intercept was interpreted as the weighted average drift velocity.

2.6.2.5 Lockhart-Martinelli model

Lockhart and Martinelli (1949) developed correlations for predicting the hold-up in horizontal cocurrent flow of gas-liquid mixtures. They presented correlations for the hold-up in terms of pressure drop in each phase. To apply the method, each phase's pressure drop is calculated as though it alone was in the line. Then the Lockhart-Martinelli parameter, X, is calculated as

$$X = \sqrt{\frac{\Delta P_G}{\Delta P_L}} \tag{2.19}$$

The X factor is then related to either ϵ_L or ϵ_G. Whichever one is chosen is multiplied by its companion pressure drop to obtain the total pressure drop. The following equation is based on points taken from ϵ_L or ϵ_G curves in Perry and Green (1999) for both phases in turbulent flow (the most common case).

$$\varepsilon_L = 4.6X^{-1.78} + 12.5X^{-0.68} + 0.65 \tag{2.20}$$

$$\varepsilon_G = X^2 \varepsilon_L \tag{2.21}$$

The X range for Lockhart-Martinelli curves is 0.01 to 100.

Besides, many other investigators have also proposed empirical and semi-empirical correlations for gas hold-up which are valid under different operating conditions (Otake et al., 1982; Zahradnik et al., 1982; Ogawa et al., 1983; Radhakrishnan and Mitra, 1984; Rylek et al., 1984; Bhutada et al., 1987; Cramers et al., 1992; Kundu et al., 1995; Zahradnik et al., 1997 and Majumder et al., 2006).

2.7 Summary

From the review of the literature, it can be observed that gas dispersion technology has been studied and developed from the simplest kind of experiments to more complex

researches with more improved and meticulous methodology. Liquid-gas ejectors are being vastly utilized in many researches and industrial applications for gas-liquid dispersion, mixing, mass and heat transfer operation, etc. because of the simple construction with no mechanically moving parts, large interfacial area generation and intense mixing between the phases. Moreover, such devices can be used to handle chemical reactions as they combine the functions of flow inducing devices and mixing reactors. However, detail knowledge of how to make a system consisting liquid-gas ejector fitted with an upflow bubble column becomes a highly efficient gas-liquid contactor is still felt essential. Therefore, understanding one of its important physical parameters like nozzle geometry on several vital aspects of the performance of ejector-induced bubble column such as pressure drop, energy dissipation and gas hold-up would be of considerable interest.

CHAPTER 3

RESEARCH METHODOLOGY

3.1 Introduction

This research work is mainly divided into five major activities. They include observation of pressure profiles and gas entrainment rate, measurement of pressure drop, calculation of energy dissipation and measurement of gas hold-up in ejector-induced cocurrent upflow bubble column. The experimental setup used in this study is described in Section 3.2. Experiments have been carried out using water and air as motive fluid and suction fluid in the ejector, respectively. In this present work, experiments have been conducted for different nozzle geometries and sizes with variations in water flow rate for each nozzle.

In order to understand the flow behavior in the ejector and bubble column, pressure profiles have been observed by means of pressure transducers mounted along the axial position of the column. Moreover, since pressure drop is one of important factors in designing and optimizing gas-liquid contactors, its measurement is necessary. The values of pressure drop have been determined from the readings on the pressure transducers. These pressure drop information can be used to calculate energy dissipation in the column to know the amount of energy that has been consumed for gas dispersion into liquid phase.

The gas fraction in the mixture in the column can be determined from the measurement of gas hold-up. Gas hold-up has been measured using flow isolation technique by switching off all inlet valves simultaneously. Analysis of experimental gas hold-up data using model developed by Zuber-Findlay (1965) have also been performed. The outline of these research activities is presented in a flow diagram as shown in Figure 3.1.

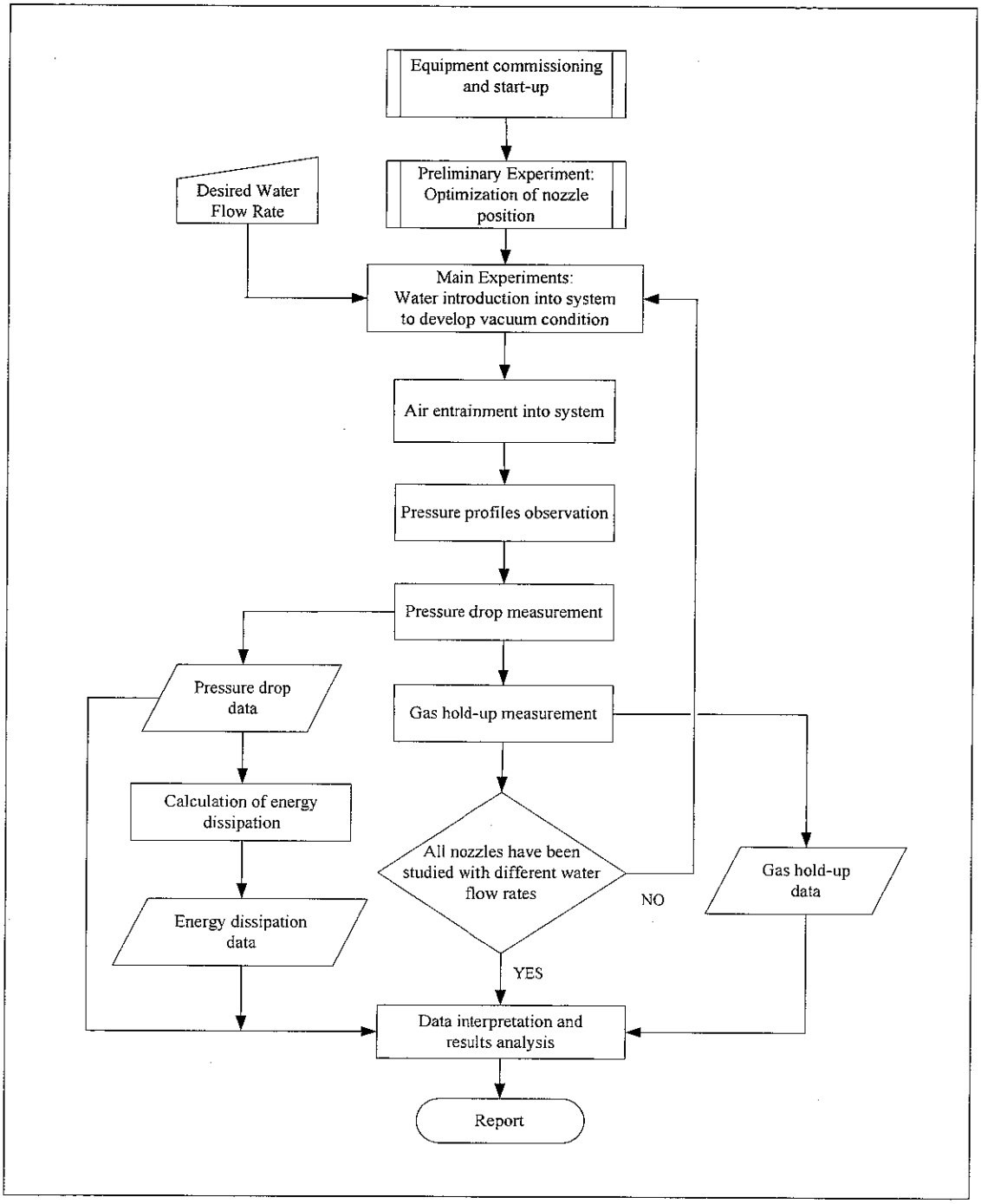

Figure 3.1. Research flow diagram

3.2. Experimental Setup

The schematic diagram of the experimental set up is shown in Figure 3.2. The apparatus consists of an ejector E, a bubble column C, and a gas-liquid separator SE, mounted vertically on a slotted-angle frame work. Water, the motive fluid, is pumped into the

system from the reservoir T, by the centrifugal pump P. Water enters the system through the water entrance line WE. The water flow rate to the ejector is controlled by adjusting the globe valves V-64 and V-66 in the bypass line and in the ejector inlet, respectively. The flow rate, temperature and pressure of the liquid are measured by magnetic flow meter FI-14a, J type thermocouple TI-03, and pressure transducer PI-04, respectively. Air, the suction fluid, is sucked into the suction chamber from the surroundings through air inlet line AE due to the vacuum generated in the ejector. The air flow rate is measured by rotameter FI-12. Pressure readings at nine positions along the axis of the column are measured by pressure transducers PI-06 to PI-15.

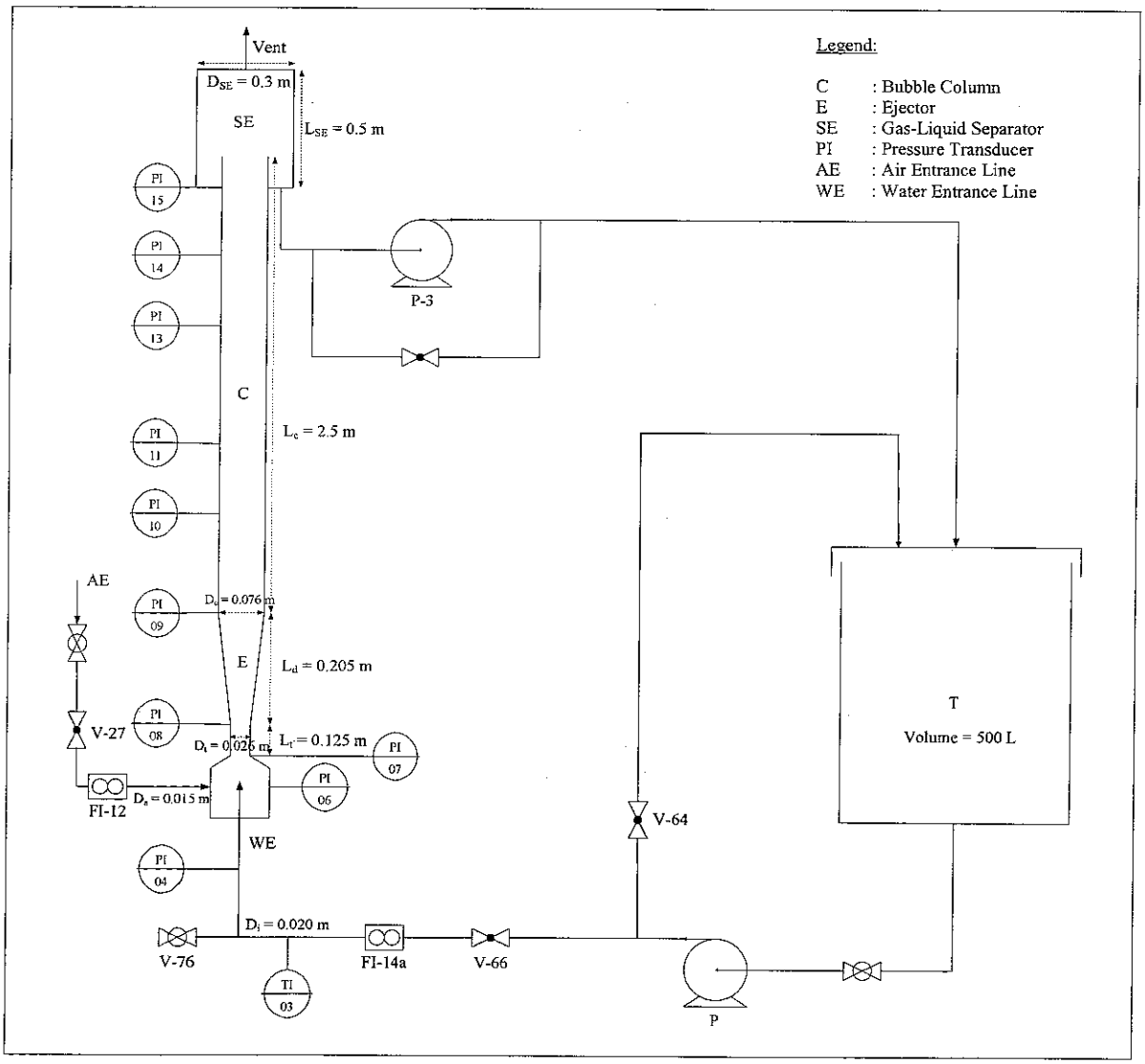

Figure 3.2. Schematic diagram of ejector-induced bubble column experimental setup

Figure 3.3 shows a sectional drawing of ejector-induced cocurrent upflow bubble column, which consists of nozzle, suction chamber, throat, diffuser, bubble column and gas-liquid separator. The column is fabricated from transparent borosilicate glass, to enable visual observation of the process. The nozzle is fixed on a long hollow spindle fitted through the bottom of the suction chamber. The spindle could be moved axially by a screw arrangement, thus permitting accurate adjustment of the distance between the nozzle tip and the throat entry. A checknut is used to secure the spindle to the suction chamber. The suction fluid, air, enters the suction chamber through an inlet line located at its side.

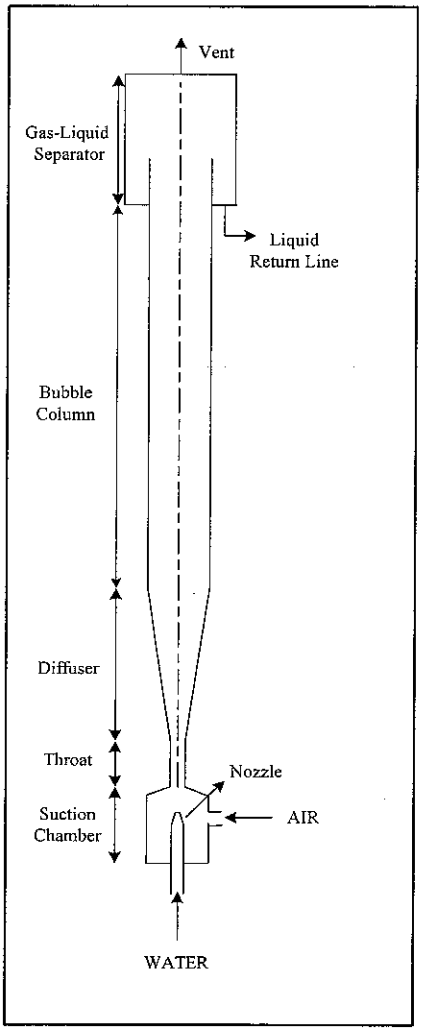

Figure 3.3. Sectional drawing of ejector-bubble column assembly

The section of the assembly consisting of throat, diffuser and bubble column has been fabricated as a single piece using borosilicate glass. The various parts of experimental setup are designed on the basis of standard dimensions recommended for optimum performance as discussed below.

a. Throat

Earlier investigators such as Smith (1951) and Lapple (1956) have shown that ejectors with parallel throat give better performance compared to those with a convergent-divergent section. According to Lapple (1956), to insure perfect mixing between the two phases, the ratio of throat length (L_t) to throat diameter (D_t) should be in range of 4 to 10. In the present investigation, a parallel throat with diameter of 26 mm and length of 125 mm has been used, giving a L_t/D_t ratio of 4.9.

b. Diffuser

A divergent section after the parallel throat decelerates the fluid and thus recovers the fluid pressure. It has been reported by Smith (1951) that a diffuser with an angle of 5 to 7 degree gives the maximum pressure recovery. In the present study a diffuser angle of 7 degrees with 205 mm length has been used.

c. Nozzle

In the present study, convergent and orifice nozzles, as shown in Figure 3.4, in various sizes have been employed. These types of nozzle are much simpler to fabricate compared to convergent-divergent nozzle. The dimensions of the different nozzle used in this study are shown in Table 3.1.

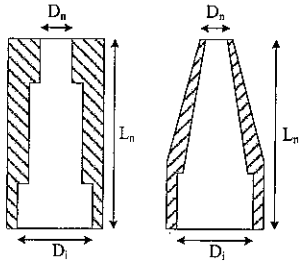

(a) (b)

Figure 3.4. Detail drawing of nozzle construction
(a) Orifice and (b) Convergent

Table 3.1. Sizes of nozzles

Type	Nozzle Inlet Diameter, D_i, mm	Nozzle Diameter, D_n, mm	Nozzle Length, L_n, mm
Convergent	20	6	37.5
	20	8	34.5
	20	10	31.5
Orifice	20	6	40
	20	8	40

d. Bubble column C

The bubble column is a cylindrical pipe of 76 mm in diameter and 2500 mm height. The upper end of the bubble column is projected into the gas-liquid separator, with the column end about 250 mm inside the separator. The column is fitted with nine pressure transducers along the axis of the column for measuring the pressure drop across the system. The locations of the pressure transducers are given in Table 3.2 (refer to Figure 3.2 for equipment identification).

Table 3.2. Distance of pressure transducers from the air inlet line

Pressure Transducers	Distance from air inlet line, mm
PI-06	0
PI-07	90
PI-08	250
PI-09	540
PI-10	1150
PI-11	1560
PI-13	2160
PI-14	2560
PI-15	2960

e. Gas-liquid separator SE

A cylindrical vessel made of stainless steel of 300 mm in diameter and 500 mm height is used as gas-liquid separator at the top of the column. The separator is

also provided with a gas vent, liquid outlet and liquid level indicator. The liquid level in the separator is controlled well below the top of the bubble column to ensure the accuracy of measurements in gas holdup. The level is controlled in a close range by an ON/OFF controller which activates a pump at the liquid outlet line.

f. Liquid feed pump P

Liquid feed pump P is used to deliver water as the motive fluid to the column at high flow and pressure. Liquid feed pump P is a vertical multi-stage centrifugal pump with capacity of 400 L/min, maximum head of 230 m, power of 15 kW, and made of stainless steel.

g. Suction pump P-3

Suction pump P-3 is used to transfer water as the motive fluid from the gas-liquid separator SE to the water storage tank T. Suction pump (P-3) is a centrifugal pump with capacity of 250 L/min, maximum head of 23 m, power of 65 W, and made of stainless steel.

The important dimensions of the ejector-induced bubble column are summarized in Table 3.3 (refer to Figure 3.2 for equipment identification).

Table 3.3. Dimensions of the ejector-bubble column assembly

Description	Dimension (m)
Height of the suction chamber, H_s	0.120
Diameter of suction chamber, D_s	0.060
Diameter of throat, D_t	0.026
Length of throat, L_t	0.125
Length of diffuser, L_d	0.205
Diameter of bubble column, D_c	0.076
Diameter of water inlet line (nozzle upstream), D_i	0.020
Diameter of gas inlet, D_a	0.015
Length of bubble column	2.5
Diameter of nozzle used, D_n	0.006, 0.008, 0.010

3.3 Experimental Procedure

3.3.1 Equipment start-up procedures

Tank T is filled with water initially before starting any experiments (refer to Figure 3.2 for equipment identification). Water is pumped through the nozzle using the high-pressure centrifugal pump P with the air inlet line closed. Water flow rate for all experiments has been selected such that an appreciable vacuum is developed in the suction chamber. The desired water flow rate is maintained by adjusting the bypass valve V-64 and the globe valve V-66 in the water inlet. After the water flow had stabilized and vacuum condition is developed, air is admitted into the system by fully opening the air inlet valve V-27. Under the action of water jet, the air is sucked into the suction chamber and dispersed into fine bubbles, and a bubbly two-phase flow is established in the ejector throat, diffuser and bubble column. After allowing 5 minutes for the establishment of steady state conditions, which is shown by stable bubble flow in the system, flow rates and pressure transducer readings are noted. To ensure the correctness of the readings and to detect any malfunctioning of the instruments, the data are noted at three different times with steady-state conditions.

3.3.2 Preliminary experiments

When water at high pressure is pumped through the nozzle, vacuum is generated in the suction chamber. The vacuum level generated varies with the position of the tip of the nozzle with respect to the throat inlet. The position also differs for different nozzle types and dimensions. Preliminary experiments are performed to determine the optimum nozzle position for each nozzle for generating the maximum vacuum as explained below. Distance between the nozzle tip and the throat entry (z_{nt}) is varied by referring the chamber base as the zero-point. Then, water is introduced into the system with a constant flow rate for each nozzle type and distance variation. The vacuum level developed in the suction chamber is then measured using PI-06. The heights of nozzle tip from the chamber base are varied within range 1 – 11 cm. By plotting the suction pressure against the height of nozzle tip from the chamber base (h_n), the position at which the maximum vacuum occurs can be observed (refer to Figure B.1 and B.2 in Appendix B). All other

experiments are conducted with the nozzle fixed at this optimum position. Moreover, in order to ensure the accuracy and reproducibility of the results, the preliminary experiment is repeated three times. Figure 3.5 shows the schematic drawing of important sections in this preliminary experiment while Table 3.4 presents the obtained optimum position for each nozzle by taking the chamber base as the zero reference of nozzle height in the suction chamber.

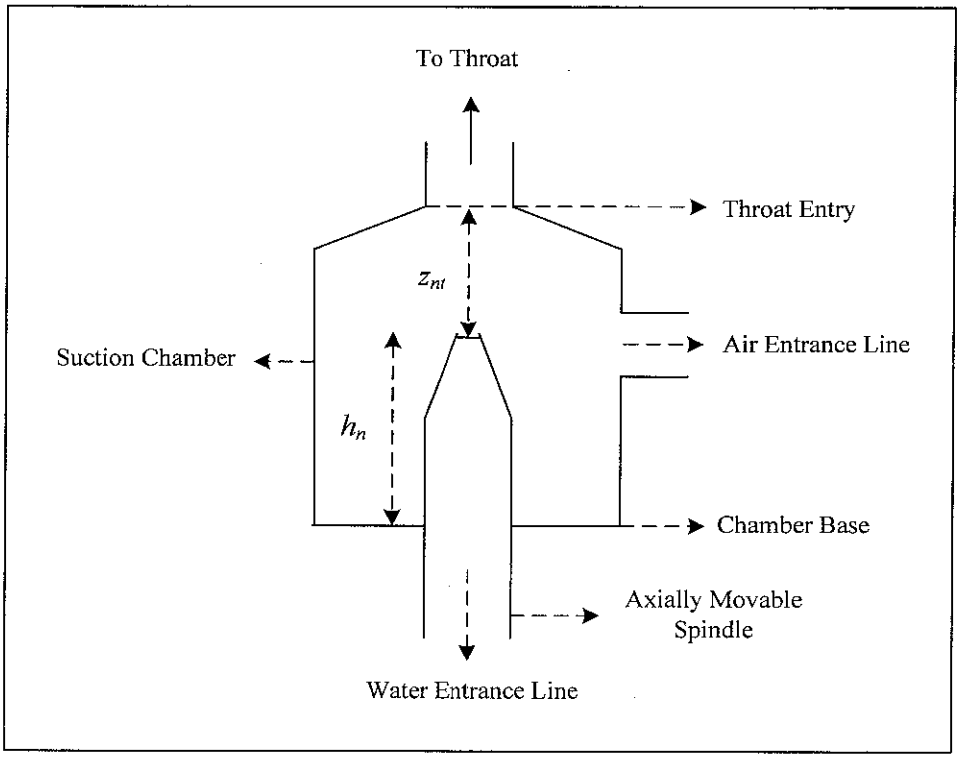

Figure 3.5 Schematic drawing of important sections in preliminary experiments

Table 3.4 Optimum position of nozzle in the suction chamber

Nozzle	**Nozzle height from chamber base (h_n), cm**
Convergent Nozzle 6 mm (NC6)	4.0
Convergent Nozzle 8 mm (NC8)	6.0
Convergent Nozzle 10 mm (NC10)	9.0
Orifice Nozzle 6 mm (NO6)	8.0
Orifice Nozzle 8 mm (NO8)	9.0

3.3.3 Pressure drop measurement

Pressure drop experiments have been carried out at maximum entrained air flow rate given by different water flow rates and conducted under steady conditions of flow. The water flow rates that have been used in the experiments extend within range 0.00058 – 0.00251 m^3/s. Pressure at any axial position in the column is measured using pressure transducers with a measurement range 0 – 4.5000 bar-a with an accuracy ± 0.0001 of the range that correspond to a linear velocity in the column. After the flow has reached steady condition, pressure readings from each pressure transducers along the axial position of the column are noted. Three repeated runs have been taken to ensure accuracy and reproducibility in the measurements. Nozzle pressure drop have been obtained by subtracting readings of PI-06 from PI-04; while the ejector pressure drop is achieved from PI-09 and PI-06 (refer to Figure 3.2). Total pressure drop in the system have been calculated as a difference between the readings of PI-06 and PI-15.

3.3.4 Gas hold-up measurement

The overall gas hold-up for the system have been measured by flow isolation technique as reported in literature Radhakrishnan et al., (1984); Kundu et al., (1995); Mandal et al., (2005). The column is equipped with a volumetric scale starting from the top section to the bottom section of the column. After the flow of gas and liquid in the column has attained a steady condition, the total volume of gas-liquid mixture is noted. Then, the system is isolated completely by closing the liquid inlet and gas inlet valves simultaneously. The gas-liquid mixture inside the column gets arrested and is allowed to settle for some time whereby the gas gets separated. The volume of the unoccupied space inside the column is then noted. Using the information of volume of total mixture and unoccupied space in the column, fractional gas hold-up (ε_G) can be calculated using the Equation (3.1). Three repeated runs have been carried out to avoid error caused by a time delay between the closures of liquid and gas inlet valves.

$$\varepsilon_G = \frac{V_G}{V_T} \tag{3.1}$$

3.3.5 Shut down procedures

The procedures to shut down the system after doing experiments are as follow:

1. Close the air inlet valve V-27
2. Close all connecting valves at the pressure transducers to avoid damage that might occur due to hydrostatic pressure
3. Reduce the water flow rate into the system by opening bypass valve V-64 and after that pump P can be switched off
4. Pump P-3 is automatically switched off according to the level in the gas-liquid separator SE
5. Allow water to drain from gas-liquid separator SE into reservoir T
6. Drain all remaining water in the column by opening valve V-76
7. Switch off the control panel

3.3.6 Changing and aligning the nozzles

Vertical alignment of the nozzle is important to ensure that the jet flow of the motive fluid comes out from the nozzle in a straight line. Moreover, alignment of the nozzle is also crucial in determining the highest vacuum level in the suction chamber as discussed in Section 3.3.2. There are several steps that need to be carried out in changing and aligning nozzles which can be described as follows:

1. Before changing the nozzle at the ejector-induced cocurrent upflow bubble column, water must be fully drained out from the system. Air is released to the atmosphere from the vent line, while water is flushed out by opening valve V-76
2. Loosen the cap holding the nozzle assembly at the bottom of the ejector and pull out the assembly
3. Unscrew the original nozzle from the assembly and attach the new nozzle
4. Reinsert the nozzle assembly into the ejector
5. Adjust the desired nozzle height in the ejector
6. Tighten the cap holding the nozzle and make sure that the spindle position is not inclined

3.4 Data Processing

3.4.1 Pressure drop

Data processing for pressure drop measurement for each nozzle is carried out by tabulating all the experimental data according to Table 3.5. Air entrainment rate (Q_G) for each water flow rate (Q_L) is measured using rotameter FI-12 (refer to Figure 3.2). Pressure readings from all transducers are noted and the pressure drop in the ejector and total system can be subsequently determined.

Table 3.5 Data table for pressure drop measurement

Q_L	Q_G	$Q_M = Q_L + Q_G$	PI-04	PI-06	PI-...	PI-15	ΔP_e	ΔP_T
m^3/s	m^3/s	m^3/s	Pa	Pa	Pa	Pa	Pa	Pa
Q_{L1}								
Q_{L2}								
Q_{Ln}								

3.4.2 Friction factor

Calculation of frictional pressure drop and friction factor is carried out by assuming that the water-air mixture inside the system is homogeneous. Therefore, Equations (2.4) and (2.10) are applied to calculate friction factor for the two-phase flow, respectively. Data processing for frictional pressure drop and friction factor for each nozzle is done by tabulating all necessary data according to Table 3.6.

Table 3.6 Data table for friction factor calculation

Q_L	Q_G	ϕ_m	v_L	m_L	m_G	R_m	$\frac{\Delta P_T}{\rho_L g z}$	$\frac{1+R_M}{1+\varphi_M}$	$\frac{\Delta P_F}{\rho_L g z}$	f_m
m^3/s	m^3/s		m/s	kg/s	kg/s					
Q_{L1}										
Q_{L2}										
Q_{Ln}										

3.4.3 Energy dissipation

Calculation of energy dissipation in the ejector from experimental data is performed by assuming that the system operates with single phase liquid flow, which can be expressed by the following equation.

$$E_{De} = \int Q_M dP \tag{3.2}$$

All the calculations of energy dissipation based on experimental data are compiled in Table 3.7.

Table 3.7 Data table for energy dissipation calculation

Q_L	Q_G	ΔP_e	E_{De}
m^3/s	m^3/s	Pa	W
Q_{L1}			
Q_{L2}			
Q_{Ln}			

3.4.4 Derivation of Bernoulli Equation for water flow through nozzle

In this present work, an attempt to elucidate the relationship between nozzle pressure drop and water flow rate has been carried out using Bernoulli principle. Bernoulli equation for the nozzle between the entry and exit points can be written as

$$\frac{P_l}{\rho_L} + \frac{v_{L,l}^{\ 2}}{2} = \frac{P_s}{\rho_L} + \frac{v_{L,s}^{\ 2}}{2} \tag{3.3}$$

Rewriting Equation (3.3), we get

$$P_l - P_s = \frac{\rho_L}{2}(v_{L,s}^{\ 2} - v_{L,l}^{\ 2}) \tag{3.4}$$

which can be rearranged as

$$P_i - P_s = \frac{\rho_L}{2} v_{L,s}^{\ 2} \left(1 - \frac{v_{L,i}^{\ 2}}{v_{L,s}^{\ 2}}\right) \tag{3.5}$$

Substituting for v_s in Equation (3.5) with $v_{L,s} = \dfrac{Q_L}{\pi/4 D_n^{\ 2}}$, we have

$$P_i - P_s = \frac{\rho_L}{2} \frac{Q_L^{\ 2}}{\left(\frac{\pi}{4} D_n^{\ 2}\right)^2} \left(1 - \frac{v_{L,i}^{\ 2}}{v_{L,s}^{\ 2}}\right) \tag{3.6}$$

Assuming constant water density and application of continuity equation yields,

$$P_i - P_s = \frac{8}{\pi^2} \frac{\rho_L Q_L^{\ 2}}{D_n^{\ 4}} \left(1 - \frac{A_n^{\ 2}}{A_i^{\ 2}}\right) \tag{3.7}$$

Equation (3.7) can be rewritten as

$$P_i - P_s = \frac{8}{\pi^2} \frac{\rho_L Q_L^{\ 2}}{D_n^{\ 4}} \left(1 - \frac{D_n^{\ 4}}{D_i^{\ 4}}\right) \tag{3.8}$$

The theoretical values of pressure drop across the nozzle can be determined using Equation (3.8) and subsequently compared with the experimental values.

3.4.5 Determination of coefficient of discharge, C_v

The coefficient of discharge, C_v is determined for different nozzles using experimental pressure drop data and applying Equation (4.2). Plotting (P_i-P_s) against ($\rho_L Q_L^{\ 2}/D_n^{\ 4}$)(1-($D_n^{\ 4}/D_i^{\ 4}$)) gives ($8/\pi^2 C_v^{\ 2}$) as the slope. From the slope information, C_v for different nozzles are calculated accordingly. The value is then plotted against Reynolds number to get a mathematical correlation between Reynolds number and C_v for each nozzle.

3.4.6 Derivation of Bernoulli Equation for air flow through air inlet line

By neglecting frictional and hydrostatic losses, and eliminating external work factor, Bernoulli equation for the air inlet line between the atmosphere and the suction chamber (points A and S, respectively, in Figure 4.11) can be written as (Perry, R.H and Green, D.W., 1999)

$$\frac{v_{G,A}^{\ 2}}{2} - \int_{A}^{S} \frac{1}{\rho} dP = \frac{v_{G,S}^{\ 2}}{2} \tag{3.9}$$

which can be rearranged as

$$-\int_{A}^{S} \frac{1}{\rho} dP = \frac{v_{G,S}^{\ 2}}{2} - \frac{v_{G,A}^{\ 2}}{2} \tag{3.10}$$

For isothermal flow of a perfect gas, $-\int_{A}^{S} \frac{dP}{\rho} = \frac{RT}{M} \ln \frac{P_A}{P_S}$. Hence, Equation (3.10) becomes

$$\frac{RT}{M} \ln \frac{P_A}{P_S} = \frac{1}{2}\left(v_{G,S}^{\ 2} - v_{G,A}^{\ 2}\right) \tag{3.11}$$

which can be rewritten as

$$\frac{RT}{M} \ln \frac{P_A}{P_S} = \frac{1}{2} v_{G,S}^{\ 2} \left(1 - \frac{v_{G,A}^{\ 2}}{v_{G,S}^{\ 2}}\right) \tag{3.12}$$

Assuming the air flow rate measurement is done at suction pressure and substituting for $v_{G,S}$ in Equation (3.12) with $v_{G,S} = \frac{Q_G}{\pi/4 D_a^{\ 2}}$, we have

$$\ln \frac{P_A}{P_S} = \frac{M}{2RT} \frac{Q_G^{\ 2}}{\left(\frac{\pi}{4} D_a^{\ 2}\right)^2} \left(1 - \frac{v_{G,A}^{\ 2}}{v_{G,S}^{\ 2}}\right) \tag{3.13}$$

Applying continuity equations and rearranging Equation (3.13) results

$$\ln\frac{P_A}{P_s}=\frac{8}{\pi^2}\frac{MQ_G^{\,2}}{RTD_a^{\,4}}\left(1-\frac{A_a^{\,2}}{A_A^{\,2}}\right) \tag{3.14}$$

Since the area of the atmosphere is assumed very large, the ratio of the square of air inlet area to that of atmosphere area can be neglected. Consequently, we get the final equation as

$$\ln\frac{P_A}{P_s}=\frac{8}{\pi^2}\frac{MQ_G^{\,2}}{RTD_a^{\,4}} \tag{3.15}$$

3.4.7 Gas hold-up

In gas hold-up measurement, first the total volume of the column, V_T, is noted, which is 14400 mL. After sudden termination of the flow, the volume of unoccupied space in the column is also noted. Then, gas hold-up can be calculated by applying Equation (3.1). Table 3.8 shows how the gas hold-up data are arranged.

Table 3.8 Data table for gas hold-up measurement

Q_L	Q_G	$Q_M = Q_L + Q_G$	V_G	$\varepsilon_G = V_G / V_T$	$\varepsilon_L = (1-\varepsilon_G)$
m^3/s	m^3/s	m^3/s	mL		
Q_{L1}					
Q_{L2}					
Q_{Ln}					

Gas hold-up is analyzed using Zuber-Findlay's (Zuber and Findlay, 1965) drift-flux model. Analysis of gas hold-up data using drift-flux model also comprises of several steps.

1. Gas and liquid superficial velocity are calculated from (Q_L/A_c) and (Q_G/A_c), respectively
2. Mixture superficial velocity is defined by summing water and air superficial velocities ($v_M = v_G + v_L$)

3. True air velocity is calculated (u_G) from (v_G / ε_G)
4. True air velocity is plotted against mixture superficial velocity in a graph for each nozzle
5. Slope of the graph represents distribution parameter (C_o), while the line interception shows the local relative velocity (v_D)

Data tabulation for gas hold-up analysis with drift-flux model is presented in Table 3.9 and Figure 3.6.

Table 3.9 Data table for gas hold-up analysis with drift-flux model

Q_L	Q_G	v_L	v_G	v_M	ε_G	u_G
m^3/s	m^3/s	m/s	m/s	m/s		m/s
Q_{L1}						
Q_{L2}						
Q_{Ln}						

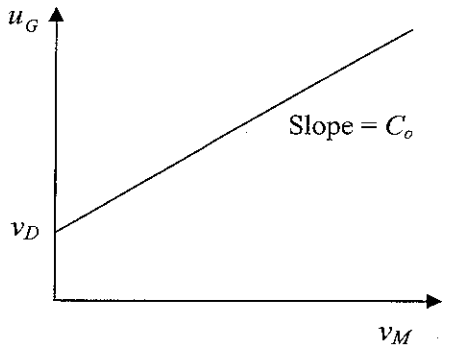

Figure 3.6 Drift-flux correlation chart

3.5 Equipment Identification

Figure 3.7 shows the experimental setup consisting of cocurrent upflow bubble column, ejector, pressure transducers and the control panel.

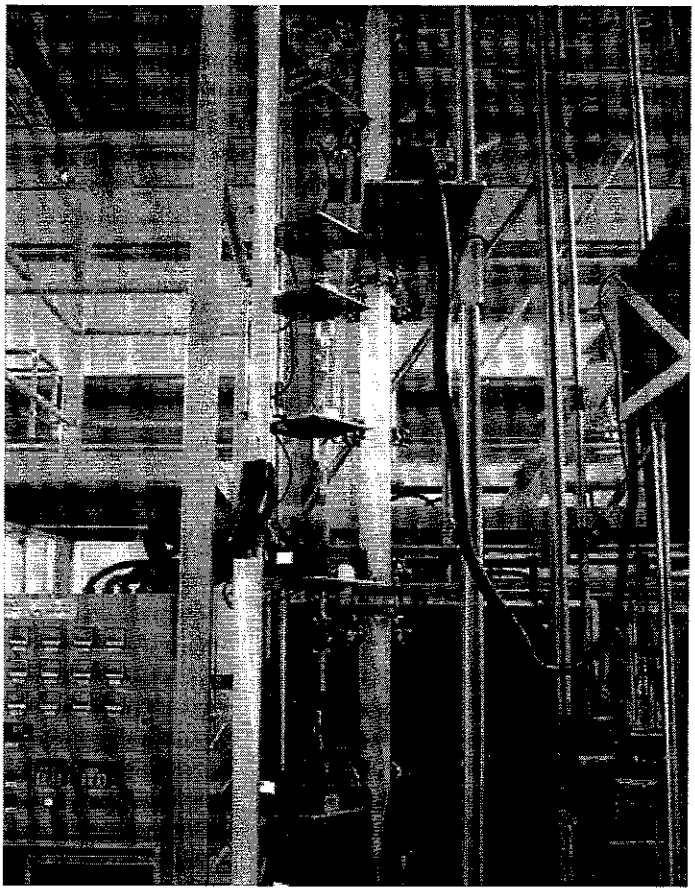

Figure 3.7 Ejector-Induced Cocurrent Upflow Bubble Column

In Figure 3.8, pictures of ejector, air inlet line, rotameter FI-12 and pressure transducers PI-06 up to PI-09 are shown.

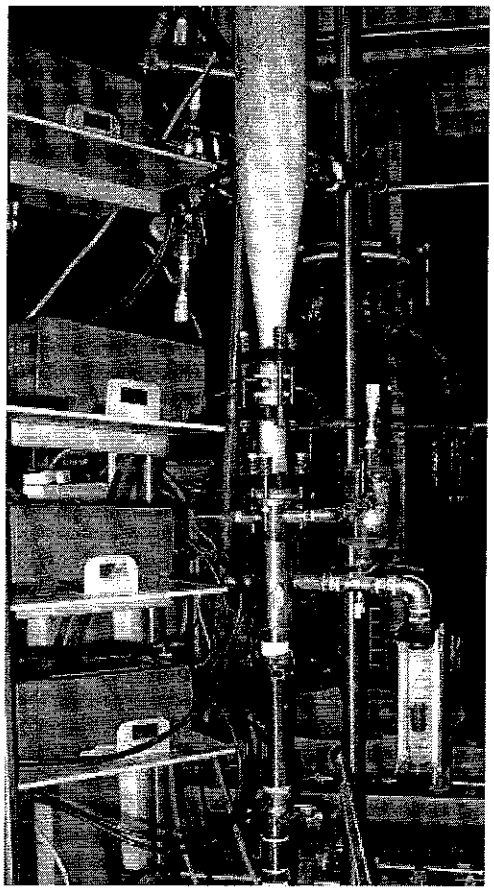

Figure 3.8 Ejector Assembly (E), air inlet line,
rotameter FI-12 and pressure transducers (PI)

Five different nozzles with different sizes in diameter have been employed in the experiments as presented in Figure 3.9 (refer to Table 3.4 for the nozzle coding).

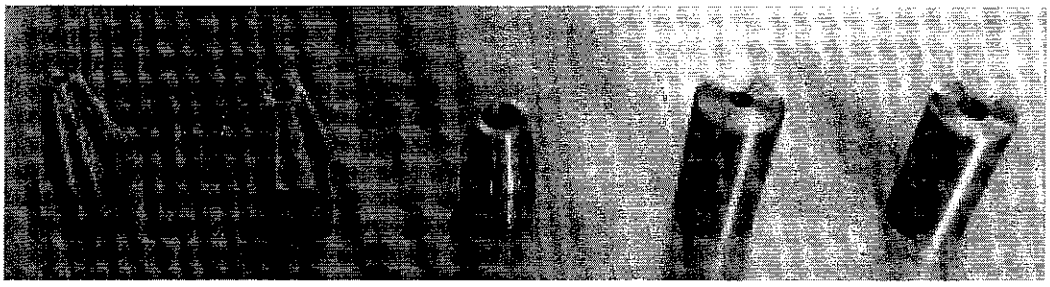

Figure 3.9 Nozzles used in the experiments from left to right:
NC6, NC8, NC10, NO6 and NO8

Figure 3.10 shows the image of storage tank T where water as the motive fluid is reserved before being pumped into system.

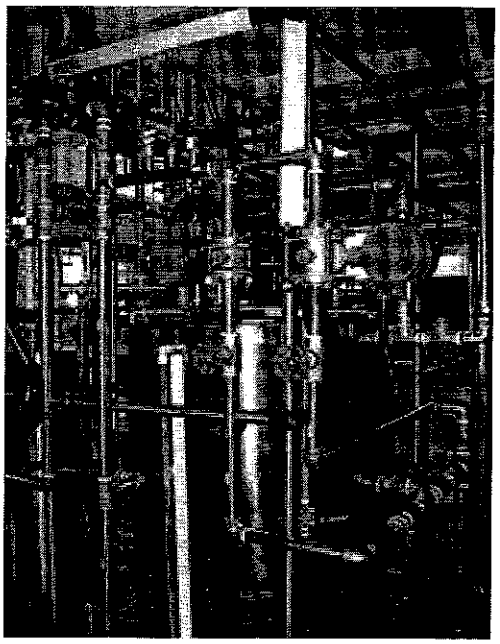

Figure 3.10 Water storage tank (T)

A centrifugal pump P is used to transfer the water from the storage tank T into the system, and to measure its flow rate, a magnetic flow meter FI-14a is provided as presented in Figure 3.11.

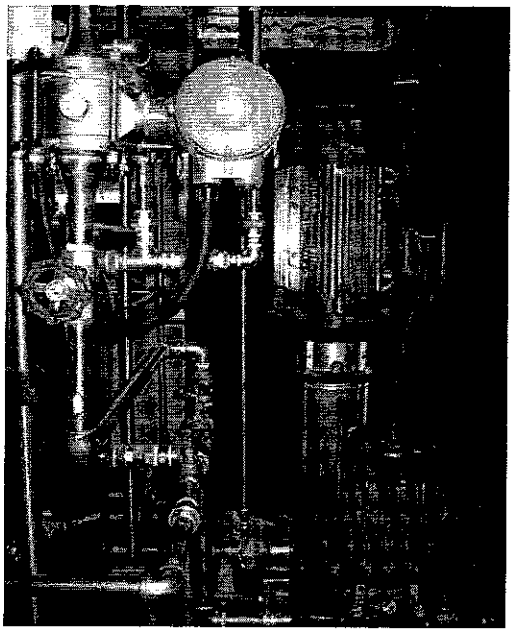

Figure 3.11 Flow meter (FI-14a) and pump (P)

After flowing upward through the column, the mixture of water and air gets separated in gas-liquid separator SE. Figure 3.12 shows the gas-liquid separator SE which is mounted at the top of the ejector-bubble column.

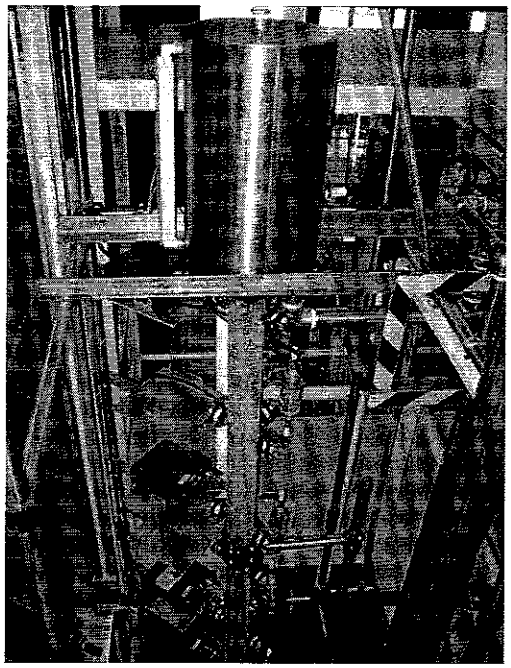

Figure 3.12 Gas-liquid separator (SE)

Water is then sent back to the water storage tank T by means of suction pump P-3 as presented in Figure 3.13.

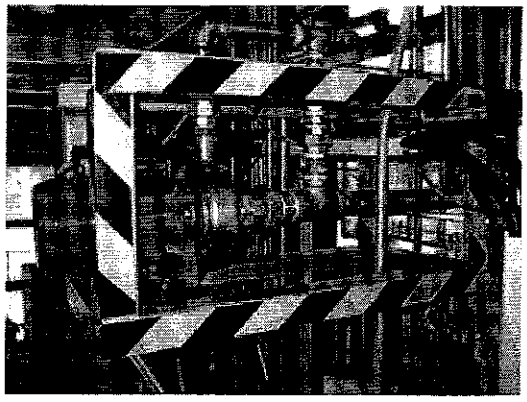

Figure 3.13 Suction pump (P-3)

3.6 Summary

This chapter presented research activities, equipment identification, experimental procedure and data analysis procedure to achieve the objective of this research. The experimental activities include observation of pressure profiles and gas entrainment rate, measurement of pressure drop, calculation of energy dissipation and measurement of gas hold-up in an ejector-induced cocurrent upflow bubble column. Experimental setup consists of an ejector integrated with upflow bubble column and gas-liquid separator (refer to Figure 3.2). Water and air have been used as the motive and suction fluid in the ejector, respectively. Sets of experiment have been performed using convergent and orifice nozzles with different sizes in nozzle diameter. Procedures for data treatment have been described in Section 3.4.

CHAPTER 4

RESULTS AND DISCUSSIONS

Experiments have been conducted in the ejector-induced cocurrent upflow bubble column using water-air system. In the ejector, water and atmospheric air act as the motive fluid and suction fluid, respectively. Two types of nozzles, orifice and convergent, with different sizes in nozzle diameter have been used in the experiments. Minimum water flow rate for all experiments has been selected such that an appreciable vacuum is developed in the suction chamber. In Sections 4.1 to 4.6, experimental results are provided and some preliminary experiments are presented. In Sections 4.7 to 4.9, Bernoulli principle has been applied for analyzing the water and air flow across nozzle and air inlet line, respectively. Analysis on energy dissipation and gas hold-up are presented in the subsequent sections.

4.1 Pressure Profile Observations

Pressure profile in the system is measured using nine different pressure transducers mounted along the axis of the column as shown in Figure 4.1. Water at high pressure is pumped through the nozzle at high velocity into the suction chamber. As a result, air is sucked into the chamber and entrained into the throat. In the throat, air disperses into the water and forms two-phase flow. The two-phase fluid then flows into the diffuser where the pressure is recovered. Subsequently, the water-air mixture flows upward through the bubble column in which the pressure decreases gradually due to the hydrostatic loss. This phenomenon is studied using five different nozzles with different sizes in nozzle diameter. Three of which are convergent nozzles, and the other two are orifice nozzles. Experimental data of this study are presented in Figures 4.1 to 4.5.

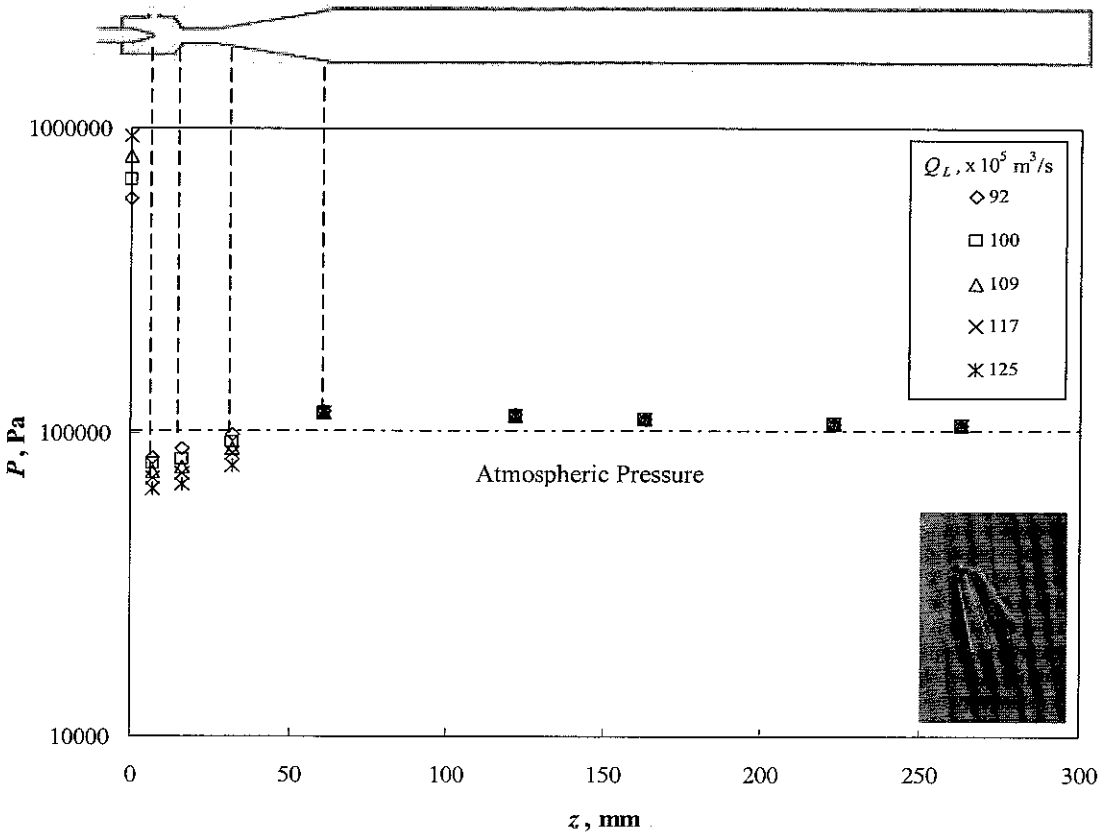

Figure 4.1. Observed pressure profiles for different water flow rates in the system using 6 mm convergent nozzle (NC6), with distance, z, measured from the tip of the nozzle

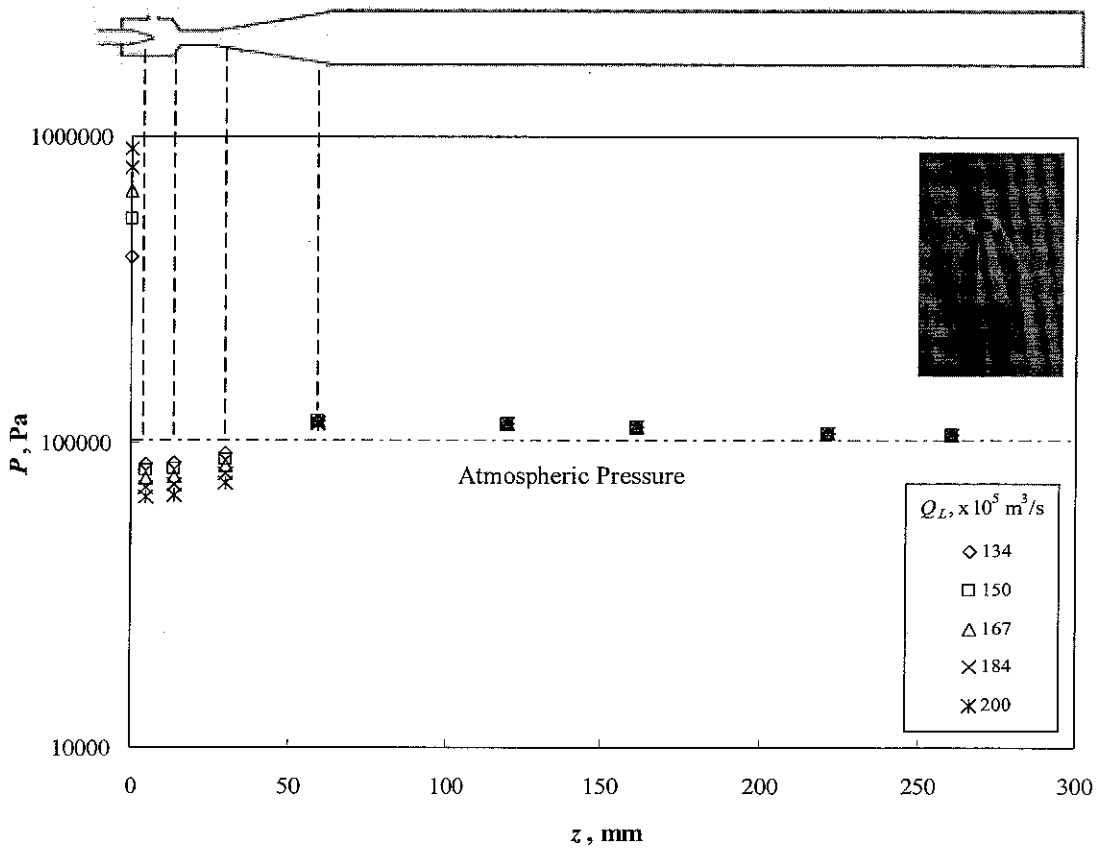

Figure 4.2. Observed pressure profiles for different water flow rates in the system using 8 mm convergent nozzle (NC8), with distance, z, measured from the tip of the nozzle

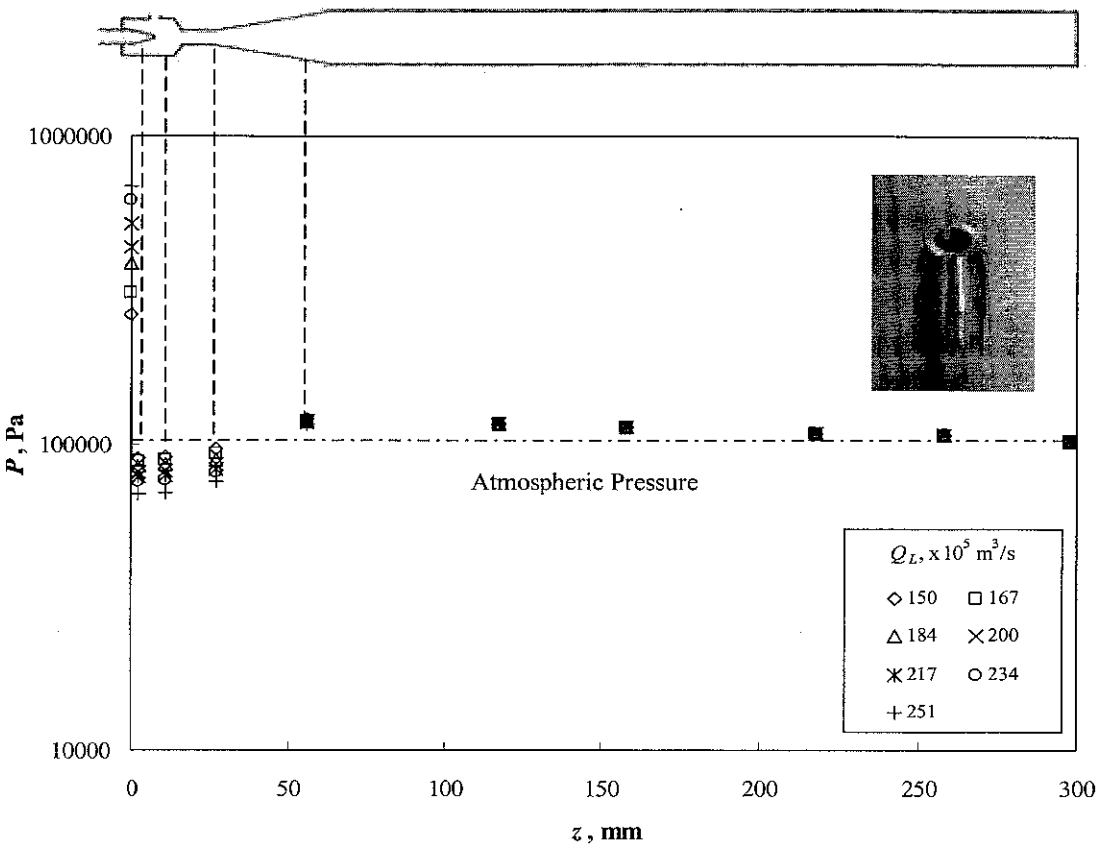

Figure 4.3. Observed pressure profiles for different water flow rates in the system using 10 mm convergent nozzle (NC10), with distance, *z*, measured from the tip of the nozzle

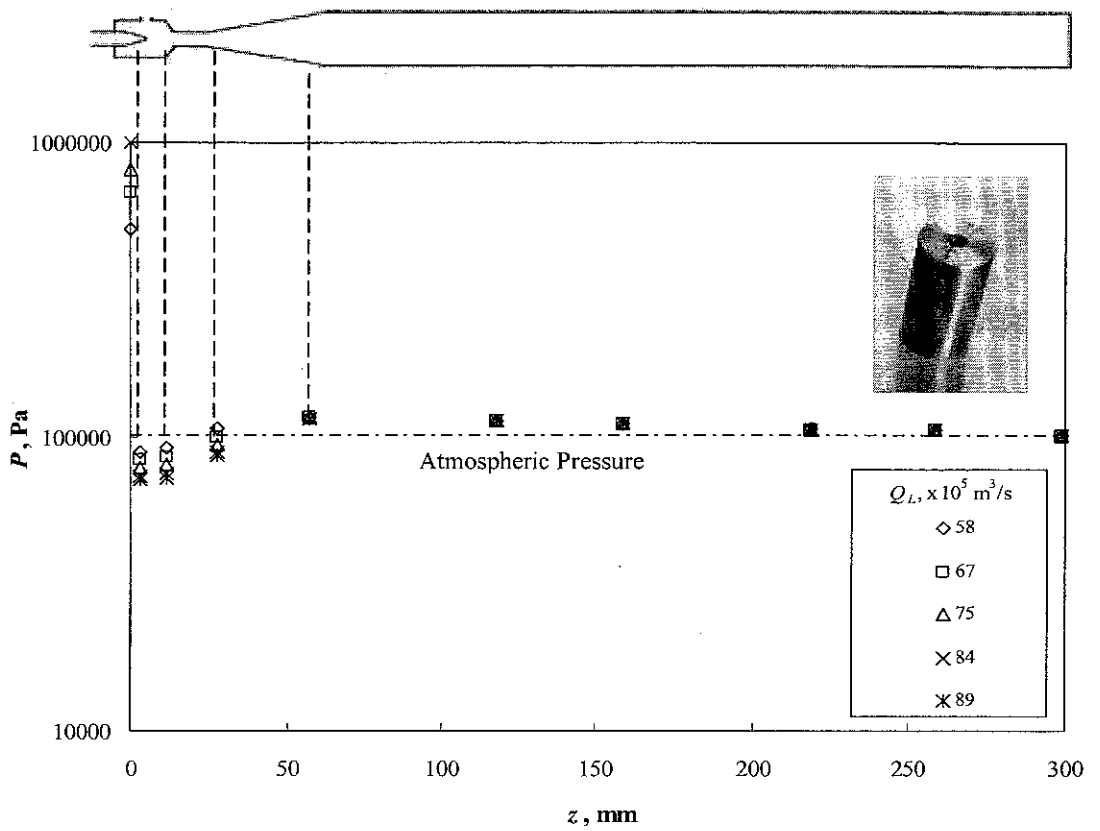

Figure 4.4. Observed pressure profiles for different water flow rates in the system using 6 mm orifice nozzle (NO6), with distance, *z*, measured from the tip of the nozzle

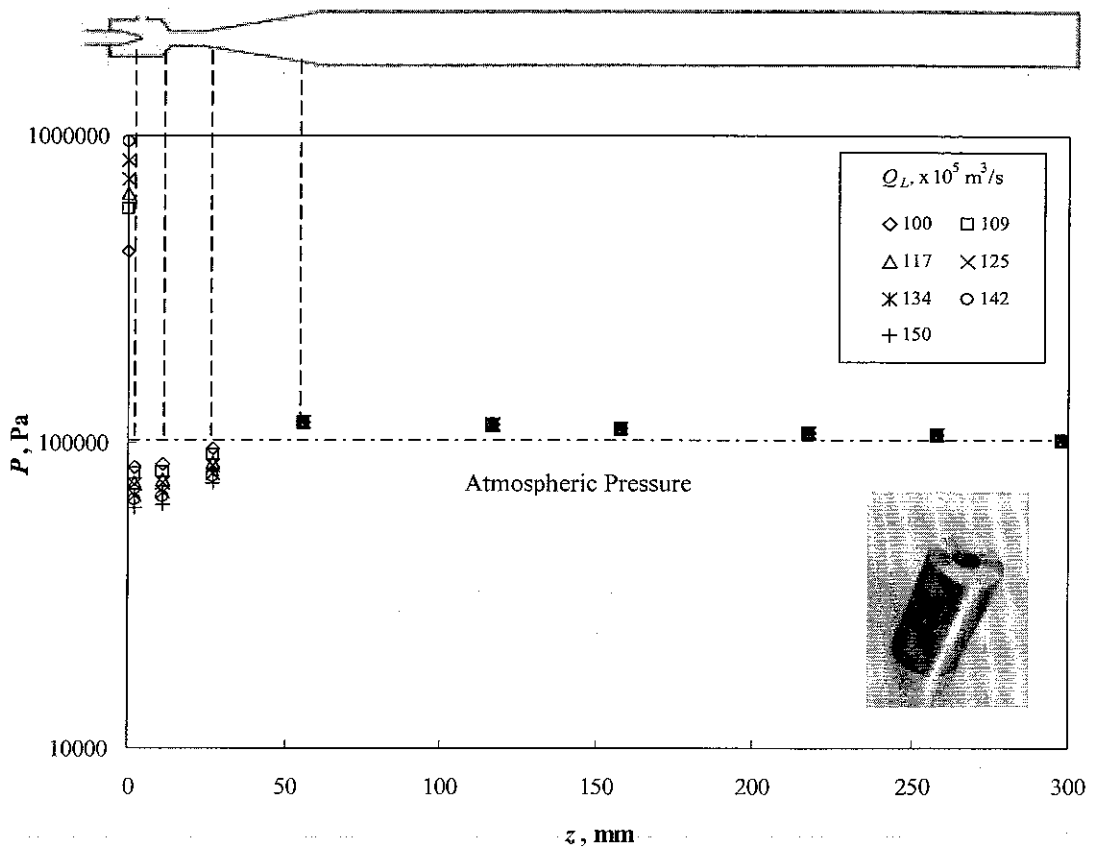

Figure 4.5. Observed pressure profiles for different water flow rates in the system using 8 mm orifice nozzle (NO8), with distance, *z*, measured from the tip of the nozzle

From the pressure profiles shown in Figures 4.1 to 4.5, it can be seen that maximum decrease in pressure occurs across the nozzle. This is due to the acceleration of the motive fluid as the pressure energy is converted into kinetic energy. This sudden pressure drop reaches vacuum condition and because of this, air is sucked into the chamber and entrained into the throat. However, as air disperses into the water along the throat and divergent diffuser, the fluid flow pressure is recovered and its velocity decelerates due to increasing crossectional area. The pressure recovery reaches its maximum condition at the diffuser outlet. In the bubble column section, the two-phase flow experiences gradual pressure drop due to the hydrostatic and frictional losses and finally reaches atmospheric pressure at the end of the column.

4.2 Pressure Drop across the Nozzle

Pressure drop across the nozzle is the difference between the pressures at the upstream of the nozzle (P_l) and at the nozzle tip (P_s). Figure 4.6 shows the schematic diagram of important locations at the nozzle for measuring water pressure drop across nozzle.

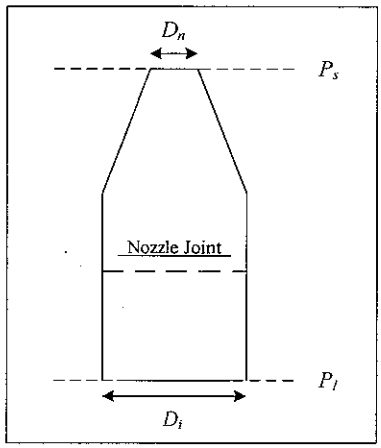

Figure 4.6. Schematic diagram of important locations at the nozzle for measuring water pressure drop across nozzle

Figure 4.7 shows the relationship between upstream water pressure (P_l) and water flow rate (Q_L) observed during the experiment (refer to Table 3.4 for the nozzle codes).

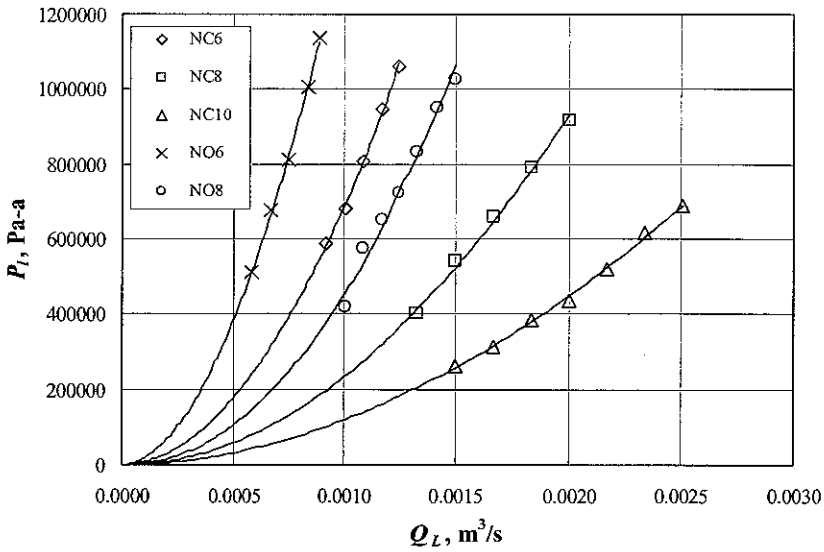

Figure 4.7. Upstream pressure (P_l) developed as a function of water flow rates for different nozzles

From Figure 4.7, it can be seen that for the same water flow rate, 6 mm nozzles have higher water pressure compared to 8 mm and 10 mm nozzles. This can be explained by the fact that greater flow restriction is obtained using nozzles with smaller nozzle diameter. In terms of nozzle type, due to their mechanical design, orifice nozzles provide greater water pressure than convergent nozzles for a given water flow rate.

As water passes through the nozzle, its pressure decreases and vacuum condition is created in the suction chamber. It is observed that suction pressure developed in the chamber depends highly on the water flow rate and nozzle diameter. The effect of water flow rate on the suction pressure is illustrated in Figure 4.8.

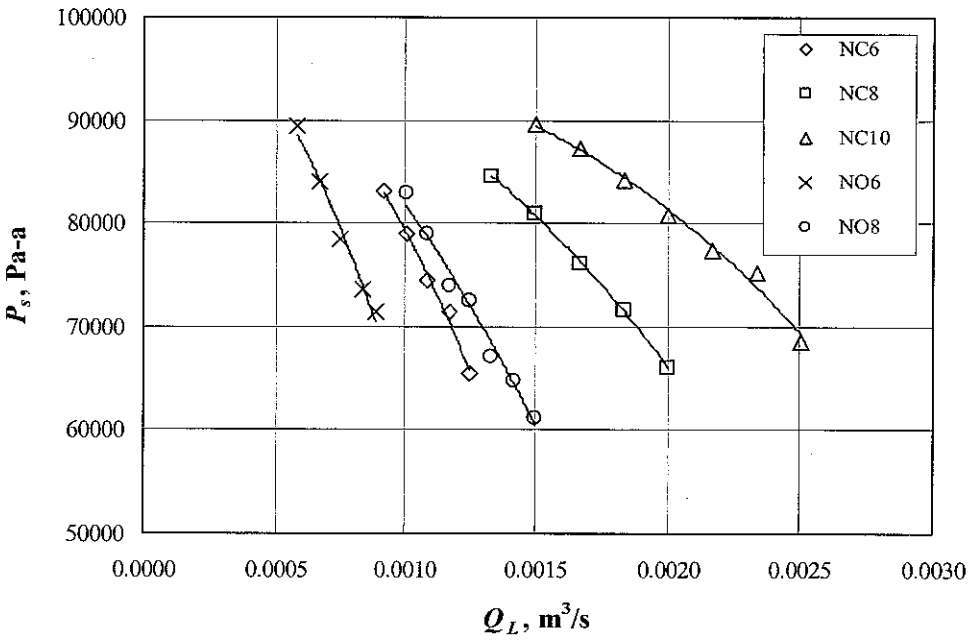

Figure 4.8. Effect of water flow rates on the suction pressure (P_s) developed for different nozzles

Figure 4.8 shows decreasing trends of suction pressure with increasing water flow rates. For the same water flow rate, 6 mm nozzle develops lower suction pressure than 8 and 10 mm nozzles. In view of the nozzle type, usage of orifice nozzles in the ejector give lower suction pressure for the same nozzle size and water flow rate.

In order to get more comprehensive view of water pressure drop across the nozzle, relationship between nozzle pressure drop and water flow rate is plotted in Figures 4.9 and 4.10.

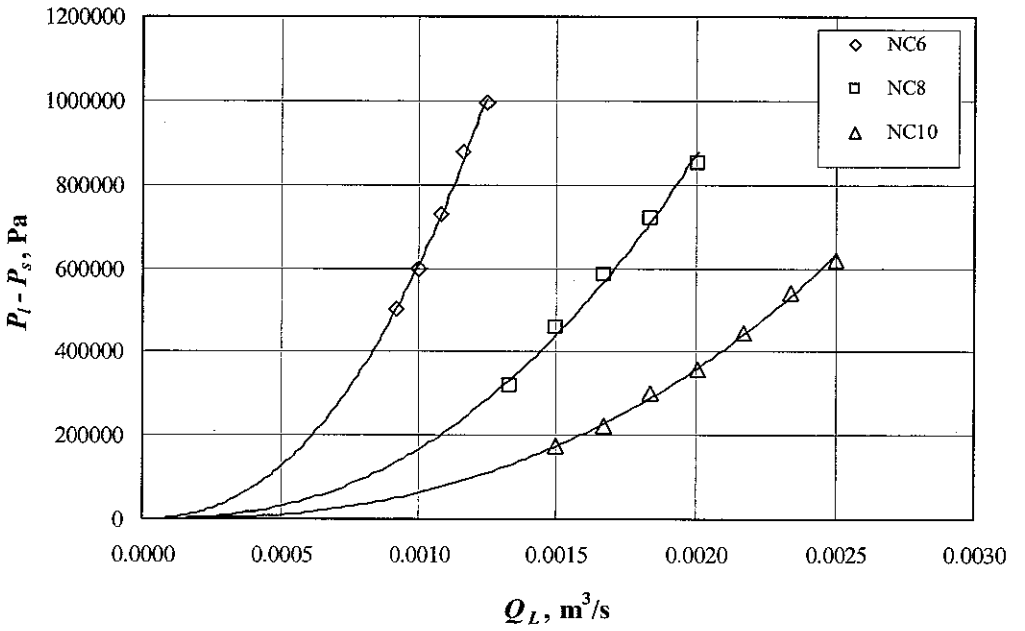

Figure 4.9. Effect of water flow rate on the pressure drop across the convergent nozzles

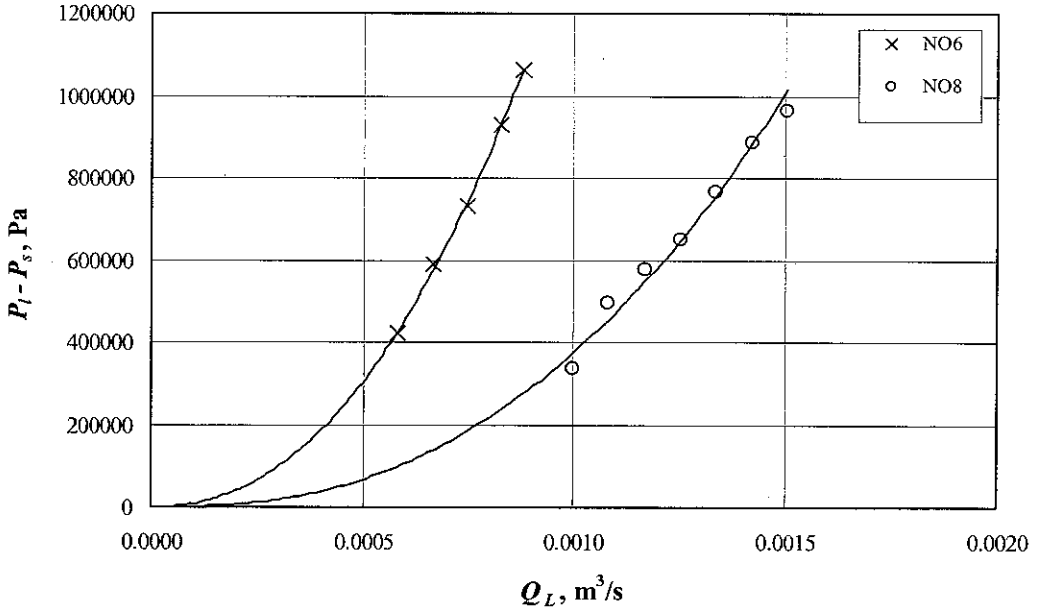

Figure 4.10. Effect of water flow rate on the pressure drop across the orifice nozzles

Figures 4.9 and 4.10 show that greater pressure drop is obtained for nozzles with smaller sizes for the same water flow rate. In terms of nozzle type, orifice nozzles give larger pressure drop compared to convergent nozzles for the same water flow rate. This is because orifice nozzles give sudden contraction on the flow, while convergent nozzles have relatively smoother contraction due to their physical shapes.

4.3 Pressure Drop for Air Flow across the Air Inlet Line

The vacuum developed in the chamber allows air from the atmosphere to be sucked into the suction chamber. The rate of air entrainment into the chamber depends on the suction pressure. Air pressure drop is measured between the atmospheric pressure (P_A) and the air pressure at the air inlet line. The pressure at the air inlet line is assumed equal to the suction pressure (P_s) developed in the suction chamber. Figure 4.11 shows the schematic diagram of important locations at the suction chamber for measuring air pressure drop across air inlet line.

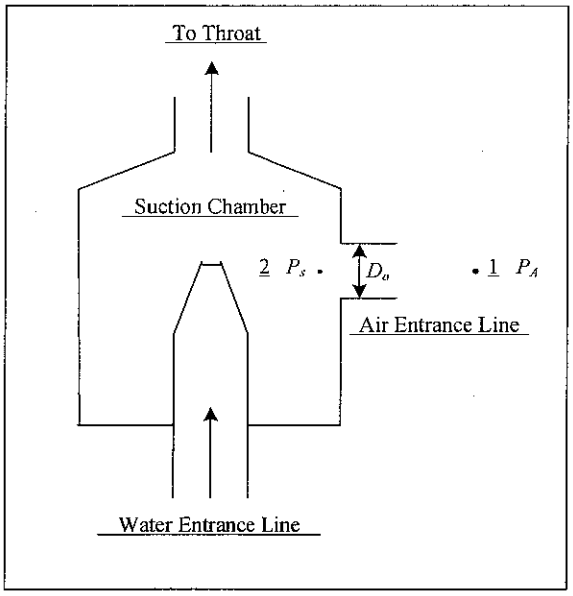

Figure 4.11 Schematic diagram of important locations at the suction chamber for measuring air pressure drop across air inlet line

The relationship of air flow rate with the air pressure drop through the air inlet line is presented in Figure 4.12.

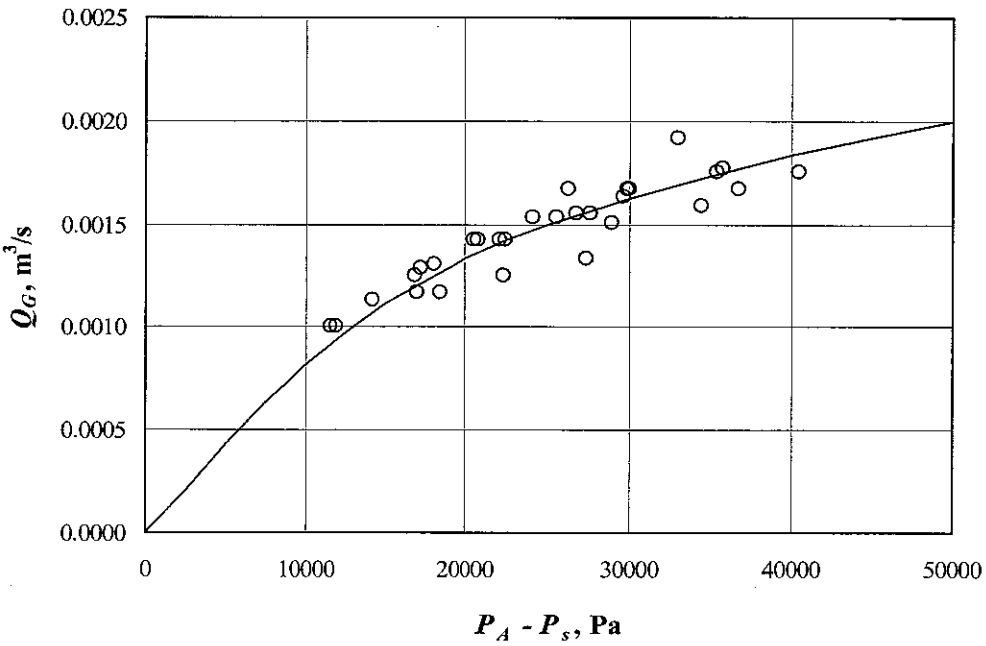

Figure 4.12. Effect of suction pressure on the air flow rate with different nozzles

From the figure, it is concluded that more air is sucked into the chamber as the suction pressure decreases or, in other words, pressure drop across the air inlet line increases. This can be explained by the fact that higher driving force is created by having greater difference in pressure through the air inlet line. This driving force causes air in the atmospheric surroundings sucked into the suction chamber of the ejector.

4.4 Observations on Water Flow Rate and Air Entrainment Rate

The relationship between the water flow rate and the air entrainment rate for various nozzles obtained experimentally is shown in Figure 4.13. From the figure, it is observed that increasing water flow rate increases the air entrainment rate into the suction chamber. It is also observed that for the same water flow rate and nozzle size, orifice nozzles have the ability to entrain greater amounts of air into the ejector than convergent nozzles. This is obvious as we have observed in Section 4.2 that orifice nozzles developed higher vacuum than convergent nozzles. Consequently, it is expected that the air flow rate to follow the same trend.

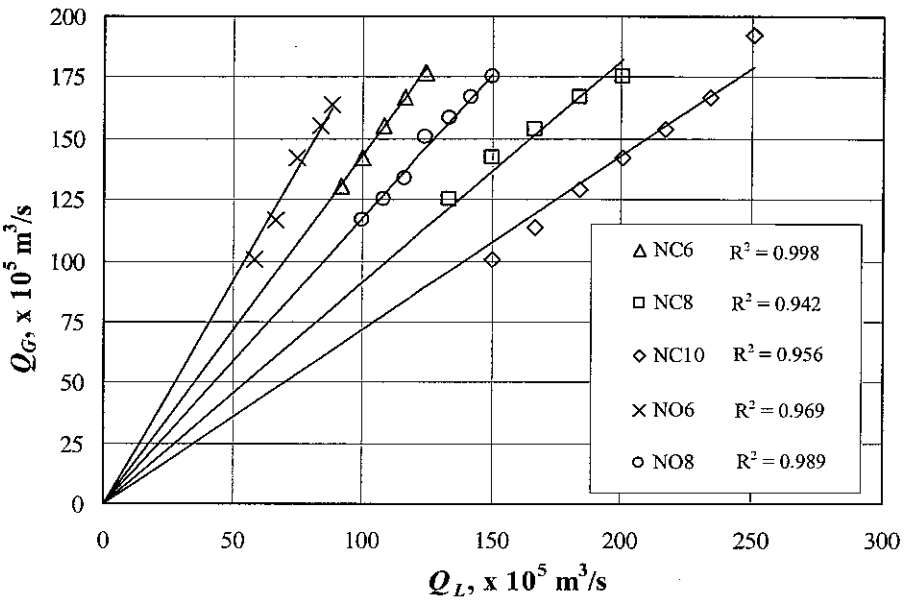

Figure 4.13. The relationship between the observed water flow rate and the air entrainment rate for different nozzles

4.5 Pressure Recovery in the Ejector

Pressure recovery in the ejector starts from the throat section up to the diffuser section and reaches its maximum value at the diffuser outlet. Besides observing the pressure values at the diffuser outlet (P_d) experimentally, an approach to verify those values has also been done using the following equation:

$$P_d = P_A + P_{hyd} \tag{4.1}$$

where P_A and P_{hyd} are atmospheric pressure at the end of the column and hydrostatic pressure in the bubble column section, respectively. By assuming that the whole section of bubble column is fully filled with water, then $P_{hyd} = \rho_L g z$. Comparison between the observed values from the experiments and the values calculated using Equation (4.1) with respect to the pressure in the suction chamber (P_s) is presented in Figure 4.14.

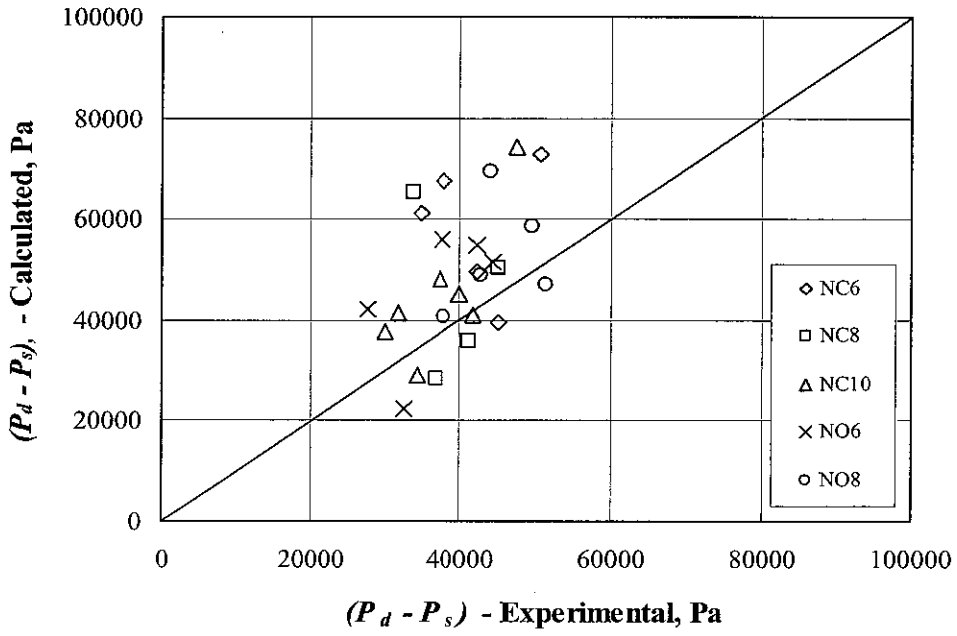

Figure 4.14 Comparison between the observed values of (P_d-P_s) and those calculated using Equation (4.1)

Figure 4.14 shows that a fair agreement between observed values from the experiments and the values calculated using Equation (4.1) is achieved. The correlation coefficient (R^2) for the fits is 0.6. Maximum deviation that can be observed from Figure 4.14 is obtained using 10 mm convergent nozzle (NC10). Deviation likely occurs due to the assumption that only water phase is considered in calculating the pressure at the diffuser outlet (P_d). This assumption influences the value of hydrostatic pressure (P_{hyd}) which consequently results in higher values of calculated P_d - P_s. However, the deviation of the parity plot only ranges from 0 – 36%, which is still considered acceptable.

4.6 Pressure Drop in the Ejector and the Total System

Pressure drop in the ejector is measured between the nozzle tip (PI-06) and the diffuser outlet (PI-09). Pressure drop across the ejector as a function of water flow rate, air entrainment rate and mixture flow rate are presented in Figures 4.15 to 4.17.

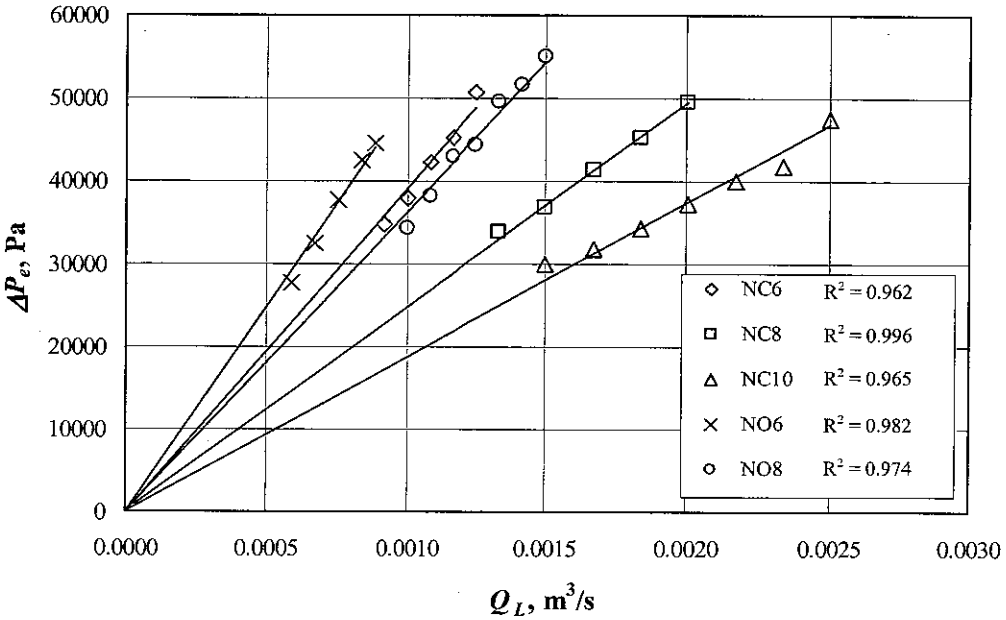

Figure 4.15. Effect of water flow rate on ejector pressure drop

Figure 4.15 shows that pressure drop in the ejector increases linearly with the increase of water flow rate (Q_L). Pressure in the diffuser outlet (P_d) does not change very much with the increase of water flow rate, while pressure at the nozzle tip (P_s) varies significantly according to water flow rate and nozzle type. Hence, the pressure drop in ejector is mainly affected by pressure at the nozzle tip which results in linear trend.

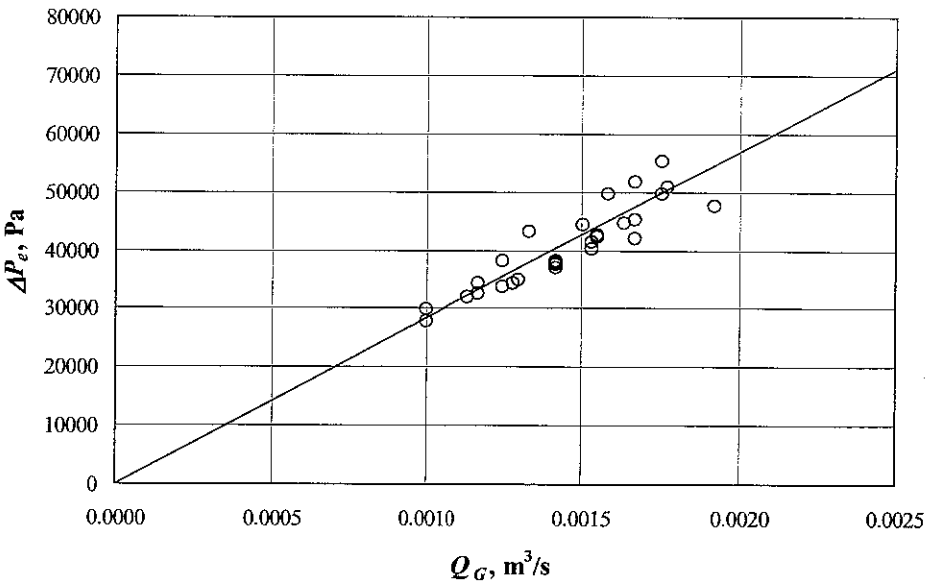

Figure 4.16. Effect of air entrainment rate on ejector pressure drop, $R^2 = 0.816$

In Figure 4.16, it is observed that pressure drop in the ejector increases with the increase of air entrainment rate. Also, ejector pressure drop have linear relationship with the air entrainment rate. This increase in pressure drop can be explained by the fact that an increase in of air entrainment rate causes higher population of gas bubbles, which in turn increases the true liquid velocity. This is also due to the fact that the amount of entrained air is only influenced by the suction pressure in the suction chamber (P_s) which is assumed to be equal to the pressure at the nozzle tip. Therefore, any changes to the suction pressure will lead to the same trend to the air entrainment rate.

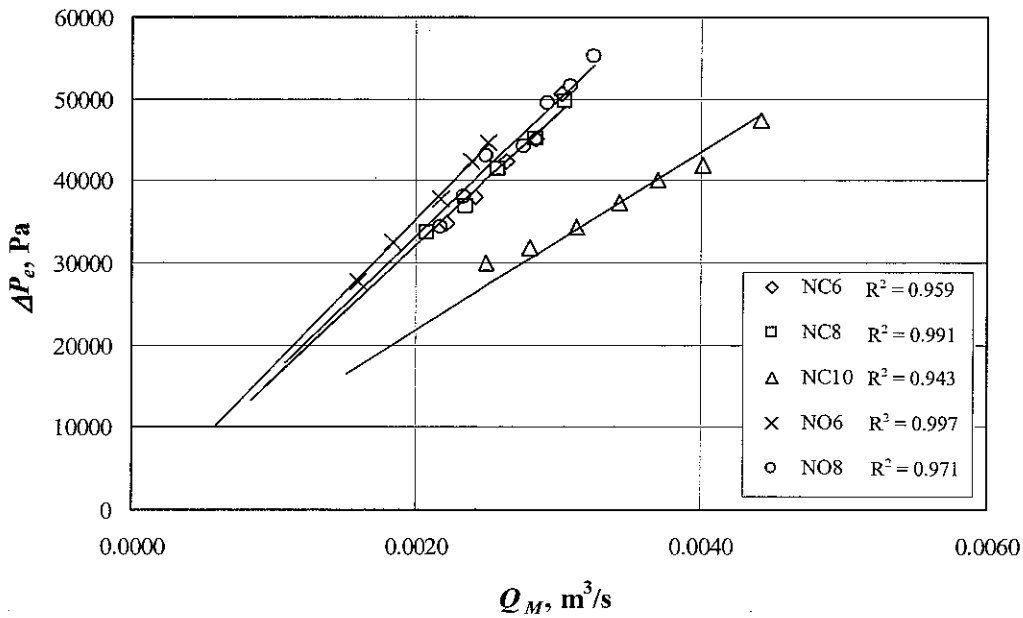

Figure 4.17. Effect of mixture flow rate at the suction chamber on ejector pressure drop

From Figure 4.17, it can be observed that pressure drop in the ejector increases with the increase of the flow rate of water-air mixture. For the same mixture flow rate, all nozzles give approximately the same pressure drop in the ejector except for NC10. Deviation for NC10 occurs because it presents higher suction pressure (P_s) compared to other nozzles. For this reason, the ejector pressure drop for NC10 becomes lower than for other nozzles.

Figure 4.18 illustrates the total pressure drop in the whole system, which is measured between the nozzle tip (PI-06) and top of the bubble column (PI-15).

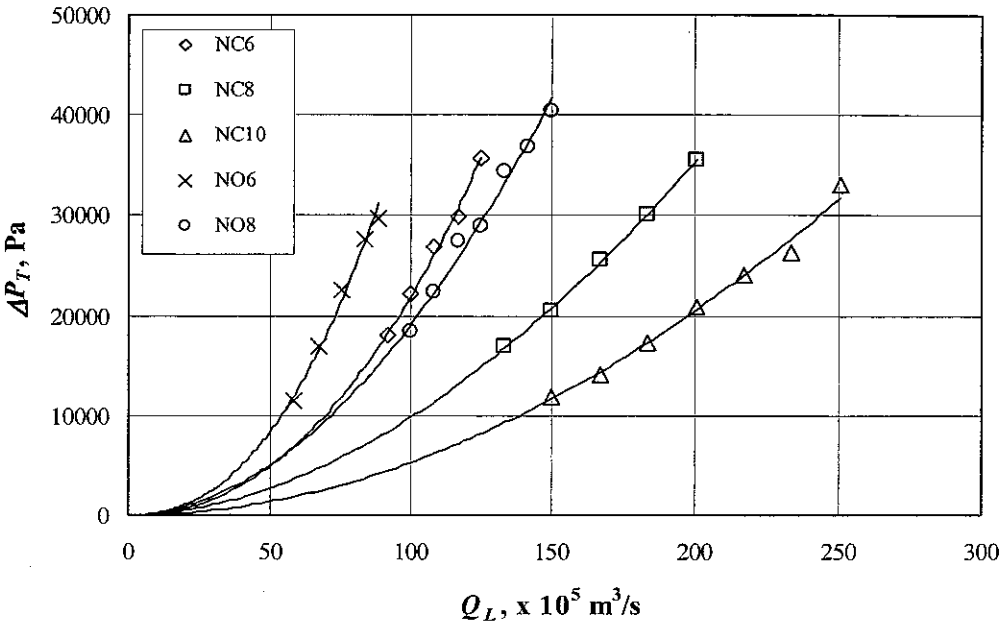

Figure 4.18. Effect of water flow rate on total system pressure drop

Pressure drop in the total system is influenced by two different shapes of vertical pipe which are divergent section at the ejector, and vertical straight pipe at the bubble column section. In the ejector, pressure recovery due to deceleration is more dominant than pressure drop caused by hydrostatic loss, while in the bubble column, by neglecting losses due to friction, pressure drop is purely influenced by hydrostatic loss. However, from Figures 4.15 and 4.18, it can be seen that the highest pressure drop is obtained in the ejector and in the total system by applying 6 mm orifice nozzle (NO6), or in other words, orifice nozzle with the smallest diameter. In addition, it is also observed that triplicate runs taken for each trend only give small deviation to the average value which range from 2 – 5 %.

4.6.1 Friction factor in the total system

Two-phase friction factor in the total system for each nozzle have been calculated using experimental data and applying Equation (2.10) as described in Section 3.4.2. Two-phase friction factor as the effect of superficial liquid Reynold's number in the column ($Re_{L,c}$) is illustrated in Figure 4.19.

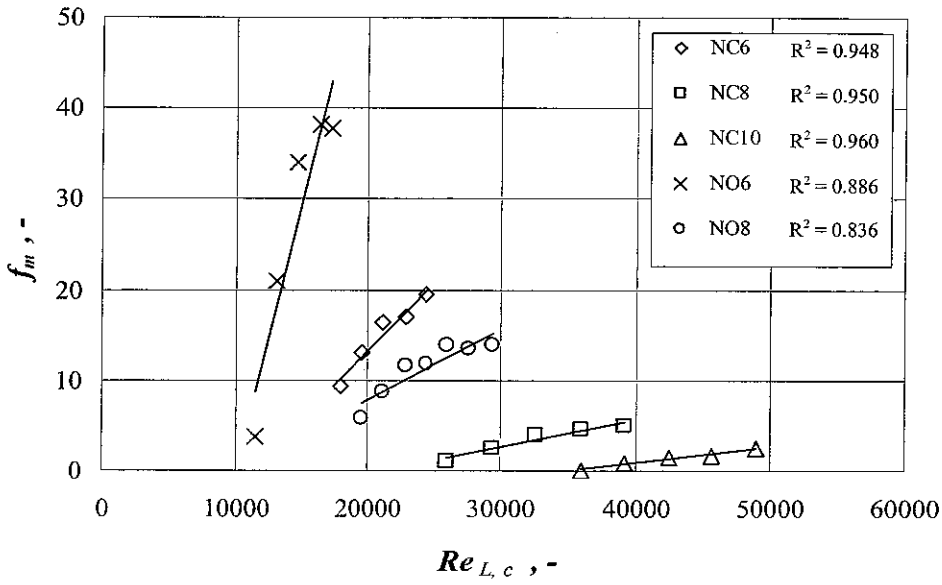

Figure 4.19 Effect of superficial water Reynold's number on the two-phase friction factor

From Figure 4.19, it can be observed that two-phase friction loss increases linearly with the increase of water Reynold's number. NO6 is found to have largest friction loss in the system of all nozzles. This is due to the fact that high water flow rate that passes through the nozzle causes high vacuum level in the suction chamber. Consequently, the total pressure drop in the column increases. As a result, frictional pressure drop is also increased as expressed by Equation (2.4). An increase in frictional pressure drop causes the increase in two-phase friction factor as shown by Equation (2.10). Friction loss in this present work ranges from 0.07 – 38.14 which is higher than ordinary pipeline contactors. This may possibly be due to the much better dispersion obtained by the use of single-jet nozzle in the ejector. In comparison with the results of Radhakrishnan and Mitra (1984), the present work gives lower values of friction factor than theirs. Radhakrishnan and Mitra (1984) obtained two-phase friction factor which ranges from 0.09 – 541.92. This is possibly due to the use of multi-jet nozzle in their system. Multi-jet nozzles are able to give higher vacuum level and entrain more amount of suction fluid than single-jet nozzle (Witte, 1969). However, they are not very common in industries and rather difficult to fabricate.

4.7 Application of Bernoulli Principle for Water Flow through the Nozzle

In this present work, Bernoulli principle has been used to interpret the water flow through the nozzle as explained in Section 3.4.4. From Equation (3.8), it is known that the pressure drop across the nozzle is proportional to the water density (ρ_L) and the square of water flow rate (Q_L^2) and inversely proportional to the fourth power of nozzle diameter (D_n^4). A plot of observed ($P_1 - P_s$) against ($\rho_L Q_L^2/D_n^4$)(1-(D_n^4/D_i^4)) is shown in Figure 4.20.

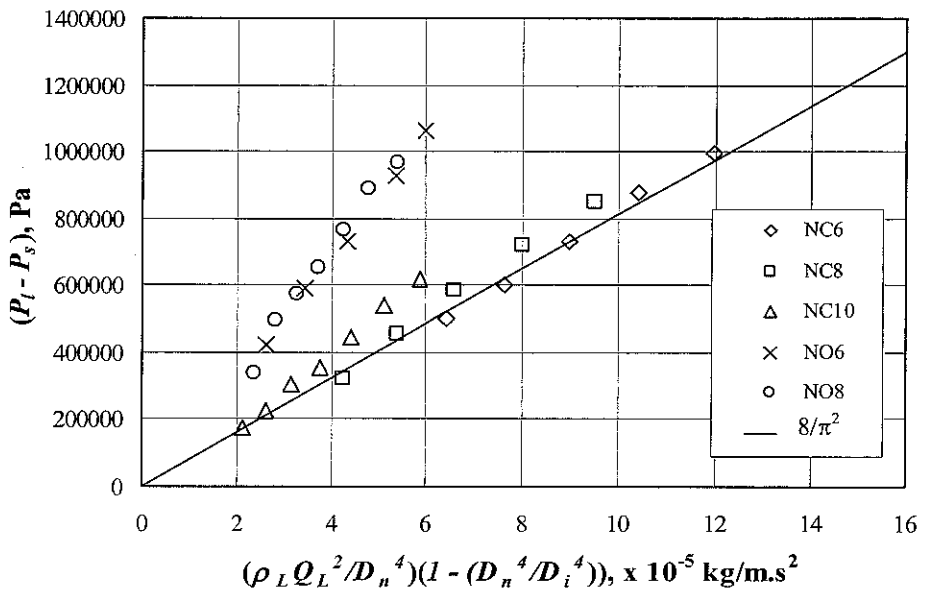

Figure 4.20. Correlation of water pressure drop across the nozzle

From the figure, it is observed that there are deviations between the experimental pressure drop values and those calculated from Equation (3.8). It is observed that the deviations for the orifice nozzles (NO6 and NO8) are larger than that for the convergent nozzles (NC6, NC8 and NC10). These deviations can be attributed to the large frictional losses in the orifice nozzles. Large frictional losses in orifice nozzles are obtained due to their physical shape that creates greater sudden contraction compared to convergent nozzles (refer to Figure 3.4). To account for the frictional losses across the nozzle, Equation (3.8) is modified by introducing a coefficient of discharge, C_v, and written as

$$P_1 - P_s = \frac{8}{\pi^2}\frac{\rho_L Q_L^2}{C_v^2 D_n^4}\left(1-\frac{D_n^4}{D_i^4}\right) \qquad (4.2)$$

The estimated C_v values for the nozzles are presented as a function of Reynolds number as shown in Table 4.1.

Table 4.1. C_v values for various nozzles

Nozzle	$Re_{L,n}$ Range	$C_v = f(Re_{L,n})$	R^2	Studied Range of Q_L (x 10^5 m^3/s)	C_v Range
NC6	227398 - 310089	C_v = -0.126 ln ($Re_{L,n}$) + 2.575	0.849	92 - 125	0.98 - 1.00
NC8	248071 - 372106	C_v = -0.198 ln ($Re_{L,n}$) + 3.474	0.849	134 - 200	0.93 - 1.00
NC10	223264 - 372106	C_v = -0.246 ln ($Re_{L,n}$) + 4.021	0.947	150 - 251	0.87 - 0.99
NO6	144708 - 219129	C_v = -0.067 ln ($Re_{L,n}$) +1.502	0.846	58 - 89	0.68 - 0.70
NO8	186053 - 279080	C_v = -0.056 ln ($Re_{L,n}$) + 1.367	0.954	100 - 150	0.66 - 0.69

For a well designed venturi-shape pipe, the constant C_v is around 0.98 – 0.99, while for orifice, C_v ranges from 0.60 – 0.70 (McCabe et al., 2004). From the table, it is observed that all convergent nozzles behave like venturis. This is shown by the fact that the C_v values for all convergent nozzles ranges from 0.87 – 1.00. C_v values for both the orifice nozzles also comply very well with the theoretical ranges for orifice shape, which is 0.66 – 0.68. Figure 4.21 shows the relationship between $(P_t\text{-}P_s)$ and $(\rho_L Q_L^2/D_n^4 C_v^2)(1\text{-}(D_n^4/D_i^4))$.

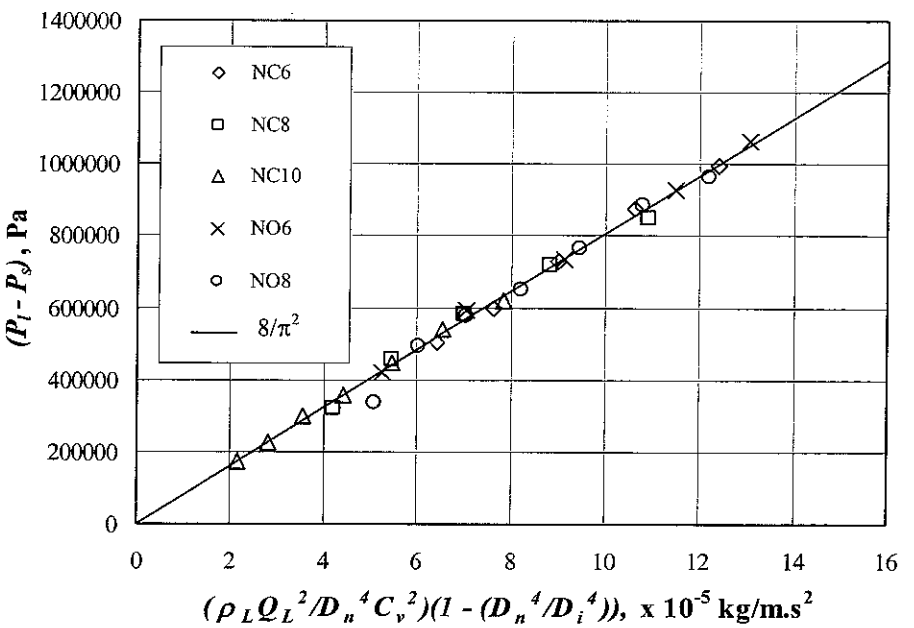

Figure 4.21. Correlation of water pressure drop across the nozzle with C_v^2

A linear trend between $(P_I\text{-}P_s)$ and $(\rho_L Q_L^2/D_n^4 C_v^2)(1\text{-}(D_n^4/D_i^4))$ is observed from Figure 4.21. The averaged slope of the trends is 0.80 which is very close to the theoretical value of 0.81. Hence, this proves the validity of the model expressed by Equation (4.2).

4.8 Application of Bernoulli Principle for Air Flow through Air Inlet Line

Suction pressure developed by the nozzle dictates the amount of air that can be sucked into the suction chamber. The relationship between suction pressure and air flow rate in the ejector can be modeled using Bernoulli equation as expressed by Equation (3.15). From the equation, it is known that $ln(P_A/P_s)$ is proportional to the square of air flow rate (Q_G^2), and inversely proportional to the fourth power of air inlet line diameter (D_a^4). An approach using this Bernoulli equation shows good theoretical match with the experimental results with only approximately 30% in error as illustrated in Figure 4.22.

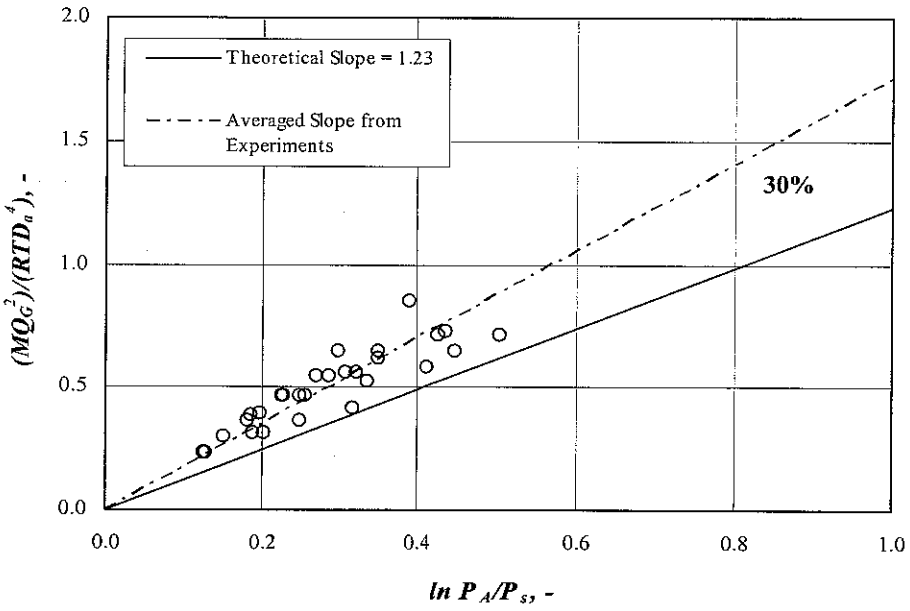

Figure 4.22. Correlation between the pressure drop across the air inlet line and the air flow rate for different nozzles, $R^2 = 0.894$

Beside random error that might have occurred during the measurement of air entrainment rate, the deviation is suspected to happen because of the assumption that has been taken in

applying the pressure in the suction chamber (P_s) to represent the pressure in the air inlet line.

4.9 Correlation between Water Flow Rate and Entrained Air Flow Rate

With the correlations developed for each phase, an attempt to predict air entrainment rate using water flow rate and nozzle size is carried out. Combining Equations (4.2) and (3.15), and eliminating P_s, we get

$$P_i - \frac{8}{\pi^2}\frac{\rho_L Q_L^{\,2}}{C_v^{\,2} D_n^{\,4}} = \frac{P_A}{\exp\left(\dfrac{8MQ_G^{\,2}}{\pi^2 RTD_a^{\,4}}\right)} \tag{4.3}$$

By simplifying Equation (4.3), a correlation between water flow rate and entrained air flow rate is obtained as

$$Q_G = \left[\left(\ln\left(\frac{P_A}{P_i - \left(\dfrac{8}{\pi^2}\dfrac{\rho_L Q_L^{\,2}}{C_v^{\,2} D_n^{\,4}}\right)}\right)\right)\left(\frac{\pi^2 RTD_a^{\,4}}{8M}\right)\right]^{1/2} \tag{4.4}$$

The calculated values of entrained air flow rate from Equation (4.4) are plotted against the experimental values and are shown in Figure 4.23.

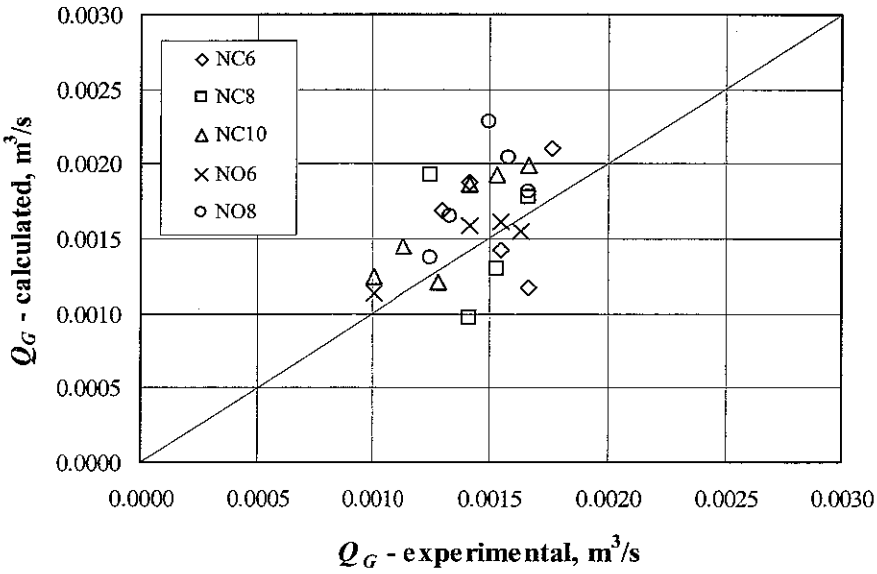

Figure 4.23. Comparison of the experimental values of entrained air flow rate with those calculated from Equation (4.4)

From Figure 4.23, it is observed that Equation (4.4) has agreeably predicted the amount of entrained air flow rate within the range of experiments. Correlation coefficient for the fits is 0.448 and maximum error of 25% is found from the parity plot. This is probably due to the fact that there are only few points that have been plotted in the graph. More points can be obtained by increasing the number of flow rates variation in the experiments. This will expectantly give clearer and better representation of the plot. However, Figure 4.23 has already proven that air entrainment rate in this system can be predicted with reasonably good accuracy with the availability of operating conditions (P_l, Q_l, and T) and the dimension of ejector (D_n and D_a) data.

4.9.1 Correlation between predicted values of water flow rate and air entrainment rate

Water flow rate is predicted using experimental values of water pressure drop across the nozzle and by applying Equation (4.2). Figure 4.24 shows the correlation between the predicted values of water flow rate and air entrainment rate.

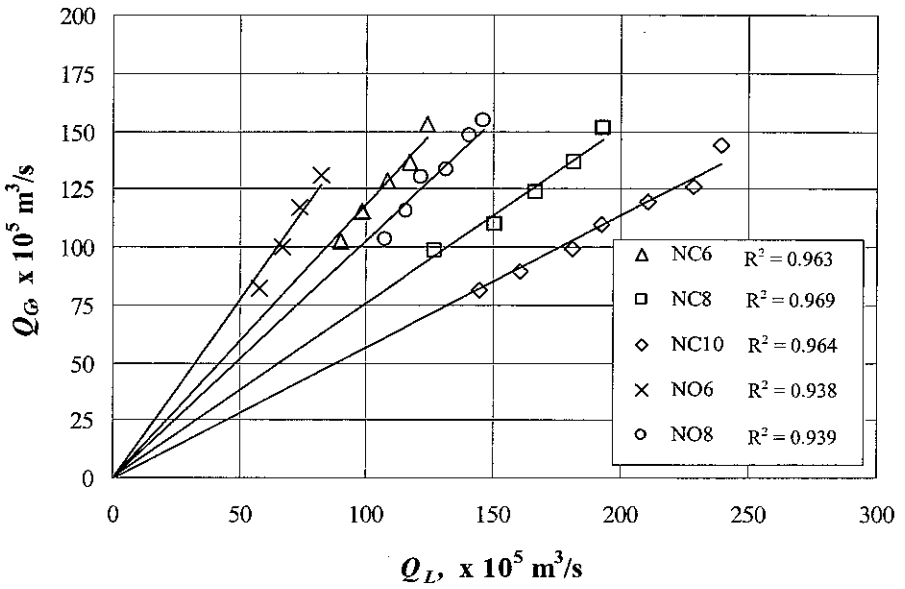

Figure 4.24. Correlation between the predicted values of water flow rate and air entrainment rate

By comparing plots obtained from Figure 4.24 with those shown in Figure 4.13, it is known that the predicted values of water and air flow rates are found lower than the experimental values. Deviation between predicted and experimental water flow rates is found very small with an average error of 3 %. On the other hand, deviation for air entrainment rate is found quite big with an average error of 20 %. This can be explained by the fact that the calculation of air entrainment rate involves several steps. First, suction pressure (P_s) is calculated through Equation (4.2). Apparently, this step of calculation provides certain amount of error. This error gets larger when suction pressure (P_s) is used further to calculate the air entrainment rate through Equation (3.15). As a result, the predicted values of air entrainment rate give rather big deviation to the experimental values.

4.10 Energy Dissipation in the Ejector

Air dispersion into the water in the ejector causes pressure loss. This pressure loss indicates the amount of energy being used to create intense mixing between water and air in the system. This phenomenon can be explained by Equation (3.2). The dissipated

energy is represented by E_D, while dP and Q_M are differential pressure in the ejector and mixture flow rate, respectively. Equation (3.2) can be written further as:

$$E_D = (P_d Q_{M,d}) - (P_s Q_{M,s}) \tag{4.5}$$

Figure 4.25 illustrates the effect of mixture flow rates at the suction chamber on the dissipated energy in the ejector.

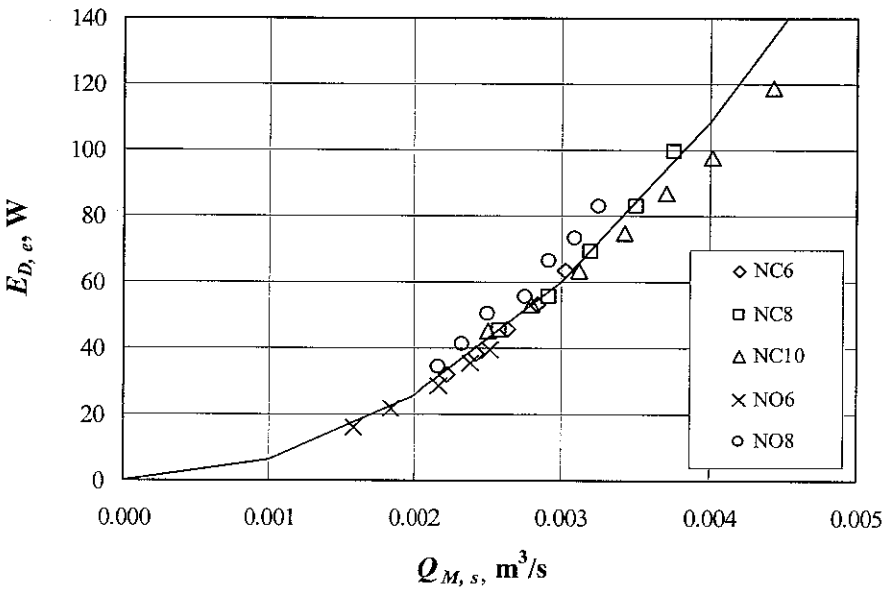

Figure 4.25. Effect of mixture flow rate at the suction chamber on the dissipated energy for different nozzles

It is known from Equation (4.2) that pressure drop in the system is proportional to the square of flow rate. Therefore, by applying this relationship in Equation (4.5) results that energy dissipation is proportional to the third power of mixture flow rate. The relationship between energy dissipation in the ejector and mixture flow rate at the suction chamber is shown in Figure 4.26. It is observed from the plot, that E_D varies linearly with Q_M^3.

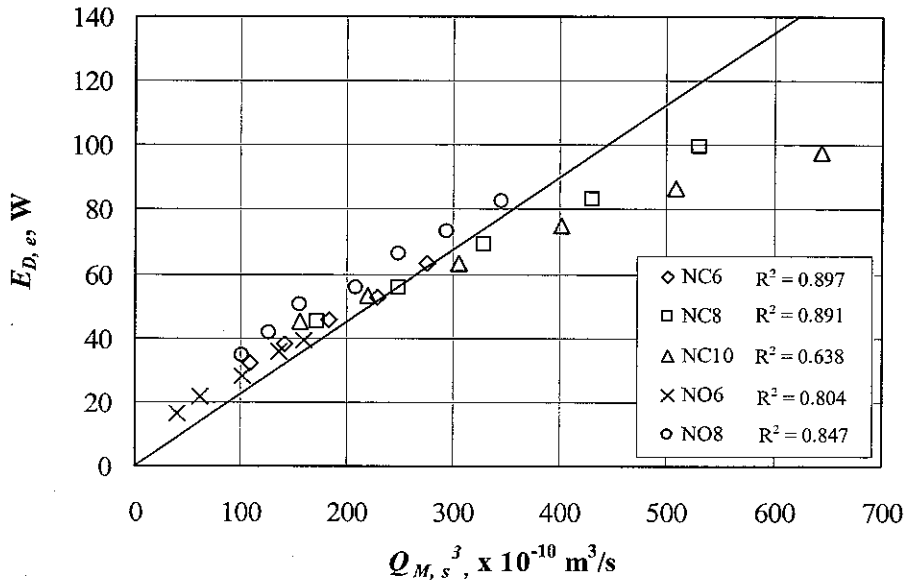

Figure 4.26. Relationship between energy dissipation in the ejector and the third power of mixture flow rate at the suction chamber

However, it can be observed from Figure 4.26 that NC8 and NC10 perform deviation from the straight line. This is due to the fact that NC8 and NC10 have lower air entrainment rate for the same water flow rate than NO6, NC6 and NO8. As a result, it is found that NC8 and NC10 have lower mixture flow rate at the diffuser outlet compared to other nozzles. Therefore, by referring to Equation (4.5), this condition makes the dissipated energy in the ejector for NC8 and NC10 lower than for NO6, NC6 and NO8.

The energy dissipation in the ejector calculated based on the pressure drop information extends within range 16.2 – 118.9 W. These values are higher compared to the results of Zahradnik et al. (1997) which only ranges from 0 – 22.4 W. This is due to the ability of the present system to provide wider range of water flow rate and perform better dispersion between the two phases.

4.11 Gas Hold-Up Analysis

Gas hold-up have been measured using flow isolation technique as described in Section 3.4.7. Experiments have been conducted using five different nozzles and atmospheric air

as suction fluid. The effect of entrained air flow rate on the gas hold-up with different nozzles is illustrated in Figure 4.27.

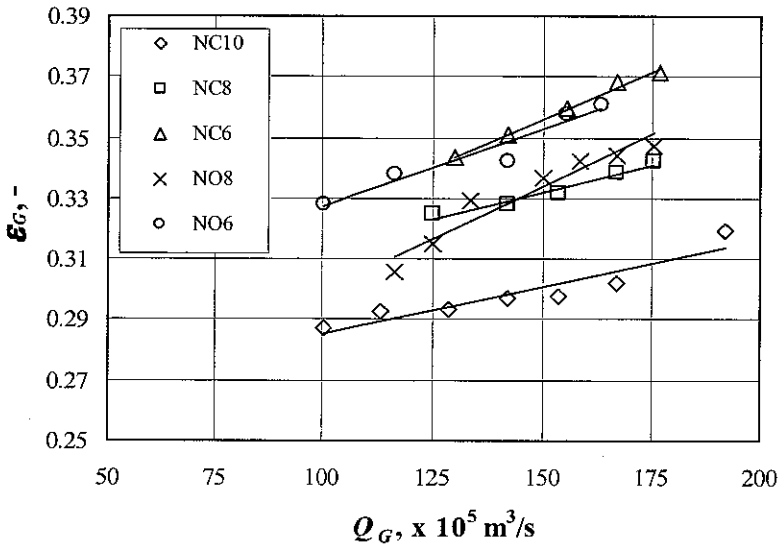

Figure 4.27. The effect of entrained air flow rate on gas hold-up for various nozzles

It is found from the experiment that gas hold-up profiles are clustered according to the nozzle sizes (6 mm, 8 mm and 10 mm nozzles). Higher gas hold-up values are provided by 6 mm nozzles. This is due to higher vacuum level obtained using smaller nozzles. This condition causes more air sucked into the system. This corroborates the results of Radhakrishnan and Mitra (1984), Zahradnik et al. (1997) and Mandal et al. (2005). A comparative picture comprising superficial velocities and gas hold-up of the present work and previous works with different jet type is presented in Table 4.2.

Table 4.2 Comparison of gas and liquid superficial velocities, and gas hold-up for different types of jet bubble column

Investigator	**Type of Reactor**	**Superficial Liquid Velocity, v_L, m/s**	**Superficial Gas Velocity, v_G, m/s**	**Gas hold-up, ε_G, -**
Radhakrishnan and Mitra, (1984)	Upflow ejector bubble column	0.04 – 0.17	0.73 – 1.00	0.13 – 0.41
Huynh et al. (1991)	Upward venturi column	0.175 – 0.353	0.05 – 0.25	0.05 – 0.30
Briens et al. (1992)	Downflow venturi column	0.20 – 0.50	0.01 – 0.10	0.15 – 0.40
Zahradnik et al. (1997)	Upflow ejector	0.01 – 0.03	0.02 – 0.06	0.06 – 0.22
Mandal et al. (2003)	Downflow ejector bubble column	0.07 – 0.16	0.01 – 0.08	0.40 – 0.60
Present work (2008)	**Upflow ejector bubble column**	**0.13 – 0.55**	**0.22 – 0.42**	**0.28 – 0.37**

From Table 4.2, it can be observed that gas hold-up value obtained in the present work is higher than Huynh et al. (1991), Briens et al. (1992) and Zahradnik et al. (1997). This is due to the fact that the present work has higher gas superficial velocity than theirs. Moreover, it can also be concluded that ejectors as is a very effective equipment to be used as gas distributor as they can entrain more amount of suction fluid into the system compared to venturi or other gas distributors for the same flow rate of motive fluid. Furthermore, this current work provides quite similar values of gas hold-up to the results of Radhakrishnan and Mitra (1984). However, Radhakrishnan and Mitra (1984) used multi-jet nozzles in their system which enables motive fluid with low flow rate to produce greater vacuum level and entrain more amount of suction fluid compared to single-jet nozzle. It is also found that the present work have lower gas hold-up value compared to the results of Mandal et al. (2003). This is because downflow column in their work has longer residence time than upflow column which is used in this current work. However, downflow columns cannot be applied with high flow rate due to the risk of flooding. This emphasizes that upflow bubble column with ejector is an efficient and flexible gas-liquid contacting device.

Gas hold-up data is then analyzed using drift-flux model as described in Section 3.4.6. Drift-flux model provides information about the two-phase flow behavior and concentration distribution across the column as well as the effect of local relative velocity between the two phases. In this correlation, gas true velocity is plotted against the mixture velocity. Figure 4.28 shows the drift-flux correlation for each nozzle.

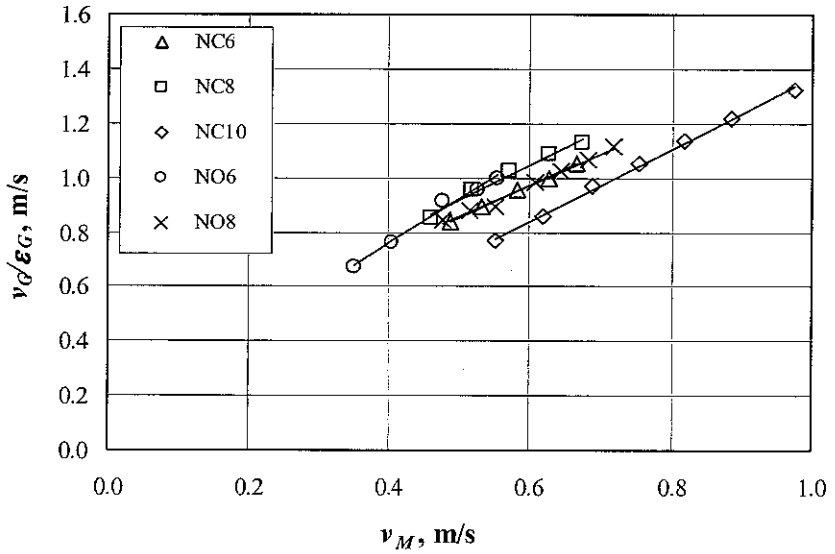

Figure 4.28. Drift-flux correlation for ejector bubble column

Slope for each line in Figure 4.28 represents the distribution parameter (C_o) which accounts for the effect of non-uniform flow and gas-phase concentration profiles, while the intercept shows the weighted average drift velocity (v_D) which accounts for the effect of local relative velocity. Table 4.3 shows the distribution parameter (C_o) and drift velocity (v_D) for each nozzle.

Table 4.3. Values of drift-flux parameters obtained from experimental data

Nozzle	C_o	v_D (m/s)
NC10	1.43	0.04
NC8	1.30	0.26
NC6	1.21	0.25
NO8	1.16	0.27
NO6	1.61	0.12

From Table 4.3, it is observed that the distribution parameters (C_o) obtained from the experiment ranges from 1.16 – 1.61. This range indicates that the fluid flows in all experiments have a center-peaked radial gas hold-up profile ($C_o > 1$) which means air travels faster than water in the column (Majumder et al., 2006). The drift velocities from the experiments extend within the range 0.04 – 0.26 m/s. The presence of nozzle has very little effect on the distribution parameter and drift velocity. Comparison between the present work and other reported works on C_o and v_D is presented in Table 4.4.

Table 4.4 Comparison of distribution parameter and drift velocity for different works

Investigator	**System**	**Distribution Parameter (C_o), -**	**Drift Velocity (v_D), m/s**
Kelkar et al. (1983)	n-butanol-Air	1.24	0.06
	n-propanol-Air	1.30	0.066
	Ethanol-Air	1.60	0.074
Clark and Flemmer (1985)	Water-Air Upflow	1.07	0.25
Chandrakar et al. (1985)	CMC-1-Air	1.37	0.22
	CMC-2-Air	1.54	0.29
	CMC-3-Air	1.70	0.25
Present work (2008)	**Water-Air Upflow**	**1.16 - 1.61**	**0.04 - 0.26**

Gas hold-up analysis with drift-flux correlation of the present work agrees well with the results achieved by Clark and Flemmer (1985). In a water-air system, Clark and Flemmer (1985) obtained an average value as 1.07 and 1.17 for conventional upflow and downflow bubble column, respectively. They also obtained the value of drift velocity 0.25 m/s for upflow bubble column and that for downflow -0.25 m/s for water-air system.

4.12 Summary

Experimental observations on air entrainment rate, pressure profiles, pressure drop and gas hold-up in an ejector-induced cocurrent upflow bubble column for various nozzles

have been conducted. Energy dissipation in the ejector section has been calculated using the pressure drop information and applying Equation (3.2).

6 mm orifice nozzle (NO6) has the ability to develop higher vacuum compared to other nozzles. Hence, it entrains more air from the atmosphere and has higher gas hold-up and energy dissipation compared to those with larger diameter. In terms of nozzle type, orifice nozzles develop higher vacuum than convergent nozzles.

Mathematical correlations have been developed to predict the water pressure drop across the nozzle, the air pressure drop across the air inlet line and air entrainment rate using fundamental principle of fluid mechanics. It is found from the models that air entrainment rate depends highly on the water flow rate and the nozzle diameter.

Experimental gas hold-up data have been presented and analyzed using drift flux model. The model shows that fluid flows in all experiments have a center-peaked radial gas hold-up profile, which means air travel faster than water in the column. The parameter values obtained from the analysis have good agreement with the previous works.

CHAPTER 5

CONCLUSIONS AND RECOMMENDATIONS

5.1 Conclusions

Application of ejector-induced cocurrent upflow bubble column is predicted to give advantageous features such as the ability to provide intimate mixing between gas phase and liquid phase, and lower power consumption as suction fluid is entrained into the system without the need of prime movers. These advantages of ejectors integrated with bubble columns make them potential candidates to replace conventional devices and be used in many chemical applications such as for carbon dioxide absorption from natural gas, desorption and scrubbing, gas-liquid reactions, aerobic fermentation, waste water treatment etc.

In the present work, the effect of nozzle geometry on hydrodynamic parameters such as gas entrainment rate, pressure drop, energy dissipation and gas hold-up have been studied for water-air system. It is observed from the experiment that the flow rate of water, as the motive fluid, and the nozzle types and sizes are important factors in determining the vacuum level developed in the suction chamber. An opportunity to develop high vacuum allows more air, as the suction fluid, to be entrained into the suction chamber. As more air entrained into the suction chamber and dispersed into the water, the gas hold-up and energy dissipation in the ejector increases. This energy dissipation indicates the amount of energy loss to create intense dispersion between air and water.

Experimental observations show that for the same nozzle type, nozzle with 6 mm in diameter develops higher vacuum and therefore entrains more air into the suction chamber compared nozzles with 8 mm and 10 mm in diameter. This also means that nozzles with smaller nozzle diameter have higher gas hold-up and dissipates greater amount of energy to create an intense contact between air and water. In terms of nozzle type, orifice nozzles present higher vacuum level than convergent nozzles for the same nozzle diameter. Pressure drop in the ejector within the studied range of water flow rate ranges from 27777 – 55080 Pa, while pressure drop in the total system ranges from 11537 – 40477 Pa. The two-phase friction factor in the total system is found to extend within

range 0.07 – 38.14 which is found to be lower than work carried out by Radhakrishnan and Mitra (1984). Furthermore, energy dissipation in the ejector have also been calculated using the pressure drop information. The values range from 16.2 – 118.9 W which is found to be higher than results obtained by Zahradnik et al. (1997). Measurement on gas hold-up shows agreeable results to the previous works and gives values in range of 0.28 – 0.37.

An attempt to analyze experimental data using fundamental principles of fluid mechanics has been successfully performed. Application of Bernoulli principle for water flow through nozzle is also performed with the introduction of coefficient of discharge, C_v, to represent the frictional losses across the nozzle. The values of coefficient of discharge for convergent and orifice nozzles in this present work agree with the theoretical values of coefficient of discharge for well-designed venturi and orifice shape, respectively. Moreover, a mathematical correlation to predict air entrainment rate have been presented. The correlation is a function of several operating conditions (P_l, Q_l, and T) and the dimension of ejector parts (D_n and D_a). Predicted values calculated using Bernoulli principle show good agreement with experimental data. Furthermore, gas hold-up data has also been analyzed using drift-flux model. It is found from the analysis that the distribution parameter, C_o, ranges from 1.16 – 1.61 which proves that the radial gas hold-up distribution in the system is center peaked. The drift velocity, v_D, found from the analysis is in range of 0.04 – 0.26 which agrees well with the previous works. However, the presence of nozzle has very little effect to the distribution parameter and drift velocity in the ejector-induced bubble column.

5.2 Recommendations

Based on this work, some recommendations as future works that may provide further insight into the development and application of ejector-induced cocurrent upflow bubble column as a good gas-liquid contactor are made. It is recommended that ejector-induced cocurrent upflow bubble column to be designed compactly. A compact design of ejector-induced cocurrent upflow bubble column can be done by reducing the height of bubble column section, since efficient dispersion between gas and liquid phase happens very intensely only in the ejector section. Calculation of interfacial area and mass transfer

coefficient should be conducted to give more understandable knowledge of the equipment characteristics. It is also suggested that experiments using CO_2-CO_2 absorbents (physical and chemical solvents) to be carried out to study the absorption performance of the equipment. Moreover, experiments using more nozzle types with different sizes are recommended for further understanding on the effect of nozzle geometry on the hydrodynamic characteristics of the column.

PUBLICATIONS

This research has been published and presented in several conferences as follows:

1. F. Rahman and M. Ramasamy, (2007). "Hydrodynamics Studies in Ejector Induced Cocurrent Upflow Bubble Column", Symposium of Malaysian Chemical Engineers, Malaysia.

2. Fauzan Rahman, M. Ramasamy and D. Subbarao, (2008). "Effect of Nozzle Geometry on the Hydrodynamics of Ejector-Induced Cocurrent Upflow Bubble Column", National Postgraduate Conference, Universiti Teknologi PETRONAS, Malaysia.

REFERENCES

1. Acharjee, D.K., Bhat, P.A., Mitra, A.K. and Roy, A.N., (1975). "Studies on momentum transfer in vertical liquid jet ejectors", *Indian Journal of Technology*, 13: 205–210.

2. Armand, A.A. and Treschev, G.G., (1946). "The resistance during the movement of a two-phase system in horizontal pipes", *Izv. Vses. Teplotek. Inst.*, 1: 16–23.

3. Balamurugan, S., Lad, M.D., Gaikar, V.G. and Patwardhan, A.W., (2007). "Hydrodynamics and mass transfer characteristics of gas-liquid ejectors", *Chem. Eng. J.*, doi:10.1016/j.cej.2006.12.026.

4. Balamurugan, S., Gaikar, V.G., Patwardhan, A.W., (2008). "Effect of ejector configuration on hydrodynamic characteristics of gas-liquid ejectors", *Chem. Eng. Sci.*, 63: 721–731.

5. Bankoff, S.G., (1960). "A Variable Density Single-Fluid Model for Two Phase Flow With Particular Reference to Steam-Water Flow", *Journal of Heat Transfer*, Vol. 82, No. 4: 265–272.

6. Bauer, W.J., Fredrickson, A.G. and Tsuchiya, H.M., (1963). "Mass transfer characteristics of a venturi liquid-gas contactor", *Ind. Eng. Chem. Process Design Dev.*, 2: 178–187.

7. Behringer, H., (1936). "The flow of liquid–gas mixtures in vertical tubes", *Zeitschrift für die Gesamte Kälte-Industrie*, 43: 55–58.

8. Bhat, P.A., Mitra, A.K.; Roy, A.N., (1972). "Momentum transfer in a horizontal liquid jet ejector", *Can. J. Chem. Eng.*, 50: 13–317.

9. Bhutada, C.L., and Pangarkar, V.G., (1992). "Gas induction and hold-up characteristics of liquid jet loop reactors", *Chemical Engineering Communication*, 61: 239–261.

10. Biswas, M. N., Mitra, A. K., Roy, A. N., (1975). "Studies on gas dispersion in a horizontal liquid jet ejector", *Second Symposium on Jet Pumps and Ejectors and Gas Lift Techniques*, Cambridge, England, March 24–26, BHRA: E3-27-42.

11. Bouaifi, M., Hebrard, G., Bastoul, D., and Roustan, M., (2001). "A comparative study of gas hold-up, bubble size, interfacial area and mass transfer coefficients in stirred gas-liquid reactors and bubble columns", *Chemical Engineering and Processing*, 40: 97–111.

12. Briens, C.L., Huynh, L.X., Large, J.F., Catros, A., Bernard, J.R., Bergougnou, M.A., (1992). "Hydrodynamics and gas–liquid mass transfer in a downward venturi-bubble column combination", *Chem. Eng. Sci.* 47: 3549–3556.

13. Brutin, D., and Tadrist, L., (2004). "Pressure drop and heat transfer analysis of flow boiling in a minichannel: influence of the inlet condition on two-phase stability", *Int. Jou. of Heat and Mass Transfer* , 47: 2365–2377.

14. Chandrakar, S.K., Biswas, M.N. and Mitra, A.K., (1985). "Two-phase gas non-Newtonian liquid flow in vertical pipe with improved gas dispersion", Paper presented at the *Second International Conference on Multiphase Flow*, London: 197–213.

15. Chaumat H., Billet-Duquennea A.M., Augierb F., Mathieub C. and Delmasa H., (2005). "Mass transfer in bubble column for industrial conditions—effects of organic medium, gas and liquid flowrates and column design", *Chem. Eng. Sci.* 60: 5930–5936.

16. Clark, N.N. and Flemmer, R.L., (1985). "Predicting the holdup in two-phase bubble upflow and downflow using the Zuber and Findlay drift-flux model", *A.I.Ch.E. Journal*, 31: 500–503.

17. Cramers, P.H.M.R., Beenackers, A.A.C.M. and Van Dierendonck, L.L., (1992). "Hydrodynamics and mass transfer characteristics of a loop-venturi reactor", *Chem. Eng. Sci.*, 47: 3557–3564.

18. Cramers, P.H.M.R. and Beenackers, A.A.C.M., (2000). "Influence of the ejector configuration, scale and the gas density on the mass transfer characteristics of gas-liquid ejectors", *Chem. Eng. Jou.*, 82: 131–141.

19. Cui, Z., (2005). "Hydrodynamics in a bubble column at elevated pressures and turbulence energy distribution in bubbling gas-liquid and gas-liquid-solid flow systems", Doctoral Dissertation, The Ohio State University.

20. Cunningham, R.G., (1974). "Gas compression with the liquid jet", *Journal of Fluids Engineering*, 96(3): 203–215.

21. Cunningham, R.G. and Dopkin, R.J., (1974). "Jet breakup and mixing throat lengths for the liquid jet gas pump", *Transcripts of ASME—Journal of Fluids Engineering*, 96: 216–226.

22. Das, S. K. and Biswas, M.N., (2006). "Studies on ejector-venturi fume scrubber", *Chem. Eng. Jou.*, 119: 153–160.

23. Dautzenberg, F. M. and de Deken, J. C., (1984). "Reactor developments in hydrotreating and conversion of residues", *Catal. Rev. Sci. Eng.*, 26: 421.

24. Davies, G.S., Mitra, A.K., Roy, A.N., (1967). "Momentum transfer studies in ejectors", *Ind. and Eng. Chem. Process Design and Development*, 6: 293–299.

25. Deckwer, W.-D., (1992). "Bubble Column Reactors", John Wiley and Sons, Chichester, England.

26. Deshpande, N.S., Prasad, C.H.V., Kulkarni, A.A. and Joshi, J.B., (2000). "Hydrodynamic Characterization of Dispersed Two-Phase Flows by Laser Doppler Velocimeter", *Trans IChemE*, Vol 78, Part A: 903–910.

27. Dhaouadi H., Poncin S., Hornut J.M. and Midoux N., (2007). "Gas–liquid mass transfer in bubble column reactor: Analytical solution and experimental confirmation", *Chem. Eng. Process.*, doi:10.1016/j.cep.2006.11.009.

28. Elenkov, D., Boyadzhiev, K., (1967). "Hydrodynamics and mass transfer in a nozzleless venturi absorber. II Absorption of sulfur dioxide in water and aqueous solutions of surfactants", *Int. Chem. Eng.* 7, 2: 191–193.

29. Evans, G.M., Jameson, G.J., Rielly, C.D., (1996). "Free jet expansion and gas entrainment characteristics of a plunging liquid jet". *Experimental Thermal and Fluid Science*, 12 (2): 142–149.

30. Flügel, G., (1951). "Berechnung von Strahlapparaten", *VDI-Forschungshefte*, nüm. 395, 2' ed. Düsseldorf.

31. Folsom, R.G., (1948). "Jet pumps with liquid drive", *Chem. Eng. Progress*, 44, 10: 765–770.

32. Fregapane, G., Rubio-Fernandez, H., Nieto, J. and Salvador, M. D., (1999). "Wine vinegar production using a noncommercial 100-litre bubble column reactor equipped with a novel type of dynamic sparger", *Biotechnology and Bioengineering*, 63: 141.

33. Gamisans, X., Sarra, M. and Lafuente, F.J., (2004). "Fluid flow and pumping efficiendy in an ejector-venturi scrubber", *Chemical Engineering and Processing*, 43: 127–136.

34. Gourich, B., El Azher, N., Vial, C., Belhaj Soulami, M., Ziyad, M. and Zoulalian, A., (2006). "Influence of operating conditions and design parameters on

hydrodynamics and mass transfer in an emulsion loop-venturi reactor", *Chemical Engineering and Processing*, doi:10.1016/j.cep.2006.05.006.

35. Govier, G.W., Radford, B.A. and Dunn, J.S.C., (1957). "The Upward Vertical Flow of Air-Water Mixtures I. Effect of Air and Water Rates on Flow Pattern, Hold-Up and Pressure Drop", *Can. J. Chem. Eng.* 35: 58–70.

36. Griffith, P. and Wallis, G.B., (1961). "Two-Phase Slug Flow", *J. Heat Transfer;*. Trans. ASME: 307–320.

37. Hagedorn, A. R. and Brown, K. E., (1964). "The effect of viscosity on. two-phase vertical flow", *J. Pet. Tech.*, 16: 203–210

38. Hagedorn, A. R. and Brown, K. E., (1965). "Experimental study of pressure gradient occurring during continuous two-phase flow in a small diameter vertical conduits", *J. Pet. Tech.*, 17: 475–484.

39. Havelka, P., Linek, V., Sinkule, J., Zahradnik, J., and Fialova, M., (1997). "Effect of the ejector configuration on the gas suction rate and gas hold-up in ejector loop reactors", *Chem. Eng. Sci.*, 52: 1701–1713.

40. Havelka, P., Linek, V., Sinkule, J., Zahradnik, J., and Fialova, M., (2000). "Hydrodynamic and mass transfer characteristics of ejector loop reactors", *Chem. Eng. Sci.*, 55: 535–549.

41. Hibiki, T., and Ishii, M., (2003). "One-dimensional drift-flux model for two-phase flow in a large diameter pipe", *Int. Jou. of Heat and Mass Transfer* , 46: 1773–1790.

42. Hills, J.H., (1976). "The operation of a bubble column at high throughputs I. Gas Measurements), *Chem. Eng. Jou.*, 12: 89–99.

43. Hoefer, K., (1922). "Experiments on vacuum pumps for condensers", *VDI Forschung*, No. 253.

44. Hughmark, G. A., Pressburg, B. S., (1961). "Holdup and pressure drop with gas-liquid flow in a vertical pipe", *AIChE J.*, 7(4): 677-682.

45. Huynh, X., Briens, C. L., Catros, A., Bernard, J. R. and Bergougnou, M. A., (1991). "Hydrodynamics and Mass Transfer in an Upward Venturi/Bubble Column Combination", *Can. J. of Chem. Eng.* 69, 711–722.

46. Isbin, H.S., Sher, N.C. and Eddy, K.C., (1957). "Void fractions in two-phase steam-water flow", *A.I.Ch.E. Journal*, 3: 136–142.

47. Jackson, M.L., (1964). "Aeration in Bernoulli types of devices", *American Institute Chem. Eng. Jou.*, 10: 836–842.

48. Jager, B. and Espinoza, R, (1995). "Advances in Low Temperature Fischer-Tropsch Synthesis", *Catal. Today*, 23: 17.

49. Jin, H., Yang, S., Wang, M. and Williams, R.A., (2007). " Measurement of gas holdup profiles in a gas liquid cocurrent bubble column using electrical resistance tomography", *Flow Measurement and Instrumentation*, 10.1016/j.flowmeasinst.2007.07.005.

50. Kandakure, M.T., Gaikar, V.G., Patwardhan, A.W., (2005). "Hydrodynamic aspects of ejectors", *Chem. Eng. Sci.*, 60: 6391–6402.

51. Kazakis, N.A., Papadopoulos, I.D. and Mouza, A.A., (2007). "Bubble columns with fine pore sparger operating in pseudo-homogeneous regime: Gas hold-up prediction and a criterion for the transition to heterogeneous regime", *Chem. Eng. Sci.*, 62: 3092–3103.

52. Kelkar, B.G., Godbole, S.P., Honath, M.F., Shah, Y.T., Carr, N.L., and Deckwer,W.D., (1983). "Effect of addition of alcohols on gas holdup and backmixing in bubble columns", *A.I.Ch.E. Journal*, 29: 361–369.

53. Kim, M.I., Kim, O.S., Lee, D.H., and Kim, S.D, (2007). "Numerical and experimental investigations of gas-liquid dispersion in an ejector", *Chem. Eng. Sci.*, 62: 7133–7139.

54. Kocamustafaogullari, G., Smits, S.R. Razi, J., (1994). "Maximum and mean droplet sizes in annular two-phase flow", *Int. J. Heat and Mass Transfer.* 37, (6): 955–965.

55. Kulkarni A. and Shah, Y. T., (1984). "Gas Phase Dispersion in a Downflow Bubble Column", *Chem Eng. Commun.*, 28: 311–326.

56. Kundu, G., Mukherjee, D. and Mitra, A.K., (1995). "Experimental studies on a co-current gas–liquid downflow bubble column", *International Journal of Multiphase Flow,* 21: 893–906.

57. Lapple, C.E., (1951). "Fluid and Particle Mechanics", *University of Delaware,* Newark, Delaware.

58. Levy, S., (1966). "Forced convection subcooled boiling prediction of vapour volumetric fraction", *Int. Jou. Heat and Mass Transfer*, 10: 951–965.

59. Lockhart, R.W. and Martinelli, R.C., (1949). "Proposed correlation of data for isothermal two-phase, two component flow in pipes", *Chem. Eng. Progress*, 45: 39–44.

60. Magaud, F., Souhar, M., Wild, G. and Boisson, M., (2001). "Experimental study on bubble column hydrodynamics", *Chem. Eng. Sci.*, 56: 4597–4607.

61. Majumder, S.K., Kundu, G. and Mukherjee, D., (2006). "Efficient dispersion in a modified two-phase non-Newtonian downflow bubble column", *Chem. Eng. Sci.*, 61: 6753–6764.

62. Mandal, A., Kundu, G. and Mukherjee, D., (2003). "Gas holdup and entrainment characteristics in a modified downflow bubble column with Newtonian and non-Newtonian liquid", *Chemical Engineering and Processing*, 42: 777–787.

63. Mandal, A., Kundu, G. and Mukherjee, D., (2004). "Studies on frictional pressure drop of gas-non-Newtonian two-phase flow in cocurrent downflow bubble column", *Chem. Eng. Sci.*, 42: 3807–3815.

64. Mandal, A., Kundu, G. and Mukherjee, D., (2005). "Comparative Study of Two-Phase Gas-Liquid Flow in the Ejector Induced Upflow and Downflow Bubble Column", *Int. Jou. of Chemical Reactor Engineering*, 3: A13.

65. Miller, J.R., (1969). "The Liquid-Gas Ejector". New Mexico State University, Sc.D., Engineering, hydraulic.

66. Moresi, M., Gianturco, G.B. and Sebastiani, E., (1983). "The ejector-loop fermenter: description and performance of the apparatus", *Biotechnol. Bioeng.*, 25 (12): 2889–2904.

67. Ogawa, S., Yamaguchi, H., Tone, S. and Otake, T., (1983). "Gas-liquid mass transfer in the jet reactor with liquid jet ejector", *J. Chem. Eng. Jpn.*, 16: 1939–1948.

68. Ohkawa, A., Kusabiraki, D., Kawai, Y. and Sakai, N., (1986). " Some flow characteristics of a vertical liquid jet system having downcomers", Chem. Eng. Sci., 41: 2347–2361.

69. Otake, T., Tone, S., Kuboi, R., Takahashi, Y. and Nakao, K., (1981). "Dispersion of a gas by liquid jet ejector", *Int. Chem. Eng.*, 21: 72–80.

70. Pal, S.S., Mitra, A.K. and Roy, A.N., (1979). "Pressure drop and gas holdup in vertical two-phase cocurrent flow with improved gas-liquid mixing", *Ind. Eng. Chem. Process Design and Development*, 19: 67–75.

71. Patel, A.K. and Thorat, B.N., (2008). "Gamma ray tomography—An experimental analysis of fractional gas hold-up in bubble columns", *Chem. Eng. Jou., Volume 137*, Issue 2: 376–385.

72. Perry, R.H and Green, D.W., (1999). "Perry's Chemical Engineer's Handbook 7th Ed.", *McGraw-Hill.*

73. Radhakrishnan, V.R. and Mitra, A.K., (1984). "Pressure drop, Holdup and Interfacial Area in Vertical Two-Phase Flow of Multi-Jet Ejector Induced Dispersions", *Can. Jou. of Chem. Eng.*, 62: 170–178.

74. Ros, N.C.J., (1961). "Simultaneous Flow of Gas and Liquid as Encountered in Well Tubing", *J. Pet. Tech.*:1037–1049.

75. Rylek, M. and Zahradnik, J., (1984). "Design of Venturi-tube gas distributors for bubble type reactors", *Coll. Czech Chem. Comm.*, 49: 1939–1948.

76. Schugerl, K., Lucke, J. and Oels, U., (1977). "Bubble column bioreactors: tower bioreactors without mechanical agitation", *Adv. Biochem. Eng.*, **7**: 1.

77. Schweitzer, J-M., Bayle, J. and Gautier, T., (2001). "Local gas hold-up measurement in fluidized bed and slurry bubble column", *Chem. Eng. Sci.*, 56: 1103–1110.

78. Smith, R.A., (1951). "Some Aspects of Fluid Flow", *Inst. of Physics.*, Edward Arnold and Co, London: 229.

79. Stepanek, J.B. and Kasturi, G., (1972). "Two phase flow – II. Parameters for void fraction and pressure drop correlations", *Chem. Eng. Sci.*, 27: 1881–1891.

80. Sun, Haiyan., Mao, Zai-Sha. and Yu, Gengzhi., (2006). "Experimental and numerical study of gas hold-up in surface aerated stirred tank", *Chem. Eng. Sci.*, 61: 4098–4110.

81. Takashima, Y., (1952). "Studies on liquid-jet gas pumps", *Jou. Scientific Research Institute (Tokyo)*, 46: 230–246.

82. Tang, C. and Heindel, T.J., (2006). "A gas holdup model for cocurrent air-water-fiber bubble columns", *Chem. Eng. Sci.*, 61: 3299–3312.

83. Tang, C. and Heindel, T.J., (2006). "Estimating gas holdup via pressure drop measurements in a cocurrent bubble column", *Int. Jou. of Multiphase Flow*, 32: 850–863.

84. Veera, U.P., Kataria, K.L. and Joshi, J.B., (2004). "Effect of superficial velocity on gas hold-up profiles in foaming liquids in bubble column reactors", *Chem. Eng. Jou.*, 99: 53–58.

85. Von Pawel-Rammingen, G., (1936). "Experiments on Ejectors", M.S. Dissertations, Pennsylvania State University.

86. Witte, J.H., (1966). "Efficiency and design of liquid-gas ejectors", *Brit. Chem. Eng.* 32: 602–607.

87. Witte, J.H., (1969). "Mixing shocks in two phase flow", *J. Fluid Mech.* 36 ((4): 639–655.

88. Woerlee, G.F., Berends, J., Olujic, Z., and de Graauw, J., (1999). "A comprehensive model for the pressure drop in vertical pipes and packed columns", *Chem. Eng. Jou.*, 84: 367–369.

89. Xie, T. Ghiaasiaan, S.M., Karrila, S. and McDonough, T., (2003). "Flow regimes and gas holdup in paper pulp-water-gas three phase slurry flow", *Chem. Eng. Sci.*, 58: 1417–1430.

90. Zahradnik, J., Kratochvil, J. and Rylek, M., (1985). "Gas holdup and interfacial mass transfer in gas-liquid tower contactors with ejector-type gas distributors", *Collect. Czech. Chem. Commun.* 50: 2535–2544.

91. Zahradnik, J., Fialova, M., Linek, V., Sinkule, J., Reznickova, J. and Kastanek, F., (1997). "Dispersion efficiency of ejector-type gas distributors in different operating modes", *Chem. Eng. Sci.*, 52: 4499–4510.

92. Zlokarnik, M., (1979). "Sorption characteristics of slot injectors and their dependency on the coalescence behaviour of the system", *Chem. Eng. Sci.,* 34: 1265–1271.

93. Zuber, N. and Findlay, J.A., (1965). "Average Volume Concentration in Two-Phase Flow Systems", *J. Heat Transfer*, Ser. C. 87: 453–468.

APPENDIX A

PHYSICAL PROPERTIES AND CONSTANTS

Table A.1 Physical properties and constants used in calculations

Properties and Constants	**Symbol**	**Unit**	**Value**
gravitational acceleration	g	m/s^2	9.8
molecular weight of air	MW_a	kg/kmol	29
molecular weight of water	MW_w	kg/kmol	18
atmospheric pressure	P_A	Pa	101325
ideal gas constant	R	m^3.Pa/mol.K	8.314
viscosity of water (25°C, 1 atm)	μ_W	Pa.s	8.5×10^{-4}
density of water (25°C, 1 atm)	ρ_L	kg/m^3	997

APPENDIX B

EXPERIMENTAL DATA

B.1 Optimization of Nozzle Position

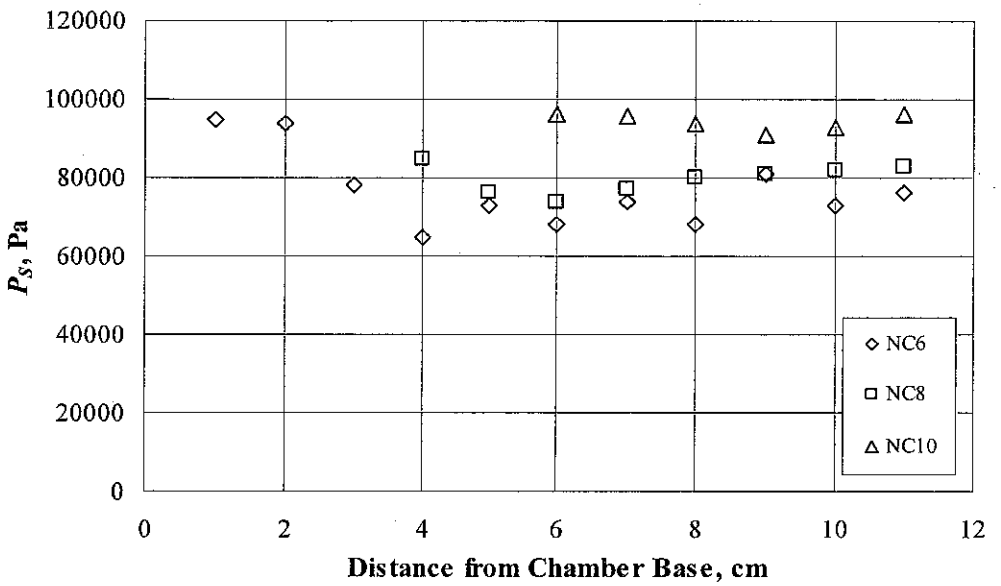

Figure B.1 Optimization of nozzle position for convergent nozzles

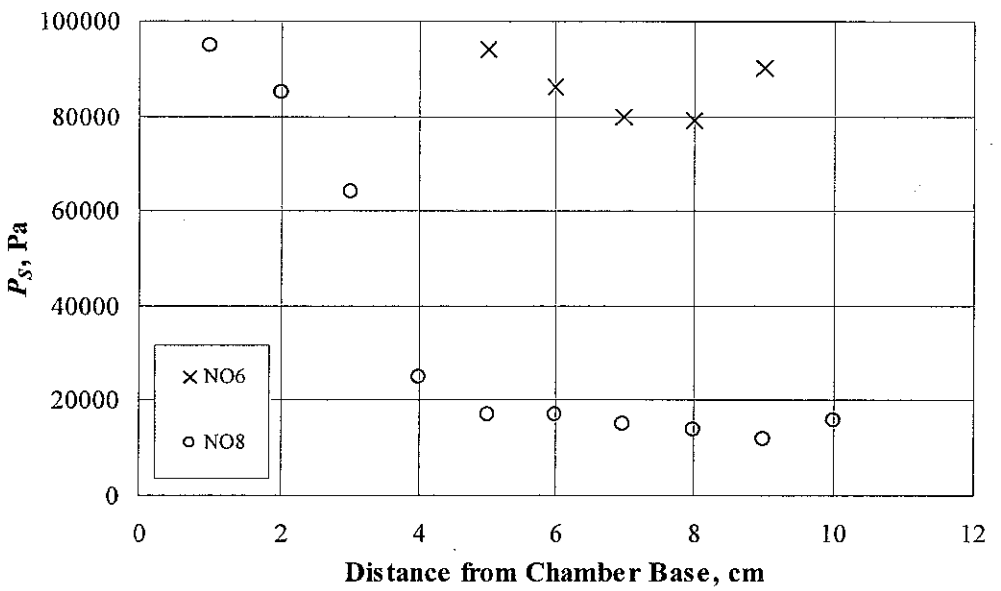

Figure B.2 Optimization of nozzle position for orifice nozzles

Table B.1. Pressure measurement for convergent nozzles

NC6

A_t/A_n: 18.78 T: 298 K

Q_L	Q_G	Q_M	Q_G/Q_L	PI-04 = P_t	PI-06 = P_s	PI-07	PI-08	PI-09 = P_d	PI-10	PI-11	PI-13	PI-14	PI-15	ΔP_T = (PI-15) - (PI-06)
m^3/s	m^3/s	m^3/s	-	Pa	Pa	Pa	Pa	Pa	Pa	Pa	Pa	Pa	Pa	Pa
0.00092	0.00130	0.00222	1.42	586000	83120	88817	98833	117900	115210	111740	107387	105857	101177	18057
0.00100	0.00142	0.00242	1.42	679000	79007	81833	93103	117013	114457	111370	106747	105883	101130	22123
0.00109	0.00155	0.00264	1.43	805000	74423	76900	88710	116747	114333	111510	107130	105973	101280	26857
0.00117	0.00167	0.00284	1.43	948000	71423	73997	85437	116640	114293	111200	106890	105957	101313	29890
0.00125	0.00177	0.00302	1.41	1060000	65477	68073	78057	116167	114160	111233	106910	105967	101277	35800

NC8

A_t/A_n: 10.56 T: 298 K

Q_L	Q_G	Q_M	Q_G/Q_L	PI-04 = P_t	PI-06 = P_s	PI-07	PI-08	PI-09 = P_d	PI-10	PI-11	PI-13	PI-14	PI-15	ΔP_T = (PI-15) - (PI-06)
m^3/s	m^3/s	m^3/s	-	Pa	Pa	Pa	Pa	Pa	Pa	Pa	Pa	Pa	Pa	Pa
0.00134	0.00125	0.00209	0.94	403000	84483	85953	92213	118257	115267	112037	107500	106213	101340	16857
0.00150	0.00142	0.00235	0.94	539000	80887	82157	88240	117767	115280	112117	107570	106197	101393	20507
0.00167	0.00154	0.00259	0.92	659000	76013	77574	83441	117385	115246	112079	107618	106351	101603	25590
0.00184	0.00167	0.00284	0.91	792000	71497	72933	79110	116673	115160	112107	107677	106287	101517	30020
0.00200	0.00175	0.00305	0.88	915000	66047	66897	73813	115680	115093	112120	107553	106397	101560	35513

NC10

A_t/A_n: 6.76 T: 298 K

Q_L	Q_G	Q_M	Q_G/Q_L	PI-04 = P_t	PI-06 = P_s	PI-07	PI-08	PI-09 = P_d	PI-10	PI-11	PI-13	PI-14	PI-15	ΔP_T = (PI-15) - (PI-06)
m^3/s	m^3/s	m^3/s	-	Pa	Pa	Pa	Pa	Pa	Pa	Pa	Pa	Pa	Pa	Pa
0.00150	0.00100	0.00251	0.67	262000	89553	90570	95840	119513	115920	112677	107903	106357	101400	11847
0.00167	0.00114	0.00281	0.68	311000	87203	88153	92180	118977	115883	112577	107890	106460	101387	14183
0.00184	0.00129	0.00312	0.70	385000	84193	85083	88813	118577	115737	112467	107940	106500	101437	17243
0.00200	0.00142	0.00342	0.71	437000	80717	81613	85277	118077	115730	112443	107857	106570	101560	20843
0.00217	0.00154	0.00371	0.71	521000	77417	78320	82443	117463	115710	112493	107807	106523	101523	24107
0.00234	0.00167	0.00401	0.71	617000	75243	76030	80443	117113	115730	112457	107957	106590	101553	26310
0.00251	0.00192	0.00443	0.77	687000	68573	69377	74710	116037	115750	112467	107983	106643	101657	33083

Table B.2. Pressure measurement for orifice nozzles

NO6

A_t/A_n: 18.78 T: 298 K

Q_L	Q_G	Q_M	Q_G/Q_L	PI-04 = P_1	PI-06 = P_s	PI-07	PI-08	PI-09 = P_d	PI-10	PI-11	PI-13	PI-14	PI-15	ΔP_T = (PI-15) - (PI-06)
m^3/s	m^3/s	m^3/s	-	Pa	Pa	Pa	Pa	Pa	Pa	Pa	Pa	Pa	Pa	Pa
0.00058	0.00100	0.00159	1.71	510000	89320	91670	107623	117097	114033	110957	106793	105540	100857	11537
0.00067	0.00117	0.00184	1.75	675000	83957	85683	99430	116500	113763	110730	106607	105487	100890	16933
0.00075	0.00142	0.00217	1.89	810000	78443	80317	94120	116127	113720	110777	106573	105620	100947	22503
0.00084	0.00155	0.00239	1.86	1004000	73497	75180	89197	115963	113693	110680	106617	105643	101100	27603
0.00089	0.00164	0.00252	1.85	1135000	71357	72940	86960	115927	113660	110730	106700	105677	101073	29717

NO8

A_t/A_n: 10.56 T: 298 K

Q_L	Q_G	Q_M	Q_G/Q_L	PI-04 = P_1	PI-06 = P_s	PI-07	PI-08	PI-09 = P_d	PI-10	PI-11	PI-13	PI-14	PI-15	ΔP_T = (PI-15) - (PI-06)
m^3/s	m^3/s	m^3/s	-	Pa	Pa	Pa	Pa	Pa	Pa	Pa	Pa	Pa	Pa	Pa
0.00100	0.00117	0.00217	1.17	418000	82863	84513	95170	117127	114293	111247	107067	105943	101217	18353
0.00109	0.00125	0.00234	1.15	573000	78993	80370	90950	117080	114233	111233	107107	105907	101290	22297
0.00117	0.00134	0.00251	1.14	650000	73847	75323	85760	116820	114333	111373	107157	106027	101307	27460
0.00125	0.00150	0.00276	1.20	722000	72455	73467	83964	116752	114297	111361	107121	106058	101391	28936
0.00134	0.00159	0.00292	1.19	833000	67050	68432	79215	116547	114506	111574	107235	106185	101485	34435
0.00142	0.00167	0.00309	1.18	952000	64753	65903	76830	116277	114647	111613	107440	106253	101550	36797
0.00150	0.00175	0.00326	1.17	1026000	61163	62367	73863	116243	114697	111757	107473	106353	101640	40477

B.3 Pressure Drop across Nozzle

Table B.3. Nozzle pressure drop calculation for various nozzles

NC6

PI-04 = P_1	PI-06 = P_s	Expr. $\Delta P_n = P_1 - P_s$	$(\rho_L Q_L^2/D_n^4)*(1-D_n^4/D_i^4)$	C_v^2	$(\rho_L Q_L^2/D_n^4)*(1-D_n^4/D_i^4)$
Pa	Pa	Pa	Pa		Pa
586000	83120	502880	643749	1.00	643749
679000	79007	599993	766114	1.00	766114
805000	74423	730577	899120	1.00	899463
948000	71423	876577	1042766	0.98	1062926
1060000	65477	994523	1197053	0.96	1241899

NC8

PI-04 = P_1	PI-06 = P_s	Expr. $\Delta P_n = P_1 - P_s$	$(\rho_L Q_L^2/D_n^4)*(1-D_n^4/D_i^4)$	C_v^2	$(\rho_L Q_L^2/D_n^4)*(1-D_n^4/D_i^4)$
Pa	Pa	Pa	Pa		Pa
403000	84483	318517	423336	1.00	423336
539000	80887	458113	535785	0.98	545310
659000	76013	582987	661463	0.94	702480
792000	71497	720503	800370	0.91	884052
915000	66047	848953	952506	0.87	1091254

NC10

PI-04 = P_1	PI-06 = P_s	Expr. $\Delta P_n = P_1 - P_s$	$(\rho_L Q_L^2/D_n^4)*(1-D_n^4/D_i^4)$	C_v^2	$(\rho_L Q_L^2/D_n^4)*(1-D_n^4/D_i^4)$
Pa	Pa	Pa	Pa		Pa
262000	89553	172447	211147	0.98	215214
311000	87203	223797	260675	0.93	280173
385000	84193	300807	315417	0.89	356118
437000	80717	356283	375372	0.85	443775
521000	77417	443583	440541	0.81	543867
617000	75243	541757	510923	0.78	657120
687000	68573	618427	586519	0.75	784259

NO6

PI-04 = P_1	PI-06 = P_s	Expr. $\Delta P_n = P_1 - P_s$	$(\rho_L Q_L^2/D_n^4)*(1-D_n^4/D_i^4)$	C_v^2	$(\rho_L Q_L^2/D_n^4)*(1-D_n^4/D_i^4)$
Pa	Pa	Pa	Pa		Pa
510000	89320	420680	260692	0.50	526297
675000	83957	591043	340495	0.48	705279
810000	78443	731557	430939	0.47	913308
1004000	73497	930503	532024	0.46	1151148
1135000	71357	1063643	597782	0.46	1308460

NO8

PI-04 = P_1	PI-06 = P_s	Expr. $\Delta P_n = P_1 - P_s$	$(\rho_L Q_L^2/D_n^4)*(1-D_n^4/D_i^4)$	C_v^2	$(\rho_L Q_L^2/D_n^4)*(1-D_n^4/D_i^4)$
Pa	Pa	Pa	Pa		Pa
418000	82863	335137	238127	0.47	506629
573000	78993	494007	279468	0.46	602466
650000	73847	576153	324117	0.46	707342
722000	72455	649545	372073	0.45	821383
833000	67050	765950	423336	0.45	944706
952000	64753	887247	477907	0.44	1077424
1026000	61163	964837	535785	0.44	1219645

B.4 Air Pressure Drop across Air Inlet Line

Table B.4. Air pressure drop calculation for various nozzles

NC6

Q_G	PI-06 = P_s	ln (P_A/P_s)	$MW_a.Q_G^2/R.T.D_a^4$
m^3/s	Pa	-	-
0.00130	83120	0.198	0.39
0.00142	79007	0.249	0.47
0.00155	74423	0.309	0.56
0.00167	71423	0.350	0.64
0.00177	65477	0.437	0.72

NO6

Q_G	PI-06 = P_s	ln (P_A/P_s)	$MW_a.Q_G^2/R.T.D_a^4$
m^3/s	Pa	-	-
0.00100	89320	0.126	0.23
0.00117	83957	0.188	0.32
0.00142	78443	0.256	0.47
0.00155	73497	0.321	0.56
0.00164	71357	0.351	0.62

NC8

Q_G	PI-06 = P_s	ln (P_A/P_s)	$MW_a.Q_G^2/R.T.D_a^4$
m^3/s	Pa	-	-
0.00125	84483	0.182	0.36
0.00142	80887	0.225	0.47
0.00154	76013	0.287	0.55
0.00167	71497	0.349	0.64
0.00175	66047	0.428	0.71

NO8

Q_G	PI-06 = P_s	ln (P_A/P_s)	$MW_a.Q_G^2/R.T.D_a^4$
m^3/s	Pa	-	-
0.00117	82863	0.201	0.32
0.00125	78993	0.249	0.36
0.00134	73847	0.316	0.41
0.00150	72455	0.335	0.52
0.00159	67050	0.413	0.58
0.00167	64753	0.448	0.64
0.00175	61163	0.505	0.71

NC10

Q_G	PI-06 = P_s	ln (P_A/P_s)	$MW_a.Q_G^2/R.T.D_a^4$
m^3/s	Pa	-	-
0.00100	89553	0.123	0.23
0.00114	87203	0.150	0.30
0.00129	84193	0.185	0.38
0.00142	80717	0.227	0.47
0.00154	77417	0.269	0.55
0.00167	75243	0.298	0.64
0.00192	68573	0.390	0.85

B.5 Pressure Recovery in the Ejector

Table B.5. Calculation of pressure recovery in the ejector for various nozzles

NC6

PI-06 = P_s	PI-09 = P_d	Expr. $(P_d - P_s)$	$P_h = \rho_L g h_b$	Calc. $P_d = P_A + P_h$	Calc. P_s (Eq. 4.8)	Calc. $(P_d - P_s)$
Pa	Pa	Pa	Pa	Pa	Pa	Pa
83120	117900	34780	23645	124970	63667	61302
79007	117013	38007	23645	124970	57381	67589
74423	116747	42323	23645	124970	75183	49787
71423	116640	45217	23645	124970	85551	39419
65477	116167	50690	23645	124970	52333	72637

NC8

PI-06 = P_s	PI-09 = P_d	Expr. $(P_d - P_s)$	$P_h = \rho_L g h_b$	Calc. $P_d = P_A + P_h$	Calc. P_s (Eq. 4.8)	Calc. $(P_d - P_s)$
Pa	Pa	Pa	Pa	Pa	Pa	Pa
84483	118257	33773	23645	124970	59508	65461
80887	117767	36880	23645	124970	96540	28430
76013	117385	41372	23645	124970	89014	35956
71497	116673	45177	23645	124970	74688	50282
66047	115680	49633	23645	124970	29565	95405

NC10

PI-06 = P_s	PI-09 = P_d	Expr. $(P_d - P_s)$	$P_h = \rho_L g h_b$	Calc. $P_d = P_A + P_h$	Calc. P_s (Eq. 4.8)	Calc. $(P_d - P_s)$
Pa	Pa	Pa	Pa	Pa	Pa	Pa
89553	119513	29960	23645	124970	87377	37593
87203	118977	31773	23645	124970	83670	41300
84193	118577	34383	23645	124970	96048	28921
80717	118077	37360	23645	124970	76924	48045
77417	117463	40047	23645	124970	79710	45259
75243	117113	41870	23645	124970	83818	41151
68573	116037	47463	23645	124970	50659	74311

NO6

PI-06 = P_s	PI-09 = P_d	Expr. $(P_d - P_s)$	$P_h = \rho_L g h_b$	Calc. $P_d = P_A + P_h$	Calc. P_s (Eq. 4.8)	Calc. $(P_d - P_s)$
Pa	Pa	Pa	Pa	Pa	Pa	Pa
89320	117097	27777	23645	124970	82966	42003
83957	116500	32543	23645	124970	102743	22227
78443	116127	37683	23645	124970	68950	56020
73497	115963	42467	23645	124970	69967	55002
71357	115927	44570	23645	124970	73326	51644

NO8

PI-06 = P_s	PI-09 = P_d	Expr. $(P_d - P_s)$	$P_h = \rho_L g h_b$	Calc. $P_d = P_A + P_h$	Calc. P_s (Eq. 4.8)	Calc. $(P_d - P_s)$
Pa	Pa	Pa	Pa	Pa	Pa	Pa
82863	117127	34263	23645	124970	6925	118045
78993	117080	38087	23645	124970	84164	40806
73847	116820	42973	23645	124970	76068	48902
72455	116752	44297	23645	124970	55537	69433
67050	116547	49497	23645	124970	66473	58497
64753	116277	51523	23645	124970	77787	47183
61163	116243	55080	23645	124970	36390	88580

B.6 Calculation of Friction Factor

Table B.6. Calculation of friction factor for convergent nozzles

NC6

Q_L	Q_G	ϕ_m	v_L	v_G	$Re_{L,e}$	$Re_{G,e}$	m_L	m_G	$(1+\phi m)$	$(1+R_m)/(1+\phi_m)$	$\Delta P_T/\rho_L.g.\Delta Z$	$\Delta P_F/\rho_L.g.\Delta Z$	f_m
m^3/s	m^3/s		m/s	m/s			(kg/s)	(kg/s)					
0.00092	0.00130	1.42	0.20	0.29	17953	1372	0.916	0.0015	2.42	0.41	0.626	0.513	9.32
0.00100	0.00142	1.42	0.22	0.31	19585	1495	0.999	0.0016	2.42	0.41	0.768	0.853	13.01
0.00109	0.00155	1.43	0.24	0.34	21217	1636	1.082	0.0018	2.43	0.41	0.932	1.263	16.42
0.00117	0.00167	1.43	0.26	0.37	22849	1759	1.165	0.0019	2.43	0.41	1.037	1.517	17.00
0.00125	0.00177	1.41	0.28	0.39	24481	1865	1.249	0.0021	2.41	0.42	1.242	1.996	19.48

NC8

Q_L	Q_G	ϕ_m	v_L	v_G	$Re_{L,e}$	$Re_{G,e}$	m_L	m_G	$(1+\phi m)$	$(1+R_m)/(1+\phi_m)$	$\Delta P_T/\rho_L.g.\Delta Z$	$\Delta P_F/\rho_L.g.\Delta Z$	f_m
m^3/s	m^3/s		m/s	m/s			(kg/s)	(kg/s)					
0.00134	0.00125	0.94	0.29	0.28	26113	1319	1.33	0.0015	1.94	0.52	0.585	0.132	1.13
0.00150	0.00142	0.94	0.33	0.31	29377	1495	1.50	0.0016	1.94	0.51	0.711	0.382	2.59
0.00167	0.00154	0.92	0.37	0.34	32641	1618	1.66	0.0018	1.92	0.52	0.888	0.704	3.86
0.00184	0.00167	0.91	0.41	0.37	35905	1759	1.83	0.0019	1.91	0.52	1.042	0.987	4.48
0.00200	0.00175	0.88	0.44	0.39	39169	1847	2.00	0.0020	1.88	0.53	1.232	1.309	4.99

NC10

Q_L	Q_G	ϕ_m	v_L	v_G	$Re_{L,e}$	$Re_{G,e}$	m_L	m_G	$(1+\phi m)$	$(1+R_m)/(1+\phi_m)$	$\Delta P_T/\rho_L.g.\Delta Z$	$\Delta P_F/\rho_L.g.\Delta Z$	f_m
m^3/s	m^3/s		m/s	m/s			(kg/s)	(kg/s)					
0.00184	0.00129	0.70	0.41	0.28	35905	1354	1.83	0.0015	1.70	0.59	0.598	0.016	0.07
0.00200	0.00142	0.71	0.44	0.31	39169	1495	2.00	0.0016	1.71	0.59	0.723	0.235	0.89
0.00217	0.00154	0.71	0.48	0.34	42433	1618	2.16	0.0018	1.71	0.59	0.836	0.427	1.39
0.00234	0.00167	0.71	0.52	0.37	45697	1759	2.33	0.0019	1.71	0.58	0.913	0.564	1.58
0.00251	0.00192	0.77	0.55	0.42	48961	2023	2.50	0.0022	1.77	0.57	1.148	1.027	2.51

Table B.7. Calculation of friction factor for orifice nozzles

NO6

Q_L	Q_G	ϕ_m	v_L	v_G	$Re_{L,e}$	$Re_{G,e}$	m_L	m_G	$(1+\phi m)$	$(1+R_m)/(1+\phi_m)$	$\Delta P_T/\rho_L.g.\Delta Z$	$\Delta P_F/\rho_L.g.\Delta Z$	f_m
m^3/s	m^3/s		m/s	m/s			(kg/s)	(kg/s)					
0.00058	0.00100	1.71	0.13	0.22	11424	1055	0.583	0.001	2.71	0.37	0.400	0.084	3.78
0.00067	0.00117	1.75	0.15	0.26	13056	1231	0.666	0.001	2.75	0.36	0.587	0.614	21.05
0.00075	0.00142	1.89	0.17	0.31	14688	1495	0.749	0.002	2.89	0.35	0.781	1.253	33.98
0.00084	0.00155	1.86	0.18	0.34	16320	1636	0.832	0.002	2.86	0.35	0.958	1.737	38.14
0.00089	0.00164	1.85	0.20	0.36	17300	1724	0.882	0.002	2.85	0.35	1.031	1.935	37.82

NO8

Q_L	Q_G	ϕ_m	v_L	v_G	$Re_{L,e}$	$Re_{G,e}$	m_L	m_G	$(1+\phi m)$	$(1+R_m)/(1+\phi_m)$	$\Delta P_T/\rho_L.g.\Delta Z$	$\Delta P_F/\rho_L.g.\Delta Z$	f_m
m^3/s	m^3/s		m/s	m/s			(kg/s)	(kg/s)					
0.00100	0.00117	1.17	0.22	0.26	19585	1231	0.999	0.0014	2.17	0.46	0.637	0.378	5.77
0.00109	0.00125	1.15	0.24	0.28	21217	1319	1.082	0.0015	2.15	0.46	0.774	0.665	8.64
0.00117	0.00134	1.14	0.26	0.29	22849	1407	1.165	0.0015	2.14	0.47	0.953	1.040	11.65
0.00125	0.00150	1.20	0.28	0.33	24481	1583	1.249	0.0017	2.20	0.46	1.004	1.207	11.78
0.00134	0.00159	1.19	0.29	0.35	26113	1671	1.332	0.0018	2.19	0.46	1.195	1.612	13.83
0.00142	0.00167	1.18	0.31	0.37	27745	1759	1.415	0.0019	2.18	0.46	1.277	1.777	13.50
0.00150	0.00175	1.17	0.33	0.39	29377	1847	1.498	0.0020	2.17	0.46	1.404	2.041	13.84

B.8 Energy Dissipation in the Ejector

Table B.9. Calculation of energy dissipation in the ejector for various nozzles

NC6

Q_L	$Q_{G,s}$	$Q_{G,d}$	$Q_{M,s}$	$Q_{M,d}$	PI-06 = P_s	PI-09 = P_d	$P_d \cdot Q_{M,d}$	$P_s \cdot Q_{M,s}$	$E_{D,e}$
m^3/s	m^3/s	m^3/s			Pa	Pa	W	W	W
0.00092	0.00130	0.00092	0.00222	0.00184	83120	117900	216.56	184.62	31.95
0.00100	0.00142	0.00096	0.00242	0.00196	79007	117013	229.40	191.31	38.08
0.00109	0.00155	0.00099	0.00264	0.00208	74423	116747	242.32	196.37	45.94
0.00117	0.00167	0.00102	0.00284	0.00219	71423	116640	255.63	202.77	52.86
0.00125	0.00177	0.00100	0.00302	0.00225	65477	116167	261.41	197.92	63.49

NC8

Q_L	$Q_{G,s}$	$Q_{G,d}$	$Q_{M,s}$	$Q_{M,d}$	PI-06 = P_s	PI-09 = P_d	$P_d \cdot Q_{M,d}$	$P_s \cdot Q_{M,s}$	$E_{D,e}$
m^3/s	m^3/s	m^3/s			Pa	Pa	W	W	W
0.00134	0.00125	0.00089	0.00259	0.00223	84483	118257	263.81	218.69	45.12
0.00150	0.00142	0.00097	0.00292	0.00248	80887	117767	291.82	236.39	55.43
0.00167	0.00154	0.00099	0.00321	0.00266	76013	117385	312.82	243.73	69.09
0.00184	0.00167	0.00102	0.00351	0.00286	71497	116673	333.73	250.74	82.99
0.00200	0.00175	0.00100	0.00376	0.00301	66047	115680	347.64	248.17	99.47

NC10

Q_L	$Q_{G,s}$	$Q_{G,d}$	$Q_{M,s}$	$Q_{M,d}$	PI-06 = P_s	PI-09 = P_d	$P_d \cdot Q_{M,d}$	$P_s \cdot Q_{M,s}$	$E_{D,e}$
m^3/s	m^3/s	m^3/s			Pa	Pa	W	W	W
0.00150	0.00100	0.00075	0.00251	0.00225	89553	119513	269.36	224.33	45.03
0.00167	0.00114	0.00083	0.00281	0.00250	87203	118977	297.72	244.66	53.06
0.00184	0.00129	0.00091	0.00312	0.00275	84193	118577	326.09	262.93	63.16
0.00200	0.00142	0.00097	0.00342	0.00297	80717	118077	351.20	276.33	74.87
0.00217	0.00154	0.00101	0.00371	0.00318	77417	117463	373.96	287.01	86.94
0.00234	0.00167	0.00107	0.00401	0.00341	75243	117113	399.47	301.58	97.89
0.00251	0.00192	0.00113	0.00443	0.00364	68573	116037	422.37	303.47	118.90

NO6

Q_L	$Q_{G,s}$	$Q_{G,d}$	$Q_{M,s}$	$Q_{M,d}$	PI-06 = P_s	PI-09 = P_d	$P_d \cdot Q_{M,d}$	$P_s \cdot Q_{M,s}$	$E_{D,e}$
m^3/s	m^3/s	m^3/s			Pa	Pa	W	W	W
0.00058	0.00100	0.00076	0.00159	0.00135	89320	117097	157.94	141.71	16.24
0.00067	0.00117	0.00084	0.00184	0.00151	83957	116500	175.97	154.23	21.74
0.00075	0.00142	0.00096	0.00217	0.00171	78443	116127	198.62	170.30	28.32
0.00084	0.00155	0.00098	0.00239	0.00182	73497	115963	210.98	175.52	35.46
0.00089	0.00164	0.00101	0.00252	0.00189	71357	115927	219.39	179.94	39.45

NO8

Q_L	$Q_{G,s}$	$Q_{G,d}$	$Q_{M,s}$	$Q_{M,d}$	PI-06 = P_s	PI-09 = P_d	$P_d \cdot Q_{M,d}$	$P_s \cdot Q_{M,s}$	$E_{D,e}$
m^3/s	m^3/s	m^3/s			Pa	Pa	W	W	W
0.00109	0.00125	0.00085	0.00234	0.00193	78993	117080	226.03	184.69	41.34
0.00117	0.00134	0.00084	0.00251	0.00201	73847	116820	235.22	184.99	50.24
0.00125	0.00150	0.00093	0.00276	0.00219	72455	116752	255.13	199.65	55.48
0.00134	0.00159	0.00091	0.00292	0.00225	67050	116547	262.08	195.95	66.13
0.00142	0.00167	0.00093	0.00309	0.00235	64753	116277	273.19	200.06	73.14
0.00150	0.00175	0.00092	0.00326	0.00243	61163	116243	281.96	199.18	82.79

B.9 Gas Hold-up Measurement and Calculation

Table B.10. Calculation of gas hold-up in the ejector for various nozzles

NC6

A_f/A_n: 18.78 T: 298 K

Q_L	Q_G	Q_M	v_L	v_G	v_M	V_T	V_G	ε_G	$\varepsilon_L = 1 - \varepsilon_G$	$u_G = v_G/e_G$
m^3/s	m^3/s	m^3/s	m/s	m/s	m/s	mL	mL	-	-	m/s
0.00092	0.00130	0.00222	0.20	0.29	0.49	14400	4950	0.34	0.66	0.84
0.00100	0.00142	0.00242	0.22	0.31	0.53	14400	5050	0.35	0.65	0.89
0.00109	0.00155	0.00264	0.24	0.34	0.58	14400	5175	0.36	0.64	0.95
0.00117	0.00167	0.00284	0.26	0.37	0.63	14400	5300	0.37	0.63	1.00
0.00125	0.00177	0.00302	0.28	0.39	0.67	14400	5350	0.37	0.63	1.05

NC8

A_f/A_n: 10.56 T: 298 K

Q_L	Q_G	Q_M	v_L	v_G	v_M	V_T	V_G	ε_G	$\varepsilon_L = 1 - \varepsilon_G$	$u_G = v_G/e_G$
m^3/s	m^3/s	m^3/s	m/s	m/s	m/s	mL	mL	-	-	m/s
0.00134	0.00125	0.00209	0.29	0.28	0.46	14400	4675	0.32	0.68	0.85
0.00150	0.00142	0.00235	0.33	0.31	0.52	14400	4725	0.33	0.67	0.95
0.00167	0.00154	0.00259	0.37	0.34	0.57	14400	4775	0.33	0.67	1.02
0.00184	0.00167	0.00284	0.41	0.37	0.63	14400	4875	0.34	0.66	1.09
0.00200	0.00175	0.00305	0.44	0.39	0.67	14400	4925	0.34	0.66	1.13

NC10

A_f/A_n: 6.76 T: 298 K

Q_L	Q_G	Q_M	v_L	v_G	v_M	V_T	V_G	ε_G	$\varepsilon_L = 1 - \varepsilon_G$	$u_G = v_G/e_G$
m^3/s	m^3/s	m^3/s	m/s	m/s	m/s	mL	mL	-	-	m/s
0.00150	0.00100	0.00251	0.33	0.22	0.55	14400	4138	0.29	0.71	0.77
0.00167	0.00114	0.00281	0.37	0.25	0.62	14400	4213	0.29	0.71	0.86
0.00184	0.00129	0.00312	0.41	0.28	0.69	14400	4225	0.29	0.71	0.97
0.00200	0.00142	0.00342	0.44	0.31	0.76	14400	4275	0.30	0.70	1.05
0.00217	0.00154	0.00371	0.48	0.34	0.82	14400	4290	0.30	0.70	1.14
0.00234	0.00167	0.00401	0.52	0.37	0.88	14400	4350	0.30	0.70	1.22
0.00251	0.00192	0.00443	0.55	0.42	0.98	14400	4400	0.31	0.69	1.39

NO6

A_t/A_n: 18.78 T: 298 K

Q_L	Q_G	Q_M	v_L	v_G	v_M	V_T	V_G	ε_G	$\varepsilon_L = 1 - \varepsilon_G$	$u_G = v_G/e_G$
m^3/s	m^3/s	m^3/s	m/s	m/s	m/s	mL	mL	-	-	m/s
0.00058	0.00100	0.00159	0.13	0.22	0.35	14400	4725	0.33	0.67	0.67
0.00067	0.00117	0.00184	0.15	0.26	0.41	14400	4863	0.34	0.66	0.76
0.00075	0.00142	0.00217	0.17	0.31	0.48	14400	4925	0.34	0.66	0.92
0.00084	0.00155	0.00239	0.18	0.34	0.53	14400	5150	0.36	0.64	0.96
0.00089	0.00164	0.00252	0.20	0.36	0.56	14400	5200	0.36	0.64	1.00

NO8

A_t/A_n: 10.56 T: 298 K

Q_L	Q_G	Q_M	v_L	v_G	v_M	V_T	V_G	ε_G	$\varepsilon_L = 1 - \varepsilon_G$	$u_G = v_G/e_G$
m^3/s	m^3/s	m^3/s	m/s	m/s	m/s	mL	mL	-	-	m/s
0.00100	0.00117	0.00217	0.22	0.26	0.48	14400	4400	0.31	0.69	0.84
0.00109	0.00125	0.00234	0.24	0.28	0.52	14400	4538	0.32	0.68	0.88
0.00117	0.00134	0.00251	0.26	0.29	0.55	14400	4738	0.33	0.67	0.90
0.00125	0.00150	0.00276	0.28	0.33	0.61	14400	4850	0.34	0.66	0.98
0.00134	0.00159	0.00292	0.29	0.35	0.64	14400	4925	0.34	0.66	1.02
0.00142	0.00167	0.00309	0.31	0.37	0.68	14400	4960	0.34	0.66	1.07
0.00150	0.00175	0.00326	0.33	0.39	0.72	14400	5000	0.35	0.65	1.11